Optical Cavities as Single Photon Sources

by

Veronica Øverbye

Thesis for the degree of

Master of Science

Department of Physics
Faculty of Mathematics and Natural Sciences
University of Oslo

December 2012

Acknowledgements

First of all, I would like to express my outmost gratitude towards my supervisor Jon Magne Leinaas. Thank you for all your help and patience, our interesting conversations and your friendship.

A big thank you goes to Andreas Nakkerud for spending an entire weekend proof-reading my thesis. I would also like to thank my fellow master students for making the last years so interesting.

Next, I express my deepest appreciation for my family. I thank my loving parents for all your support, encouragement and understanding. I thank my wonderful sister, for being there for me during this last strenuous semester.

I am forever indebted to three of my dearest friends and fellow students, Thea Marcelia Sletten, Tone Melvær Ruud and Sarah Thaysen, for your irreplaceable company through the struggle that is higher education. You have taught me so much, and I am sincerely grateful for your friendship.

Finally, I thank my best friend and beloved, John Christian Ottem, for your endless love and encouragement.

Veronica Øverbye, Oslo, December 2012

Abstract

Recent work within quantum information technology suggests combining single atoms and photons to form quantum networks and processors. In such set-ups the ability to produce and manipulate single photons is a crucial factor.

This thesis is devoted to the topic of single photon sources, based on single atoms inside optical cavities. We discuss the basic features of cavity quantum electrodynamics, and present the concept of an optical cavity and the quantization of the cavity field. The characteristics of a cavity-based single photon source are studied in the two-level Jaynes-Cummings model, and we evaluate the photon emission efficiency for variations in the system parameters.

Next, we extend the two-level system to a three-level Λ-model, coupled to an adjustable laser field. We demonstrate numerically a laser-controlled procedure for adiabatic manufacturing of single photons. We use a numerical Monte Carlo wavefunction method for modeling the Lindblad master equation of the Λ-system. We also show how to apply the laser to produce photons with a predefined temporal profile.

Contents

Introduction

The Theory of Quantum Mechanics was carefully assembled during the first decades of the 20th century, by a handful of the greatest physicists of that time. The idea that natures fundamental variables are quantized on the microscopic scale would turn out to have ground-breaking consequences. From the new theory, strange and counterintuitive predictions were made, foretelling particle wave properties, exclusion principles and quantum entanglement.

Quantum mechanical states are fragile constructions that are easily destroyed by even the weakest of external influences. In the early 1900s the experiments one were able to conduct with quantum systems were therefore limited. Controlled manipulation of single particles or single quanta of light were exclusively reserved for thought experiments. As time passed our technology and knowledge improved, making it possible to demonstrate in practice the strange predictions of quantum mechanics. Today scientists have come a long way in the laboratory. As we speak, methods enabling detailed control on single atom and single photon level are being developed. In fact, the Nobel Prize in Physics was in 2012 awarded to Haroche and Wineland, "for ground-breaking experimental methods that enable measuring and manipulation of individual quantum systems" [1].

With means available to control individual quantum entities, new areas of quantum research and applications have formed. In recent years, the potentially revolutionary applications of quantum mechanics in information theory have been brought to attention. What happens if the classical two-state information carrier, known as a bit, is replaced by a quantum mechanical two-state system? This question motivated the establishment of a new scientific field known as Quantum Information Theory.

In quantum information theory the bit is traded for a new basic unit of information, namely the quantum bit or qubit. The physical representation of a qubit is a quantum mechanical system composed of two orthogonal states, usually denoted $|0\rangle$ and $|1\rangle$. A general qubit is a superposition of these states

$$|q\rangle = \alpha\,|0\rangle + \beta\,|1\rangle\,,$$

where the coefficients α and β are complex numbers. While the possible values of a bit is restricted to 0 and 1, the qubit takes values in a two-dimensional Hilbert space spanned by the states $|0\rangle$ and $|1\rangle$.

The long-term goal for quantum information scientists is to utilize the quantum mechanical properties of the qubit to construct quantum processors and communication networks. The latter would provide new methods for secure communication, while

quantum processors may be used to solve certain types of mathematical problems in an extremely efficient way. The essential building blocks of both quantum processors and quantum networks are, in a wide sense, nodes and wires. The nodes are stations, where the qubits are stored or manipulated. The wires are qubit highways, connecting the nodes and allowing them to exchange information.

At the moment, an effort is being made to find suitable physical realizations of qubits, and methods enabling us to perform different quantum operations on them. In theory, any quantum mechanical system having a pair of well-defined orthogonal states may serve as a qubit. If the system is suitable depends upon its ability to store information in a robust way, and how efficiently the information may be manipulated and transported. Currently there are several candidates for qubits. In the field of quantum optics photons in combination with trapped atoms or ions are giving promising results.

The photon is outstanding when it comes to velocity and resistance to interactions with its environment. This means it can travel fast over long distances, without losing data. The loss of information from a quantum mechanical system is often referred to as decoherence. The decoherence process robs the system of its quantum mechanical properties, properties that carry the information necessary for quantum processing and communication. The difficulties in successfully isolating a system from its surroundings, makes decoherence one of the most demanding challenges of handling quantum systems in practice. In this respect the photons intrinsic robustness is a great advantage.

What appears as a strength in one situation can be a weakness in another. Photons are hasty creatures; they are not easily restrained for manipulation or storage of information. In this regard atoms are much better suited. An ideal set-up would therefore be to construct a quantum network or processor scheme consisting of atomic nodes, for quantum state manipulation and storage, combined with single photons to transport information from one node to another.

For quantum computing and quantum networking schemes combining atoms and single photons, our ability to produce single photons in a controlled manner, as well as to efficiently transfer information between atoms and photons, will be of great importance. Quantum mechanical set-ups utilizing photons are often referred to as optical. Some of the most crucial requirements for the successful implementation of an optical quantum computer or quantum communication network, as listed in [14], are

- Deterministic single photon emission with 100% efficiency.
- Directed emission into a single mode of the electromagnetic field.
- Reversible quantum state transfer and entanglement between atoms and photons.

The term single mode refers to a mode of the electromagnetic field with a well-defined frequency and polarization.

When it comes to producing single photons, the atom is certainly a natural choice. After all, most of the light surrounding us is the collected result of a great number of atomic de-excitation processes. It is a well-known fact that the coupling between a

specific atomic transition and an electromagnetic mode will depend on the frequency of the mode in question. The interaction will be strongest for the modes with an energy matching the atomic transition, and decrease as the discrepancy grows. This means that the emitted light associated with a specific atomic transition has a rather accurately determined frequency. However, an atom interacting with the electromagnetic field in open space has no preferred destination in mind for its emitted photons. Consequently, the direction of the produced light is certainly not well defined. This makes the emitted photons hard to collect, and results in poor efficiency.

It turns out that providing the atom with the accommodations of an optical cavity will, influence its emission properties in an advantageous way. An optical cavity in its simplest manifestation is a construction of highly reflective mirrors, which is able to capture light in an effective manner. Inside such a device the electromagnetic field is discretized, and can be considered as a collection of clearly separated standing wave modes. Each mode having a specified polarization and frequency.

Under these circumstances the atom can be made to effectively couple to only a single cavity mode. For sufficiently small cavity volume the atom-cavity coupling will grow strong, causing the atomic radiation into the cavity to completely dominate over emission into non-cavity modes. Supplying one of the cavity mirrors with a finite transparency will cause the produced photons to leak out in a specified direction. The final result is a single photon source, emitting photons into a single mode of the electromagnetic field with a well-defined direction of propagation.

The first observations of atoms strongly coupled to an optical cavity were made in the early 1990's. Since then a wide range of application for this phenomenon has been discovered. By using atoms of different energy structures and varying the set-up parameters in terms of coupling strength and decay processes, we can construct several types of schemes. Procedures enabling nearly lossless production of single photons by the means of a laser [12] and the production of predefined photon shapes [29], have recently been uncovered.

The enhancement of atom-field interactions caused by optical cavities is also one of the main ingredients in the experiments performed by the Nobel Prize winning Haroche and his team. In the experiment that got special attention from the Nobel commitee [23], non-destructive measurements of single cavity photons where performed, by sending an atom through the cavity, and subsequently measuring its state.

In this thesis we will look into the characteristics of some of the current state-of-the-art models of single photon sources, based on single atoms trapped inside optical cavities. We will attempt to answer the questions of how single photons can be deterministically manufactured and how their properties may be controlled. As a guide through the different topics of discussion the article *Cavity-based single-photon sources* by Kuhn and Ljunggren [14] is used.

Chapter 1 provides a solid footing within the world of cavity quantum electrodynamics. The concepts of optical cavities and the quantization of the electromagnetic field inside a cavity are introduced. Furthermore, the interaction of the quantized cavity

field and a single two-level atom is described through the Jaynes-Cummings model. The Jaynes-Cummings Hamiltonian is thoroughly derived, and the Schrödinger equation is solved analytically, to reveal the system dynamics.

In Chapter 2 the Jaynes-Cummings model is extended to include interactions with the environment. This allows it to describe cavity photon emission and the atomic coupling to non-cavity modes. A short introduction to the description of open quantum mechanical systems is given, where the density operator and the Lindblad master equation are presented. It is shown how the master equation can, for a certain type of incoherent transitions, be formulated as an effective Schrödinger equation. Finally, analytic expressions revealing the system dynamics are found.

Further, the decaying Jaynes-Cummings model is enriched with a third atomic energy level and the electromagnetic field of an adjustable laser. The new composition forms a so-called Λ-model, to which we devote Chapter 3. In this chapter we focus on an adiabatic scheme for producing single cavity photons. With the introduction of the time dependent laser, the system dynamics must be found numerically. The chapter concludes with a discussion of numerical results.

In Chapter 4 the full Lindblad equation is put to use, when a second type of incoherent transitions are included in the Λ-model. Further we introduce a procedure for numerically simulating the Lindblad dynamics through a Monte Carlo wavefunction method. An in-depth review of the corresponding algorithm is given, before the method is applied to model the decaying Λ-system.

Our theoretical study of the Λ-model is rounded off with Chapter 5. Here it is demonstrated how the laser can be used to customize photons with a specified temporal shape. After predefining the photon profile, we find a unique analytic expression for the corresponding laser profile. At last we apply the method for a few example photons, and calculate their required laser profiles.

The thesis is concluded with Chapter 6, where we turn our attention to the experimental side of cavity quantum electrodynamics. We review a real life Λ-model experiment, and briefly look into some of its technical details. We round off with concluding remarks on this thesis.

Chapter 1

Theory of Light, Matter and Cavitites

In our pursuit of revealing the secrets of the cavity-based single photon sources we need to understand the interaction of light and matter inside a cavity. In this chapter we will conceptually build a simple atom-cavity system, piece by piece.

We start by introducing the electric scalar potential and magnetic vector potential from Maxwell's equations. Next follows a brief introduction to optical cavities and an outline of the quantization of the electromagnetic field inside a cavity. A single electromagnetic cavity mode and a single atom are then brought together to form the so-called Jaynes-Cummings model. The chapter is concluded with the investigation of the Jaynes-Cummings dynamics.

1.1 The Electromagnetic Potentials

The very first section of this thesis is intended to give an introduction to the concepts of the electric scalar potential and the magnetic vector potential, as is commonly used in the field of quantum optics. The material presented on this subject can be found in most introductory literature concerning quantum optics, such as [19] and [16].

The theory of electromagnetism is neatly summarized by Maxwell's four famous equations

$$\boldsymbol{\nabla} \cdot \mathbf{E} = \frac{\rho}{\epsilon_0}, \tag{1.1}$$

$$\boldsymbol{\nabla} \times \mathbf{B} - \frac{1}{c^2}\frac{\partial \mathbf{E}}{\partial t} = \mu_0 \mathbf{j}, \tag{1.2}$$

$$\boldsymbol{\nabla} \cdot \mathbf{B} = 0, \tag{1.3}$$

$$\boldsymbol{\nabla} \times \mathbf{E} + \frac{\partial \mathbf{B}}{\partial t} = 0, \tag{1.4}$$

with $\mathbf{E}$ and $\mathbf{B}$ as the electric and magnetic fields, ρ as the charge density and $\mathbf{j}$ as the current density. The constants ϵ_0 and μ_0 are the vacuum permittivity and vac-

uum permeability. Equation (1.3) and (1.4) allows for the definition of electromagnetic potentials as follows

$$\mathbf{B} = \boldsymbol{\nabla} \times \mathbf{A}, \quad \mathbf{E} = -\boldsymbol{\nabla}\phi - \frac{\partial \mathbf{A}}{\partial t}, \tag{1.5}$$

where ϕ is called the electric scalar potential, and $\mathbf{A}$ is known as the magnetic vector potential.

These definitions do not, however, specify the potentials uniquely. For an arbitrary function $f(\mathbf{r}, t)$ the observable electromagnetic fields $\mathbf{E}$ and $\mathbf{B}$ will not be affected by so called gauge transformation of the form

$$\phi \to \phi' = \phi + \frac{1}{c}\frac{\partial f}{\partial t}, \qquad \mathbf{A} \to \mathbf{A}' = \mathbf{A} - \boldsymbol{\nabla} f.$$

This property is known as gauge invariance. It reflects non-physical degrees of freedom in $\mathbf{A}$, and we are free to choose a gauge condition in order to remove these. The Coulomb gauge condition (also known as the radiation gauge condition) is

$$\boldsymbol{\nabla} \cdot \mathbf{A} = 0, \tag{1.6}$$

and is the usual choice when interaction between electromagnetic fields and atoms are to be considered. With this condition the Maxwell equations reduces to

$$\begin{aligned} \boldsymbol{\nabla}^2 \phi &= -\frac{\rho}{\epsilon_0}, \\ \big(\frac{1}{c^2}\frac{\partial^2}{\partial t^2} - \boldsymbol{\nabla}^2\big)\mathbf{A} &= \mu_0 \mathbf{j} - \frac{1}{c^2}\frac{\partial}{\partial t}\boldsymbol{\nabla}\phi. \end{aligned} \tag{1.7}$$

Restricting our scope to fields in vacuum, the charge density ρ and current density $\mathbf{j}$ are both zero. The electric potential then vanish by equation (1.7), so $\phi = 0$. The electromagnetic field may thus be described through the magnetic potential $\mathbf{A}$, given by the equation

$$\big(\frac{1}{c^2}\frac{\partial^2}{\partial t^2} - \boldsymbol{\nabla}^2\big)\mathbf{A} = 0, \tag{1.8}$$

which we recognize as the electromagnetic wave equation. We also observe from (1.5) that

$$\phi = 0 \quad \Rightarrow \quad \mathbf{E} = -\frac{\partial \mathbf{A}}{\partial t} = -\dot{\mathbf{A}}. \tag{1.9}$$

This last relation turns out to be useful; since the vector potential does not represent any observable physical quantity, the physical boundary and initial conditions must be given indirectly through $\mathbf{E}$ and $\mathbf{B}$.

1.2 Cavity Quantum Electrodynamics

An optical cavity is a construction that effectively stores light through the mechanism of repeated reflections. Light confined inside the cavity is reflected multiple times resulting

in stable electromagnetic fields for certain resonant frequencies. Throughout this thesis these fields will be referred to as *cavity modes*. Optical cavities are also called optical resonators.

In the course of the last century the optical cavity has made major contributions to our understanding of light and its mysterious ways. So much so, that it has become the founding source of its own area of quantum research, namely cavity quantum electrodynamics. It turns out that the interaction of light and matter can be greatly amplified by the confinement of an optical cavity. Cavity quantum electrodynamics is devoted to the study of this interaction.

There are several ways of constructing an optical cavity. Two examples of relatively recent development are fiber cavities [8] and photonic crystal cavities. However, the most common and perhaps intuitive set-up is using mirrors. In this category we find the optical cavity in its simplest form, consisting of two facing mirrors with a uniform medium in between. This set-up is named a Fabry-Pérot cavity, after its two French inventors Charles Fabry and Alfred Pérot, who introduced their invention in a joint article in 1897 [4]. Despite its simplicity, the set-up can be made quite effective with the right design and materials, and constitutes a favorable tool in the making of collaboration agreements between light and matter. In the following we will be concerned with resonators of the Fabry-Pérot kind.

1.2.1 The Quantized Field Inside a Fabry-Pérot Cavity

With the notions of the magnetic vector potential and optical resonators in place, we can make an attempt to find quantized solutions for the cavity modes in terms of the magnetic potential. We will begin with the simplest possible type of Fabry-Pérot cavity, consisting of two plane mirrors. In the closing of this subsection we will discuss more realistic cavity set-ups.

Figure 1.1 shows the schematic set-up of a Fabry-Pérot cavity with plane parallel mirrors. The mirrors are assumed to be perfectly reflective surfaces, with a separation l along the z-axis. In addition we assume that the cavity modes are held completely captive by the mirrors, in the sense that no light will escape the cavity.
The cavity construction gives the following boundary conditions

$$\mathbf{E}(z = 0) = \mathbf{E}(z = l) = 0, \tag{1.10}$$

for components of the electric field parallel to the mirrors. From this follows the existence of an infinite range of discrete cavity modes of wavelength

$$\lambda = \frac{2l}{n}, \quad \text{for } n = 1, 2, \ldots \tag{1.11}$$

and a corresponding discretization of the wavenumber

$$k = |\mathbf{k}| = \frac{\pi n}{l}. \tag{1.12}$$

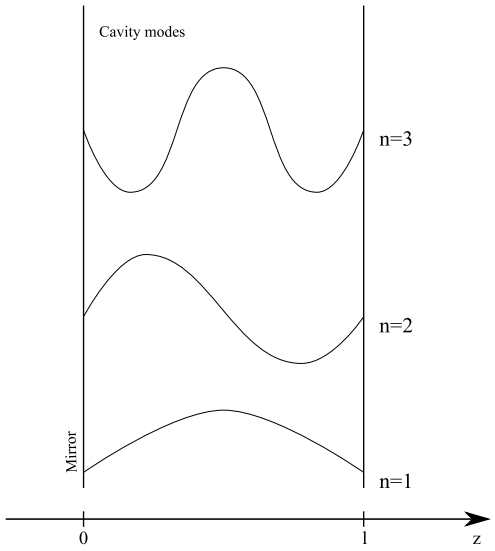

Figure 1.1: Set-up of a simple Fabry-Perot cavity. Two plane mirrors are placed parallel to each other with a separation l. The three lowest cavity modes are displayed and marked with their n-values corresponding to their wavenumber $k = \frac{\pi n}{l}$.

The total cavity field will consist of an infinite collection of modes stretching in all three spatial directions. However, we will only be interested in the modes resonating between the mirrors, with the electric field parallel to the mirror surfaces. We call these *cavity modes* and sort them into two independent linear polarization groups. Let $\boldsymbol{\epsilon}_a$, with $a \in \{||, \perp\}$, denote the two corresponding polarization vectors. For wavenumber k and polarization a, we solve the electromagnetic wave equation to find

$$E_{ak}(z,t) = E^0_{ak}(t) \sin kz, \tag{1.13}$$

and by relation (1.9) the vector potential is on the same form

$$A_{ak}(z,t) = A^0_{ak}(t) \sin kz. \tag{1.14}$$

The total vector potential may then be expressed as a sum over the two possible polarizations and all available wave numbers

$$\mathbf{A}(z,t) = \frac{1}{\sqrt{V}} \sum_{a,k} A^0_{ak}(t) \sin kz \, \boldsymbol{\epsilon}_a. \tag{1.15}$$

The constant $\frac{1}{\sqrt{V}}$ is made explicit in order to rid the factors A_{ak} of any volume dependence.

So far we have only made use of classical electromagnetic theory. The time has come to tiptoe across the border to quantum electrodynamics, taking the quantum nature of light into account. The electric field and the vector potential are quantized in the usual manner, by replacing $\mathbf{E}$ and $\mathbf{A}$ by operators $\hat{\mathbf{E}}$ and $\hat{\mathbf{A}}$. We make a change of variables

for convenience

$$\hat{A}_{ak}(t) = \sqrt{\frac{\hbar}{2\omega_k \epsilon_0}}(\hat{a}_{ak}(t) + \hat{a}^\dagger_{ak}(t)), \tag{1.16}$$

$$\hat{E}_{ak}(t) = i\sqrt{\frac{\hbar\omega_k}{2\epsilon_0}}(\hat{a}_{ak}(t) - \hat{a}^\dagger_{ak}(t)). \tag{1.17}$$

With ω_k being the frequency accompanying the wave number k. From the classical expression for the Hamiltonian we then get the quantum mechanical Hamiltonian

$$\begin{aligned} H &= \sum_{a,k} \frac{1}{2}\epsilon_0(E_{ak}E^*_{ak} + \omega_k^2 A_{ak}A^*_{ak}) \quad \rightarrow \\ \hat{H} &= \sum_{a,k} \frac{1}{2}\epsilon_0(\hat{E}_{ak}\hat{E}^\dagger_{ak} + \omega_k^2 \hat{A}_{ak}\hat{A}^\dagger_{ak}) \\ &= \sum_{a,k} \frac{1}{2}\hbar\omega_k(\hat{a}_{ak}(t)\hat{a}^\dagger_{ak}(t) + \hat{a}^\dagger_{ak}(t)\hat{a}_{ak}(t)) \\ &= \sum_{a,k} \hbar\omega_k(\hat{a}_{ak}(t)\hat{a}^\dagger_{ak}(t) + \frac{1}{2}). \end{aligned} \tag{1.18}$$

We see that with this particular choice of expressions for the quantized field operators, the field Hamiltonian takes the form of a collection of harmonic oscillators, one for each distinct pair of k and polarization a. The terms $\hat{a}_{ak}$ and $\hat{a}^\dagger_{ak}$ act as lowering and raising operators for each mode. We note that the operators may be time dependent, corresponding to the Heisenberg picture. We will prefer the Schrödinger picture, where the states carry the time dependence. From here on the operators will therefore be considered to be time independent.

Inserting the result from (1.16) into equation (1.15) gives the quantized cavity mode vector potential

$$\hat{\mathbf{A}}(z) = \sum_{a,k} \sqrt{\frac{\hbar}{2\omega_k \epsilon_0 V}}(\hat{a}_{ak} + \hat{a}^\dagger_{ak}) \sin kz\, \boldsymbol{\epsilon}_a, \tag{1.19}$$

of an idealized Fabry-Pérot cavity.

In real life Fabry-Pérot cavities are usually constellations of two curved mirrors, or one curved mirror in combination with a plane mirror. For an example, see [27]. We will in the following give a brief summary on the subject of optical resonators with spherical mirrors. These are commonly used, as presented by Yarvin [31]. For a cavity consisting of spherically shaped mirrors it can be shown that the field solutions are the so-called Gaussian beams. These are electromagnetic waves whose transverse electric field distribution is given by a Gaussian function. The fundamental transversal Gaussian wave in which the energy is propagating mainly in the z-direction is given by

$$E(x,y,z) = E_0 \frac{\omega_0}{\omega(z)} \exp\left(-i(kz - \eta(t)) - (x^2+y^2)\Big(\frac{1}{\omega^2(z)} + \frac{ik}{2R(z)}\Big)\right). \tag{1.20}$$

With

$$R(z) = z(1 + \frac{z_0^2}{z^2}), \qquad z_0 = \frac{\pi\omega_0^2 n}{\lambda}, \tag{1.21}$$

$$\omega^2(z) = \omega_0^2(1 + \frac{z^2}{z_0^2}), \qquad k = \frac{2\pi n}{\lambda}, \tag{1.22}$$

$$\eta(z) = \tan^{-1}\Big(\frac{\lambda z}{\pi\omega_0^2 n}\Big). \tag{1.23}$$

$\omega(z)$ is the so called spot size, giving the distance from the z-axis for which the field amplitude has decreased with a factor $1/e$. ω_0 is the minimum spot size, given by $\omega(0)$. Gaussian beams are found to have nearly spherical phase fronts for $z^2 \gg x^2 + y^2$, and $R(z)$ gives the corresponding radius of curvature.

Picture having a cavity set-up consisting of two spherical mirrors with radius of curvature R_1 and R_2, placed at z_1 and z_2 respectively (see Figure 1.2). By adjusting the beam such that the phase front curvature matches the curvature of the mirrors, that is $R(z_1) = R_1$ and $R(z_2) = R_2$, the beam will reflect and retrace itself, forming a resonant cavity mode. The process of tuning a beam to fit a specific cavity set-up is known as mode matching. Mode matching can be an intricate and time-consuming process.

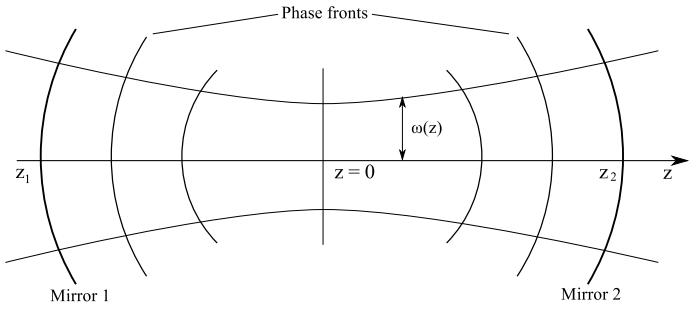

Figure 1.2: Schematic presentation of the Gaussian beam with main propagation direction along the z-axis. The spot size $\omega(z)$, spherical phase fronts and the mirrors positioned at z_1 and z_2 are indicated.

Assume we are able to get our hands on a pair of perfectly reflecting mirrors, and that we are able to completely match a Gaussian mode to our cavity set-up. The stability of our captured cavity mode will then depend on the mirror curvature and the mirror separation $l = |z_2 - z_1|$. The stability criteria is found to be

$$0 \leq \Big(1 - \frac{l}{R_1}\Big)\Big(1 - \frac{l}{R_2}\Big) \leq 1. \tag{1.24}$$

Inspecting (1.20), we observe that the familiar plane wave solutions,

$$E(z) = E_0 e^{-ikz}, \tag{1.25}$$

are just special cases of the Gaussian modes, found in the limit $R(z) \to \infty$. In order to capture a cavity mode formed from these solutions, the mirrors would have to be plane and parallel, and the resulting cavity modes would be the ones described in (1.19). From (1.24) we see that such a system is on the verge of instability, with $(1 - l/R_1)(1 - l/R_2) = 1$. Consequently, the mode stability is extremely sensitive, and small inaccuracies in the cavity set-up or mode matching can lead to a cavity of poor performance. This is the reason why realistic cavity set-ups usually involve curved mirrors, leading to better stability.

Since our work will be purely theoretical, we are free to assume that we are capable of setting up a resonator where the mirrors and modes are perfectly fitted. For our purposes it will thus suffice to consider a system of plane mirrors with plane wave solutions, not taking into account the possible obstacles we would encounter as experimentalists. This is most fortunate, seeing how plane wave solutions will make our calculations considerably simpler.

1.3 The Jaynes-Cummings Model

As previously discussed, the aim of this thesis is to describe how to manufacture single photons, using single atoms confined inside optical cavities. Having established our cavity modes in the previous section, now is the appropriate time for the atom to make its entrance. One of the simplest atom-cavity models imaginable is the so-called Jaynes-Cummings model, consisting of a two-level atom interacting with a single electromagnetic mode. The Jaynes-Cummings model was first introduced in 1963 [30], for the purpose of comparing spontaneous emission within the semiclassical and quantum theories of light. Since then it has become a widely applied model, both due to its simplicity and because it is so easily extended to describe more complex systems. We will launch our investigation of atom-cavity systems using the Jaynes-Cummings model.

The energy structure of even the simplest of atoms can be quite complex. Accordingly, the term *two-level atom* refers to a simplified picture. It turns out that it is possible to assemble atoms and electromagnetic fields in such a way that only two of the atomic energy levels effectively couples to the field. When studying the atom-field interaction, the atom can then be regarded as a two-level system. Take as an example the calcium atom, with ground state ${}^1\mathcal{S}_0(l = 0, m = 0)$, and a triplet excited state ${}^1\mathcal{P}_1(l = 1, m = 0, \pm 1)$, given in standard spectroscopic notation. Transitions between the ground state and any one of these excited states are all allowed according to the dipole selection rules. The transition with $\Delta m = 0$ couples to light with linear polarization, while the ones with $\Delta m = \pm 1$ couples to light with circular polarization. The signs of Δm refer to opposite directions of rotation. By providing a mode with energy close to the atomic transition, and the right polarization, we can thus make three different, effectively two-level systems from these two atomic energy states [20]. Naturally, if the atom is to act as a two-level system, we must assume there are no other atomic transitions matching this particular mode.

Assume we place a single atom inside the plane mirror Fabry-Perot cavity described in the preceding section, keeping it in place by some form of electromagnetic potential. In order to implement the Jaynes-Cummings model we need the atom to interact significantly with only one of the cavity modes. As noted above, this can be accomplished by making sure only one of the cavity modes possess the right polarization and energy. Fortunately, we can control the allowed cavity mode energies, by adjusting the cavity separation l. The energy of a single cavity mode photon of wavelength λ is

$$E = \frac{hc}{\lambda}. \tag{1.26}$$

In Section 1.2 we found that the possible wavelengths are $\lambda = \frac{2l}{n}$ with $n = 0, 1, \ldots$. Thus the energy difference between two adjacent cavity modes is

$$\Delta E = \frac{hc}{2l}. \tag{1.27}$$

From this expression we conclude that the smaller we make he distance between the cavity mirrors, the larger the energy gap between adjacent modes. It is therefore desirable to make the optical cavity as small as possible, in order to get a strong coupling between the atomic transition and the single mode of interest. Assuming this coupling is sufficiently strong, we may neglect the effect of the other cavity modes.

1.3.1 The Jaynes-Cummings Hamiltonian

Proceeding to determine the dynamics of the Jaynes-Cummings model, we set out to find its Hamiltonian. Complex physical systems are known to put up a good fight when it comes to preserving the secret of their Hamilton function. A common and often useful tactic is to break up complicated systems into smaller and more manageable parts. We will in the following study the atom, the cavity field and the atom-field interaction, analyzing each of them as separate systems, before finally fusing the results to form the total system description.

In the following, let $\hat{H}_A$, $\hat{H}_F$ and $\hat{H}_{AF}$ denote the Hamiltonians of the atom, the field and the atom-field interaction. The total system Hamiltonian is then

$$\hat{H} = \hat{H}_A + \hat{H}_F + \hat{H}_{AF}. \tag{1.28}$$

Let the two active atomic states be noted by $|g\rangle$ and $|x\rangle$, where the former refers to the ground state and latter to an excited state. Further assume that each of the states is accompanied by the respective energies $\hbar\omega_g$ and $\hbar\omega_x$. As a first approximation we will consider the energy levels of the atom to be of infinite lifetime. According to the spectral theorem the corresponding Hamiltonian may then be written

$$\hat{H}_A = \hbar\omega_g |g\rangle \langle g| + \hbar\omega_x |x\rangle \langle x| . \tag{1.29}$$

We will assume the atomic transition in question couples to linearly polarized modes, with polarization vector $\boldsymbol{\epsilon}_{||}$. In the following we will always concern our selves with modes of this polarization, and omit the previous notation using the symbols $||$ and $\perp$. For simplicity we will assume the energy of the lowest cavity mode to be the one close to the energy of the atomic transition. From equation (1.19) the vector potential of the selected cavity mode is then expressed

$$\hat{\mathbf{A}}(z) = \sqrt{\frac{\hbar}{2\omega_k \epsilon_0 V}}\left(\hat{a} + \hat{a}^\dagger\right) \sin kz\, \boldsymbol{\epsilon}, \tag{1.30}$$

where $\hat{a}$ and $\hat{a}^\dagger$ denotes the operators of the chosen mode, and $k = \frac{\pi}{l}$. From (1.18) the field Hamiltonian will be one of a single harmonic oscillator

$$\hat{H}_F = \hbar\omega_k(\hat{a}\hat{a}^\dagger + \frac{1}{2}). \tag{1.31}$$

Finally, we turn to the atom-field interaction. In the subsequent evaluation we will mimic the procedure followed by Leinaas [19]. Assuming that our atom is an alkali atom, an atom with one valence electron, the interaction Hamiltonian in its entirety is

$$\hat{H}_{AF} = -\frac{e}{m}\hat{\mathbf{A}} \cdot \hat{\mathbf{p}} + \frac{e^2}{2m}\hat{\mathbf{A}}^2 - \frac{e}{m}\hat{\mathbf{S}} \cdot \hat{\mathbf{B}}. \tag{1.32}$$

Here $\hat{\mathbf{p}}$ is the electron momentum operator, $\hat{\mathbf{S}}$ is the electron spin operator and $\hat{\mathbf{B}}$ the magnetic field operator. The two first terms are due to charge interactions, describing how the electron charge interacts with the field. To lowest order in perturbation expansion, the first term describes single photon processes, while the second term describes scattering and two-photon processes. The third term is due to the spin interactions between the magnetic dipole moment of the electron and the magnetic field. We will here restrict our selves to processes where only single photons are involved, and assume spin interactions between the electron and the magnetic field to be insignificant. The Hamiltonian describing the interaction of the atom and the electromagnetic field is then

$$\hat{H}_{AF} = -\frac{e}{m}\hat{\mathbf{A}}(z) \cdot \hat{\mathbf{p}}. \tag{1.33}$$

For later convenience we choose to express the interaction Hamiltonian using the basis of the atomic states $\{|g\rangle, |x\rangle\}$. Expanding $\hat{H}_{AF}$ in terms of $|g\rangle$ and $|x\rangle$ gives

$$\hat{H}_{AF} = \sum_{\alpha,\beta \in \{g,x\}} \langle\alpha|\, \hat{H}_{AF}\, |\beta\rangle \langle\beta|\, \alpha\rangle\,. \tag{1.34}$$

We need to calculate the matrix elements $\langle\alpha|\, \hat{H}_{AF}\, |\beta\rangle$ in order to reach an explicit expression for the $\hat{H}_{AF}$. These can be written in a general way as

$$\langle\alpha|\, \hat{H}_{AF}\, |\beta\rangle = -\frac{e}{m}\langle\alpha|\, \hat{\mathbf{A}} \cdot \hat{\mathbf{p}}\, |\beta\rangle = -\frac{e}{m}\sqrt{\frac{\hbar}{2\omega_k \epsilon_0 V}} \sin kz\left(\hat{a} + \hat{a}^\dagger\right)\boldsymbol{\epsilon} \cdot \hat{\mathbf{p}}_{\alpha\beta}, \tag{1.35}$$

with $\hat{\mathbf{p}}_{\alpha\beta} = \langle\alpha|\, \hat{\mathbf{p}}\, |\beta\rangle$.

It is common practice to the express atom-field interaction in terms of the position operator $\hat{\mathbf{r}}$ of the electron. This gives us an interaction Hamiltonian of an electric dipole energy-like form. The first step towards achieving this is expressing the Hamiltonian of the electron in the familiar manner

$$\hat{H}_A = \frac{\hat{p}^2}{2m} + \hat{V}(\mathbf{r}), \tag{1.36}$$

to find the commutation relation

$$[\hat{H}_A, \hat{\mathbf{r}}] = \frac{1}{2m}[\hat{p}^2, \hat{\mathbf{r}}] = \frac{1}{2m}\sum_{j\in\{x,y,z\}}[\hat{p}_j^2, \hat{j}]\mathbf{e}_j = \frac{1}{2m}\sum_{j\in\{x,y,z\}} -2i\hbar\hat{p}_j\mathbf{e}_n = -i\frac{\hbar}{m}\hat{\mathbf{p}}. \tag{1.37}$$

The matrix elements of the momentum operator are accordingly expressed

$$\hat{\mathbf{p}}_{\alpha\beta} = i\frac{m}{\hbar}\langle\alpha|\,\hat{H}_A\hat{\mathbf{r}} - \hat{\mathbf{r}}\hat{H}_A\,|\beta\rangle = i\frac{m}{\hbar}(E_\alpha - E_\beta)\hat{\mathbf{r}}_{\alpha\beta}. \tag{1.38}$$

From relation (1.38) we can rewrite the matrix elements of the interaction Hamiltonian as

$$\begin{aligned}\langle\alpha|\,\hat{H}_{AF}\,|\beta\rangle &= -i\sqrt{\frac{\hbar}{2\omega_k\epsilon_0 V}}\sin kz\Big(\hat{a}+\hat{a}^\dagger\Big)(\omega_\alpha-\omega_\beta)\boldsymbol{\epsilon}\cdot e\hat{\mathbf{r}}_{\alpha\beta}\\ &= -i\sqrt{\frac{\hbar}{2\omega_k\epsilon_0 V}}\sin kz\Big(\hat{a}+\hat{a}^\dagger\Big)\omega_{\alpha\beta}\hat{\mu}_{\alpha\beta}.\end{aligned} \tag{1.39}$$

Where $\omega_{\alpha\beta} = \omega_\alpha - \omega_\beta$ is the frequency gap between the states α and β, and $\mu_{\alpha\beta} = \boldsymbol{\epsilon}\cdot e\hat{\mathbf{r}}_{\alpha\beta}$ is the relevant component of the transition dipole moment. We can now finally express $\hat{H}_{AF}$ in terms of the energy eigenstates of the atom. Observing that $\langle\alpha|\,\hat{H}_I\,|\alpha\rangle = 0$, we get

$$\begin{aligned}\hat{H}_{AF} &= -i\sqrt{\frac{\hbar}{2\omega_k\epsilon_0 V}}\sin kz\Big(\hat{a}+\hat{a}^\dagger\Big)\Big(\omega_{gx}\mu_{gx}\,|g\rangle\langle x| + \omega_{xg}\mu_{xg}\,|x\rangle\langle g|\Big)\\ &= -i\sqrt{\frac{\hbar}{2\omega_k\epsilon_0 V}}\sin kz\Big(\hat{a}+\hat{a}^\dagger\Big)\omega_{xg}\Big(\mu_{xg}\,|x\rangle\langle g| - \mu_{xg}^*\,|g\rangle\langle x|\Big)\\ &= -\sqrt{\frac{\hbar}{2\omega_k\epsilon_0 V}}\sin kz\Big(\hat{a}+\hat{a}^\dagger\Big)\omega_{xg}\,|\mu_{xg}|\Big(e^{i\phi}\,|x\rangle\langle g| - e^{-i\phi}\,|g\rangle\langle x|\Big)\\ &\longrightarrow -\hbar\sqrt{\frac{|\mu_{xg}|^2\omega_{xg}^2}{2\omega_k\epsilon_0 V\hbar}}\sin kz\Big(\hat{a}+\hat{a}^\dagger\Big)\Big(\,|x\rangle\langle g| + |g\rangle\langle x|\,\Big).\end{aligned} \tag{1.40}$$

In the second line we have used that the polarization vector of linearly polarized light is real, $\boldsymbol{\epsilon} = \boldsymbol{\epsilon}^*$, combined with the hermiticity of the position operator, $\hat{\mathbf{r}} = \hat{\mathbf{r}}^\dagger$, to show that $\mu_{\alpha\beta} = \mu_{\beta\alpha}^*$. In the third line we have written μ_{xg} in polar form $\mu_{xg} = |\mu_{xg}|e^{i\phi}$. Attaching a phase factor onto a quantum mechanical state will make no physical changes to the state, since it will not alter the corresponding expectation values of Hermitian operators. We can therefore redefine the excited atomic energy state $|x\rangle \to e^{i\phi}\,|x\rangle$.

From (1.40) we see how the quantity

$$g(z) = g_0 \sin kz, \quad g_0 = \sqrt{\frac{|\mu_{xg}|^2 \omega_{xg}^2}{2\omega_k \epsilon_0 V \hbar}}, \quad k = \frac{\pi}{l}, \tag{1.41}$$

determines the strength of the atom-field interaction as a function of the position of the atom. We will from here on assume the interaction to be maximal, with the atom placed at the center of the optical cavity. That is

$$z = \frac{l}{2} \quad \Rightarrow \quad g(z) = g_0. \tag{1.42}$$

Inserting our findings for each subsystem into the equation for the total Hamiltonian (1.28), we find

$$\hat{H} = \hbar\omega_g |g\rangle \langle g| + \hbar\omega_x |x\rangle \langle x| + \hbar\omega_k(\hat{a}\hat{a}^\dagger + \frac{1}{2}) - \hbar g_0\Big(\hat{a} + \hat{a}^\dagger\Big)\Big(|x\rangle \langle g| + |g\rangle \langle x|\Big). \tag{1.43}$$

Note that while $\hat{a}^\dagger$ and $\hat{a}$ acts as raising and lowering operators of the cavity mode, the operators $|x\rangle \langle g|$ and $|g\rangle \langle x|$ are raising and lowering operators for the atom.

We are closing in on the final expression for the total Jaynes-Cummings Hamiltonian, but there is still one more approximation we can employ. The so-called *Rotating Wave Approximation* is a frequently applied approximation in quantum optics. It applies to atom-field couplings where the field energy is close to one of the atomic energy transitions. The approximation involves neglecting the terms $\hat{a}|g\rangle \langle x|$ and $\hat{a}^\dagger |x\rangle \langle g|$ in the interaction Hamiltonian. This is justified by doing a first order perturbation expansion in the interaction picture, and observing that the contributions to the time evolution from these terms are negligible compared to the contributions from $\hat{a}|x\rangle \langle g|$ and $\hat{a}^\dagger |g\rangle \langle x|$. For a rigorous derivation of the rotating wave approximation, see Appendix A. Within this approach the atom-cavity interaction Hamiltonian is reduced to

$$\hat{H}_{AF} = -\hbar g_0\Big(\hat{a}|x\rangle \langle g| + \hat{a}^\dagger |g\rangle \langle x|\Big). \tag{1.44}$$

With the expression in (1.44) we can finally express the Hamiltonian of the Jaynes-Cummings model

$$\hat{H} = \hbar\omega_g |g\rangle \langle g| + \hbar\omega_x |x\rangle \langle x| + \hbar\omega_k(\hat{a}\hat{a}^\dagger + \frac{1}{2}) - \hbar g_0\Big(\hat{a}|x\rangle \langle g| + \hat{a}^\dagger |g\rangle \langle x|\Big). \tag{1.45}$$

1.3.2 The Jaynes-Cummings Dynamics

To celebrate our recent unveiling of the Jaynes-Cummings Hamiltonian (1.45), we will let it make its first stage appearance. In this subsection we aim to describe the behavior of our atom-cavity system by solving the Hamiltonian eigenvalue problem.

The state space in which the evolution of the Jaynes-Cummings model can be described consists of the tensor product space of the atomic states $|g\rangle$ and $|x\rangle$ and the state space of a single mode of the field. For the mode, the photon number states acts

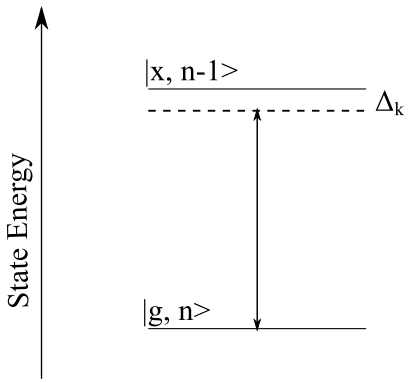

Figure 1.3: Schematic presentation of the Jaynes-Cummings model.

as a natural basis. The photon number states are denoted $|n\rangle$ with $n = 0, 1, ...$, and are also known as Fock states. We will represent the total Hamiltonian by a matrix using the product basis for a given photon number $|g, n\rangle$ and $|x, n-1\rangle$. Calculating the matrix elements of the Jaynes-Cummings Hamiltonian from Equation (1.45) results in the matrix

$$H = \begin{pmatrix} \hbar\omega_k(n+\frac{1}{2}) + \hbar\omega_g & -\hbar g_0\sqrt{n} \\ -\hbar g_0\sqrt{n} & \hbar\omega_k(n-\frac{1}{2}) + \hbar\omega_x \end{pmatrix}. \tag{1.46}$$

The time evolution of the system eigenstates can be found from solving the eigenvalue problem of the Hamilton matrix

$$H\,|\psi\rangle = E\,|\psi\rangle\,, \tag{1.47}$$

with eigenstates $|\psi\rangle$ and eigenvalues E. Solving (1.47) results in the energy eigenvalues

$$E_n^{\pm} = \hbar\omega_k(n+\frac{1}{2}) + \hbar\omega_g + \frac{1}{2}\hbar(\Delta_k \pm \sqrt{4g_0^2 n + \Delta_k^2}), \tag{1.48}$$

where $\Delta_k = \omega_x - \omega_g - \omega_k$ is the detuning between the atom and the cavity field mode. The corresponding energy eigenstates are

$$\left|\psi_n^+\right\rangle = \frac{1}{\sqrt{4g_0^2 n + (\Delta_k + \Omega_{kn})^2}}\Big(2g_0\sqrt{n}\,|g, n\rangle - (\Delta_k + \Omega_{kn})\,|x, n-1\rangle\Big), \tag{1.49}$$

$$\left|\psi_n^-\right\rangle = \frac{1}{\sqrt{4g_0^2 n + (\Delta_k - \Omega_{kn})^2}}\Big(2g_0\sqrt{n}\,|g, n\rangle - (\Delta_k - \Omega_{kn})\,|x, n-1\rangle\Big), \tag{1.50}$$

where

$$\Omega_{kn} = \sqrt{4g_0^2 n + \Delta_k^2}. \tag{1.51}$$

The time evolution operator is given by $\hat{U}(t) = e^{-i\hat{H}t/\hbar}$. Assuming the system is in the state $|\psi(0)\rangle = |x, n-1\rangle$ at time $t = 0$, then at time t the system will be in the state

$$|\psi(t)\rangle = \hat{U}(t)\,|\psi(0)\rangle\,. \tag{1.52}$$

Expressed in terms of the eigenstates the state $|x, n-1\rangle$ is written

$$|\psi(0)\rangle = |x, n-1\rangle = \frac{\sqrt{4g_0^2 n + (\Delta_k - \Omega_{kn})^2}}{2\Omega_{kn}} \Big(\left|\psi_n^-\right\rangle - \left|\psi_n^+\right\rangle \Big), \tag{1.53}$$

and the system state evolution is found to be

$$|\psi(t)\rangle = \frac{\sqrt{4g_0^2 n + (\Delta_k - \Omega_{kn})^2}}{2\Omega_{kn}} \Big(e^{-iE_n^- t/\hbar} \left|\psi_n^-\right\rangle - e^{-iE_n^+ t/\hbar} \left|\psi_n^+\right\rangle \Big). \tag{1.54}$$

The probability of finding the system in the state $|g, n\rangle$ at time t is then

$$\begin{aligned} |c_g(t)|^2 &= |\, \langle g, n|\, \psi(t)\rangle\, |^2 \\ &= \frac{2g_0^2 n}{\Omega_{kn}^2} \Big(1 - \cos\Big(\frac{E_n^+ - E_n^-}{\hbar} t \Big) \Big) \\ &= \frac{2g_0^2 n}{\Omega_{kn}^2} \Big(1 - \cos\Big(\Omega_{kn} t \Big) \Big). \end{aligned} \tag{1.55}$$

And the corresponding probability of finding the system in the state $|x, n-1\rangle$ is of course given by

$$|c_x(t)|^2 = 1 - |c_g(t)|^2. \tag{1.56}$$

The above quantitative story can be put to words in the form of a recipe. Start by taking out your idealized Fabry-Pérot cavity. Pour into it a mixture of $n-1$ perfectly prepared cavity mode photons. Next, choose a two-level atom with an energy transition matching fairly well the cavity mode, and initialize it in its excited state $|x\rangle$. Finish your creation by carefully placing the atom inside the cavity, and stand back to let nature take its course.

Your atom-cavity composition will then be initialized in the state $|x, n-1\rangle$. Due to the arising atom-cavity coupling, energy exchanges between the atom and the cavity field will arise. According to (1.55) and (1.56), the system population will start to oscillate at a frequency Ω_{kn}, between the state $|g, n\rangle$ and the initial state $|x, n-1\rangle$. In $|g, n\rangle$, the atom is in its ground state accompanied by n photons inside the cavity. In $|x, n-1\rangle$ the atom is excited and the cavity hold $n-1$ photons.

Inspecting (1.55) we conclude that the population of the energy level $|g, n\rangle$ is at its maximum when $t = \frac{\pi}{\Omega_{kn}}$, corresponding to

$$|c_g|^2 = \frac{4g_0^2 n}{\Omega_{kn}^2}. \tag{1.57}$$

So for the system to make a full transition from $|x, n-1\rangle$ to $|g, n\rangle$ we must require

$$\frac{4g_0^2 n}{\Omega_{kn}^2} = \frac{4g_0^2 n}{4g_0^2 n + \Delta_k} = 1. \tag{1.58}$$

This gives $\Delta_k = 0$, which means that the energy of the cavity mode photons and the energy transition between the atomic levels must be a perfect match for total transitions

to occur. This phenomenon is known as *Rabi oscillations*. Substituting $\Delta_k = 0$ into (1.48) and (1.51) gives the eigenstate energies

$$E_n^{\pm} = \hbar\omega_k(n + \frac{1}{2}) + \hbar\omega_g \pm \hbar g_0\sqrt{n}, \tag{1.59}$$

and the so called *Rabi frequency*

$$\Omega_{kn} = 2g_0\sqrt{n}. \tag{1.60}$$

Expression (1.59) shows that the energy gap between the system eigenstates broadens as the strength of the atom-field interaction g_0 is increased. From (1.60) We see that the oscillation frequency of the cavity population increases linearly with atom-field interaction strength.

Figure 1.4 displays the population of $|g, n\rangle$ for different values of Δ_k. It is evident that for $\Delta_k \neq 0$, the system state will fluctuate between $|x, n-1\rangle$ and a superposition of the form $c_g |g, n\rangle + c_x |x, n-1\rangle$. These oscillations are known as *effective Rabi oscillations*, and the corresponding frequency Ω_{kn} as the *effective Rabi frequency*.

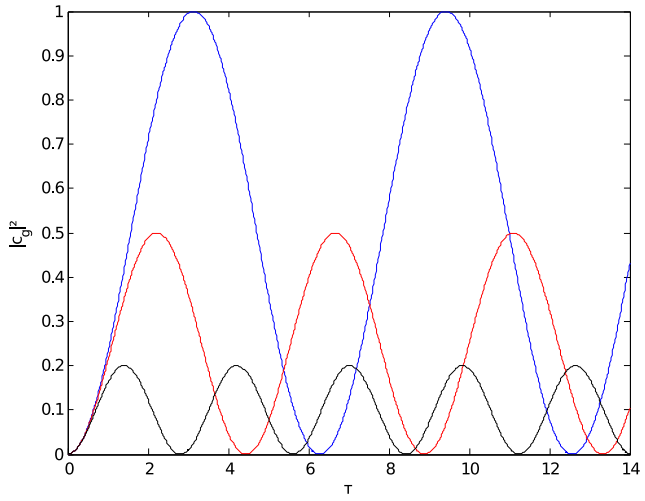

Figure 1.4: Population of the state $|g, n\rangle$ as function of the time parameter $\tau = \zeta t$, where $\zeta = 2g_0\sqrt{n}$. Δ_k is measured in units of ζ. Blue: $\Delta_k = 0$, Red: $\Delta_k = \zeta$, Black: $\Delta_k = 2\zeta$.

We round off Chapter 1 with this demonstration of the essential behavior of the Jaynes-Cummings model. Having pieced together a complete system of a single atom and a collection of photons in perfect union with an optical cavity, we are now slightly more familiar with the concepts of cavity quantum electrodynamics. Yet, it might not be obvious how the Jaynes-Cummings scheme is going to be helpful in regards to producing single photons. The answer to this question is a treat that is saved for the next chapter.

Chapter 2

A Simple Photon Source

In the previous chapter the interaction between single atoms and photons, confined within an optical cavity, was put under the microscope. The cavity, the quantized electromagnetic field and the atom all came beautifully together in the Jaynes-Cummings model. This is in itself an interesting model, because of its simplicity and wide area of applications. However, our underlying motivation for studying the scheme of Jaynes and Cummings is to investigate its properties as a single photon source.

For an atom-cavity system to be able to function as a photon source the cavity must in some way be capable of emitting photons. This means that the cavity mirrors are required to have some degree of transparency, which will eventually cause the cavity photons to leak out. Clearly, our Jaynes-Cummings model will need to be modified in order to come to deal with this new requirement.

Cavity photon emission is an example of interaction between the atom-cavity composition and its environment. It is a form of decay, where energy escapes from the system into its surroundings. In order to include photon emission in our model, we need to understand how to correctly describe the dynamics of decay processes.

Quantum mechanical systems interacting with their environment are often referred to as *open*. In this chapter we will take a first peek into the concept of open quantum systems and a possible realization of a single photon source. The first section will be dedicated to the description of open system dynamics, with an introduction to the density operator and the master equation. We will then move on to the study of a modified Jaynes-Cummings model with decay processes. We will discuss both the models system dynamics and its potential as a single photon source.

2.1 The Density Operator and The Master Equation

A quantum state that can be described by a single vector in a Hilbert space is called a *pure state*. It corresponds to the situation where we have the maximum available information about the system, and the system dynamics is ruled by the Schrödinger equation. For this to be the case the system must be completely isolated, allowing us to keep a detailed track of every part of its machinery.

In real life situations, it is not generally possible to obtain all the information about

a physical system. Perfect isolation exists only in theory, so all real quantum mechanical systems will, to some degree, interact with their environment. Under circumstances where this interaction is significant, the system can no longer be described in a satisfactory way by a pure state, and we are in need of a more general description.

For this purpose the *density operator* is introduced. It is generally defined as

$$\hat{\rho} = \sum_{k=1}^{n} p_k \left|\psi_k\right\rangle \left\langle\psi_k\right|, \tag{2.1}$$

and must satisfy

$$\hat{\rho} = \hat{\rho}^\dagger, \qquad \left\langle\psi\right| \hat{\rho} \left|\psi\right\rangle \geq 0, \qquad \mathrm{Tr}(\hat{\rho}) = 1. \tag{2.2}$$

The density operator portrays the situation of a system being described by an ensemble of state vectors $|\psi_k\rangle$, each associated with a probability p_k. The system is then said to be in a *mixed state*. All the measurable information of a mixed state is contained in the density operator, and the expectation value of an observable represented by an operator $\hat{A}$ is given by

$$\langle A \rangle = \mathrm{Tr}(\hat{\rho}\hat{A}). \tag{2.3}$$

It is easily seen that the pure state is just a special case of a mixed state, with only one state vector $|\psi\rangle$ and corresponding probability $p = 1$.

As previously mentioned, the dynamics of an isolated quantum mechanical system is determined by the Schrödinger equation. An open system on the other hand calls for different measures. The density operator offers a solution to this problem, in situations where the open system can be regarded as part of a larger isolated system.

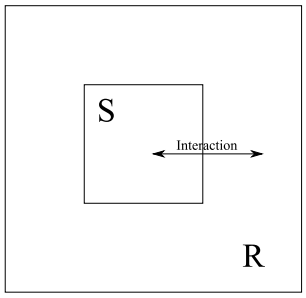

Figure 2.1: Representation of a small open quantum mechanical system $\mathcal{S}$ interacting with a large reservoir $\mathcal{R}$.

Imagine a quantum mechanical set-up composed of two subsystems, the small system of interest $\mathcal{S}$, and a large reservoir $\mathcal{R}$ of infinitely many states (see Figure 2.1). Assuming we know everything there is to know about the total system, it can be described by the

density operator of a pure state $\hat{\rho}$. The reduced density operator of subsystem $\mathcal{S}$ is then found by taking the partial trace with respect to the states of the reservoir

$$\hat{\rho}^{\mathcal{S}} = \mathrm{Tr}_{\mathcal{R}}(\hat{\rho}). \tag{2.4}$$

Since the total system is pure the time evolution of the total density operator is given by the von Neumann equation

$$\frac{d\hat{\rho}}{dt} = -\frac{i}{\hbar}[\hat{H}, \hat{\rho}], \tag{2.5}$$

which follows directly from the Schrödinger equation. The corresponding evolution of subsystem $\mathcal{S}$ is found by tracing out the reservoir degrees of freedom on both sides of (2.5). The resulting equation is called the *master equation* for the reduced density operator $\hat{\rho}^{\mathcal{S}}$.

By making certain approximations we reach the most general form of the master equation of a small quantum system coupled to a Markovian reservoir, the so-called *Lindblad equation*. The complete derivation of the Lindblad equation will not be demonstrated here, but can be found in several literary sources concerning open quantum systems. For an example, see [2]. Here we will only give an account of the key assumptions made on the way to producing it.

Initial separability It is assumed that the total system is initialized such that there are no correlations between the small system and the reservoir, and the total initial density operator can be written on the form

$$\hat{\rho}(0) = \hat{\rho}^{\mathcal{S}}(0) \otimes \hat{\rho}^{\mathcal{R}}(0). \tag{2.6}$$

The Born approximation The environment is assumed not to be significantly affected by the system. This is justified when the reservoir is very large compared to the system, and their interaction is weak. The total density operator at time t can then be approximately expressed

$$\hat{\rho}(t) \approx \hat{\rho}^{\mathcal{S}}(t) \otimes \hat{\rho}^{\mathcal{R}}. \tag{2.7}$$

This does not mean that the reservoir is not affected by the system interaction, but that changes in the reservoir caused by this interaction will die out on a quicker time scale than can be resolved by the Lindblad equation.

The Markov approximation It is assumed that the time evolution of the reduced density operator of the system, depends only on its present state $\hat{\rho}^{\mathcal{S}}(t)$. Let $\tau_{\mathcal{R}}$ be the time scale at which the two-time correlations of the reservoir operators decay, and $\tau_{\mathcal{S}}$ be the time scale at which the system changes appreciably. The above assumption is then valid for

$$\tau_{\mathcal{R}} \ll \tau_{\mathcal{S}}. \tag{2.8}$$

This means that the reservoir has a very short memory as compared to the system of interest.

Implementing these assumptions along with a few others, such as the rotating wave approximation, results in a time evolution described by the Lindblad equation, which reads

$$\begin{aligned}\frac{\partial}{\partial t}\hat{\rho}^{\mathcal{S}} &= -\frac{i}{\hbar}[\hat{H}_{\mathcal{S}}, \hat{\rho}^{\mathcal{S}}] + \hat{\mathcal{L}}\hat{\rho}^{\mathcal{S}}, \\ \hat{\mathcal{L}}\hat{\rho}^{\mathcal{S}} &= \sum_i \gamma_i (2\hat{\alpha}_i \hat{\rho}^{\mathcal{S}} \hat{\alpha}_i^\dagger - \hat{\alpha}_i^\dagger \hat{\alpha}_i \hat{\rho}^{\mathcal{S}} - \hat{\rho}^{\mathcal{S}} \hat{\alpha}_i^\dagger \hat{\alpha}_i). \end{aligned} \tag{2.9}$$

Here $\hat{H}_{\mathcal{S}}$ is the Hamiltonian of the system $\mathcal{S}$. The γ_i are non-negative quantities, given by correlation functions of the reservoir. They are associated with the decay rates of the different decay processes, referred to as decay channels, of the open system. $\hat{\alpha}_i$ and $\hat{\alpha}_i^\dagger$ are the Lindblad superoperators through which the system couples to the environment. They describe the system transitions caused by the system-reservoir interaction. When a system evolves according to the Schrödinger equation it is said to evolve coherently. This means that no information about the system is lost during its evolution. Transitions induced by the environment are a type of evolution that do cause loss of information. These transitions are therefore often referred to as incoherent transitions.

For our purposes it will be convenient to rewrite the Lindblad equation in a slightly different form. By defining the effective Hamiltonian $\hat{H}_{\text{eff}}$ and the so called jump superoperator $\hat{\mathcal{L}}_j$

$$\hat{H}_{\text{eff}} = \hat{H}_S - i\hbar \sum_i \gamma_i \hat{\alpha}_i^\dagger \hat{\alpha}_i, \tag{2.10}$$

$$\hat{\mathcal{L}}_j \hat{\rho}^S = \sum_i 2\gamma_i \hat{\alpha}_i \hat{\rho}^S \hat{\alpha}_i^\dagger, \tag{2.11}$$

we can formulate the master equation as

$$\frac{\partial}{\partial t}\hat{\rho}^S = -\frac{i}{\hbar}(\hat{H}_{\text{eff}}\hat{\rho}^S - \hat{\rho}^S \hat{H}_{\text{eff}}^\dagger) + \hat{\mathcal{L}}_j \hat{\rho}^S. \tag{2.12}$$

The term jump superoperator refers to $\hat{\mathcal{L}}_j$ being a linear operator acting on other operators. The reason for the designation jump will become evident when we return to the master equation in Chapter 4.

Writing the Lindblad equation in the latter form reveals an interesting opportunity for simplifying our description of the system dynamics. By closer inspection of (2.12) we recognize that dropping the last term involving the jump superoperator would result in a von Neumann-like equation. This equation is equivalent with the one we would get by replacing $\hat{H}$ with $\hat{H}_{\text{eff}}$ in the Schrödinger equation. If we could argue that the last term of (2.12) is insignificant, the dynamical equation of interest would be reduced to a slightly modified Schrödinger equation. In the light of the resulting effort savings of such a simplification, spending the remaining of this section examining this possibility seems well justified. This simplification would save a great deal of effort, and is therefore well worth studying.

It seems that the evolution described by the Lindblad equation in (2.12), can be understood as a combination of two different processes. One is the evolution governed by

the modified Schrödinger equation, with $\hat{H}_{\text{eff}}$, given by the bracket-term. This describes a system evolving in a similar fashion to the evolution that is found from the standard Schrödinger equation, while the populations of the decaying states dissipate at exponential rates. The other process is the one accounted for by the jump superoperator term. This term takes care of the population that has leaked out due to decay processes, and redistributes it to its rightful states, keeping the trace of the density operator $\hat{\rho}^{\mathcal{S}}$ equal to one.

We will here attempt to demonstrate the effect of the jump superoperator on the system behavior, through a general example. As previously mentioned, the Lindblad operators describe the state transitions of the system, caused by its interaction with the environment. Suppose now that we have a system that through influence from its environment is caused to decay from the state $|\chi\rangle$ to another state $|\phi\rangle$, at a rate γ_χ. The corresponding Lindblad operator of this decay channel would be

$$\hat{\alpha} = |\phi\rangle \langle\chi| \,, \tag{2.13}$$

which will contribute with the term

$$2\gamma_\chi \rho^{\mathcal{S}}_{\chi\chi} |\phi\rangle \langle\phi| \,, \quad \rho^{\mathcal{S}}_{\chi\chi} = \langle\chi| \hat{\rho}^{\mathcal{S}} |\chi\rangle \,, \tag{2.14}$$

in the jump superoperator.

In Section 2.2.2, it will be demonstrated that the population $|c_\chi|^2 = \rho^{\mathcal{S}}_{\chi\chi}$ of state $|\chi\rangle$ will change at a rate $2\gamma_\chi \rho^{\mathcal{S}}_{\chi\chi}$, due to dissipation through a decay channel with an associated decay rate γ_χ. From (2.14) it is then evident that the jump superoperator takes an amount of probability, which is exactly the amount that is lost to decay from the state $|\chi\rangle$, and places it in the state $|\phi\rangle$, where it belongs.

Now, if $|\phi\rangle$ is coupled to other states through the effective Hamiltonian, the term in (2.14) makes an important difference to the evolution of the system. It redistributes population that will continue to actively participate in new state transitions, even after it has been through a decaying process. On the other hand, if the state $|\phi\rangle$ is not coupled to any other states through $\hat{H}_{\text{eff}}$, the population that is placed in $|\phi\rangle$ will be stuck there throughout the remaining evolution. The only function of the term in (2.14) is then to preserve the system probability. From this we conclude that we can safely drop some of the terms from the jump superoperator. These are the terms associated with transitions to system states that $\hat{H}_{\text{eff}}$ does not couple to other states.

As long as we consider systems that do not allow incoherent transitions to states that are affected by $\hat{H}_{\text{eff}}$, the dynamics can be described in an exact way using the effective Schrödinger equation

$$i\hbar \frac{d}{dt} |\psi(t)\rangle = \hat{H}_{\text{eff}} |\psi(t)\rangle \,. \tag{2.15}$$

It is easily seen that the effective Hamiltonian $\hat{H}_{\text{eff}}$ in (2.10) is not Hermitian, and thus can not provide a unitary time evolution. This will result in an apparent violation of the conservation of the system probability, in the sense that the squared system state norm, $\langle\psi(t)|\, \psi(t)\rangle$, will be less than one as time goes by. As long as we keep this in mind, non-hermiticity should cause no further problems.

2.2 The Jaynes-Cummings Model with Decay

With the Lindblad equation (2.12) we are now properly equipped for upgrading the Jaynes-Cummings model. We proceed to incorporate the necessary decay processes to transform our present system into a potential photon source. In the following we will take into account the decay of the cavity mode through the cavity mirrors, enabling photon emission. In addition we will take into account that the excited state of the atom will have a finite lifetime, which may cause the atom to emit photons into non-cavity modes. These are modes with polarization perpendicular to the polarization of the cavity mode. We will open this section by formulating and solving the dynamical equation accounting for these new features in the language of the Lindblad formalism.

2.2.1 Working Out the Dynamics

Consider once again the Jaynes-Cummings system described in Chapter 1. The system consists of an atom inside an optical cavity. Two atomic energy levels, $|g\rangle$ and $|x\rangle$, interact with the lowest cavity mode. We have previously used $\{|g,n\rangle, |x,n-1\rangle\}$ as basis to describe the evolution of the Jaynes-Cummings model. As we are now mainly interested in the systems ability to manipulate and emit single photons, it seem natural to choose $n = 1$ for the following discussion. In this section we will work in the basis $\{|g,1\rangle, |x,0\rangle\}$.

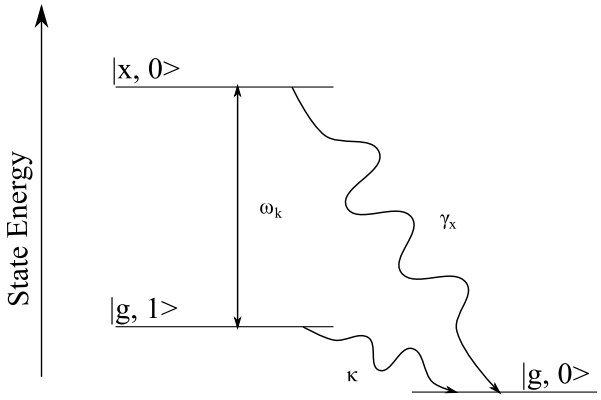

Figure 2.2: Schematic presentation of the Jaynes-Cummings model with decaying excited atomic state and cavity mode. Here the rippled arrow represents transitions caused by incoherent interactions with the environment, while the straight arrows represents coherent transitions.

Taking into account the finite lifetime of the excited atomic state and the photon leakage from the cavity, the system has two decay channels. Let us take a moment to determine their respective Lindblad operators, which should describe the state transitions for each decay channel. Starting with the atomic decay, we imagine the system is in the state in which the atom is excited, $|x,0\rangle$. Emission of a non-cavity photon

would result in a situation with the atom in its ground state inside an empty cavity, corresponding to $|g,0\rangle$. So the Lindblad operator representing this process is

$$\alpha_{xg} = |g,0\rangle \langle x,0| . \tag{2.16}$$

We continue with the decay of the cavity mode, starting with the system state in which the cavity contains a photon, $|g,1\rangle$. When the photon escapes, the resulting system state will equal the result of atomic decay, with the atom in its ground state inside an empty cavity. This gives the Lindblad operator

$$\alpha_{10} = |g,0\rangle \langle g,1| , \tag{2.17}$$

describing cavity photon emission.

Let γ_x be the decay rate of the excited state and κ be the rate at which photons leak out from the cavity. From (2.10) the effective Hamiltonian of the system then reads

$$\hat{H} = \hat{H}_{\mathcal{S}} - i\hbar\gamma_x |x,0\rangle \langle x,0| - i\hbar\kappa |g,1\rangle \langle g,1| . \tag{2.18}$$

$\hat{H}_{\mathcal{S}}$ being the plain Jaynes-Cummings Hamiltonian in (1.45).

The situation is schematically depicted in Figure 2.2. The state $|g,0\rangle$, which is the resulting state for both of the included decay channels, is not accounted for by the effective Hamiltonian describing our atom-cavity composition. According to our argumentation in the previous section, the system evolution can then be described in a satisfactory way by introducing an effective Hamilton operator into the Schrödinger equation (2.15). Consequently, once we have the explicit expression for the effective Hamiltonian, we can once again expose the atom-cavity behavior by solving the Hamiltonian eigenvalue problem.

Now expressing the total Hamiltonian using the states $|g,1\rangle$ and $|x,0\rangle$ as basis gives

$$H = \begin{pmatrix} \frac{3}{2}\hbar\omega_k + \hbar\omega_g - i\hbar\kappa & -\hbar g_0 \\ -\hbar g_0 & \frac{1}{2}\hbar\omega_k + \hbar\omega_x - i\hbar\gamma_x \end{pmatrix} . \tag{2.19}$$

For the sake of simplicity we will assume the cavity mode to be tuned perfectly with the energy transition between the levels of the atom, so $\omega_k = \omega_x - \omega_g$. Defining the constant $E_0 = \frac{3}{2}\hbar\omega_k + \hbar\omega_g$ and observing that $\omega_x = \omega_k + \omega_g$, simplifies the Hamiltonian to

$$H = \begin{pmatrix} E_0 - i\hbar\kappa & -\hbar g_0 \\ -\hbar g_0 & E_0 - i\hbar\gamma_x \end{pmatrix} = \begin{pmatrix} -i\hbar\kappa & -\hbar g_0 \\ -\hbar g_0 & -i\hbar\gamma_x \end{pmatrix} + E_0\mathbb{I} = A + E_0\mathbb{I}. \tag{2.20}$$

In order to find the time evolution of the system eigenstates we proceed to solve the Hamiltonian eigenvalue problem. We can find the eigenvalues of the total matrix by first identifying the eigenvalues of the matrix A, and then adding E_0. The eigenvalue equation of the matrix A reads

$$\lambda^2 + i\hbar(\kappa + \gamma_x)\lambda - \hbar^2(\kappa\gamma_x + g_0^2) = 0.$$

Solving the equation for λ yields

$$\lambda_\pm = \frac{\hbar}{2}\Big(- i(\kappa+\gamma_x) \pm \sqrt{4g_0^2 - (\kappa-\gamma_x)^2}\Big). \tag{2.21}$$

The energies of the eigenstates are then

$$E_\pm = E_0 + \lambda_\pm, \tag{2.22}$$

with corresponding eigenstates

$$|\psi_-\rangle = \frac{1}{\sqrt{\hbar^2 g_0^2 + |i\hbar\kappa + \lambda_-|^2}}\Big(\hbar g_0 |g,1\rangle - (i\hbar\kappa+\lambda_-)|x,0\rangle\Big), \tag{2.23}$$

$$|\psi_+\rangle = \frac{1}{\sqrt{\hbar^2 g_0^2 + |i\hbar\kappa + \lambda_-|^2}}\Big(\hbar g_0 |g,1\rangle - (i\hbar\kappa+\lambda_+)|x,0\rangle\Big). \tag{2.24}$$

Simple calculations show that $|i\hbar\kappa+\lambda_-|^2 = |i\hbar\kappa+\lambda_+|^2$. For convenience we therefore express the normalization factors of both $|\psi_+\rangle$ and $|\psi_-\rangle$ with λ_-.

We will assume the system starts out with an excited atom inside an empty cavity, which correspond to the state $|x,0\rangle$. Expressing the initial state $|x,0\rangle$ in terms of the eigenstates gives

$$|x,0\rangle = \frac{\sqrt{\hbar^2 g_0^2 + |i\hbar\kappa+\lambda_-|^2}}{\lambda_+ - \lambda_-}\Big(|\psi_-\rangle - |\psi_+\rangle\Big). \tag{2.25}$$

Once again the time evolution operator $\hat{U}(t) = e^{-i\hat{H}t/\hbar}$ determines the systems time evolution

$$|\psi(t)\rangle = \hat{U}|x,0\rangle = \frac{\sqrt{\hbar^2 g_0^2 + |i\hbar\kappa+\lambda_-|^2}}{\lambda_+ - \lambda_-}\Big(e^{-iE_-t/\hbar}|\psi_-\rangle - e^{-iE_+t/\hbar}|\psi_+\rangle\Big). \tag{2.26}$$

Finally writing the eigenstates in terms of $|g,1\rangle$ and $|x,0\rangle$ results in

$$\begin{aligned}|\psi(t)\rangle =& \frac{1}{\lambda_+-\lambda_-}\Big(\hbar g_0(e^{-iE_-t/\hbar} - e^{-iE_+t/\hbar})|g,1\rangle \\ &+ ((i\hbar\kappa+\lambda_+)e^{-iE_+t/\hbar} - (i\hbar\kappa+\lambda_-)e^{-iE_-t/\hbar})|x,0\rangle\Big).\end{aligned} \tag{2.27}$$

The probabilities of finding the system in either of the states $|g,1\rangle$ and $|x,0\rangle$ at time t are then

$$\begin{aligned}|c_g|^2 = |\langle g,1|\psi(t)\rangle|^2 &= \Big|\frac{\hbar g_0}{\lambda_+-\lambda_-}(e^{-iE_-t/\hbar} - e^{-iE_+t/\hbar})\Big|^2 \\ &= \frac{\hbar^2 g_0^2}{|\lambda_+-\lambda_-|^2}\Big(e^{-i(\lambda_- - \lambda_-^*)t/\hbar} - e^{i(\lambda_+^*-\lambda_-)t/\hbar)} - e^{-i(\lambda_+-\lambda_-^*)t/\hbar} + e^{-i(\lambda_+-\lambda_+^*)t/\hbar}\Big),\end{aligned} \tag{2.28}$$

$$\begin{aligned}|c_x|^2 = |\langle x,0|\psi(t)\rangle|^2 &= \Big|\frac{1}{\lambda_+-\lambda_-}((i\hbar\kappa+\lambda_+)e^{-iE_+t/\hbar} - (i\hbar\kappa+\lambda_-)e^{-iE_-t/\hbar})\Big|^2 \\ &= \frac{1}{|\lambda_+-\lambda_-|^2}\Big(|i\hbar\kappa+\lambda_+|^2 e^{-i(\lambda_+-\lambda_+^*)t/\hbar} - 2Re\Big((i\hbar\kappa+\lambda_+)(i\hbar\kappa+\lambda_-)^* e^{-i(\lambda_+-\lambda_-^*)t/\hbar}\Big) \\ &+ |i\hbar\kappa+\lambda_-|^2 e^{-i(\lambda_- - \lambda_-^*)t/\hbar}\Big).\end{aligned} \tag{2.29}$$

Note that since our Hamiltonian is not Hermitian, probability is not conserved during time evolution, so $|c_x|^2 \neq 1 - |c_g|^2$, as was the case for the plain Jaynes-Cummings system in Chapter 1. From here on our calculations will depend on the sign of $4g_0^2 - (\kappa - \gamma_x)^2$.

For $4g_0^2 - (\kappa - \gamma_x)^2 < 0$ the eigenvalues $\lambda_\pm$ will be purely imaginary

$$\lambda_\pm = i\frac{\hbar}{2}\Big(- (\kappa + \gamma_x) \pm \sqrt{(\kappa - \gamma_x)^2 - 4g_0^2}\Big). \tag{2.30}$$

The corresponding state probabilities are

$$|c_g|^2 = \frac{2g_0^2}{(\kappa - \gamma_x)^2 - 4g_0^2} e^{-(\kappa+\gamma_x)t}\Big(\cosh\Big(\sqrt{(\kappa - \gamma_x)^2 - 4g_0^2}t\Big) - 1\Big), \tag{2.31}$$

and

$$\begin{aligned} |c_x|^2 = \frac{1}{(\kappa - \gamma_x)^2 - 4g_0^2} e^{-(\kappa+\gamma_x)t}\Big(&((\kappa - \gamma_x)^2 - 2g_0^2)\cosh\Big(\sqrt{(\kappa - \gamma_x)^2 - 4g_0^2}t\Big) \\ &+ \frac{1}{2}(\kappa - \gamma_x)\sqrt{(\kappa - \gamma_x)^2 - 4g_0^2}\sinh\Big(\sqrt{(\kappa - \gamma_x)^2 - 4g_0^2}t\Big) - 2g_0^2\Big). \end{aligned} \tag{2.32}$$

For $4g_0^2 - (\kappa - \gamma_x)^2 > 0$ the $\lambda_\pm$ will have both a real and an imaginary part

$$\lambda_\pm = \frac{\hbar}{2}\Big(- i(\kappa + \gamma_x) \pm \sqrt{4g_0^2 - (\kappa - \gamma_x)^2}\Big). \tag{2.33}$$

Leading to the state probabilities

$$|c_g|^2 = \frac{2g_0^2}{4g_0^2 - (\kappa - \gamma_x)^2} e^{-(\kappa+\gamma_x)t}\Big(1 - \cos\Big(\sqrt{4g_0^2 - (\kappa - \gamma_x)^2}t\Big)\Big), \tag{2.34}$$

and

$$|c_x|^2 = \frac{1}{4g_0^2 - (\kappa - \gamma_x)^2} e^{-(\kappa+\gamma_x)t}\Big(2g_0^2 + (2g_0^2 - (\kappa - \gamma_x)^2)\cos\Big(\sqrt{4g_0^2 - (\kappa - \gamma_x)^2}t\Big) \tag{2.35}$$

$$+ (\kappa - \gamma_x)\sqrt{4g_0^2 - (\kappa - \gamma_x)^2}\sin\Big(\sqrt{4g_0^2 - (\kappa - \gamma_x)^2}t\Big)\Big). \tag{2.36}$$

Figure 2.3 shows the state populations of $|g, 1\rangle$ and $|x, 0\rangle$ as functions of time, with each of the parameter ranges, $4g_0^2 - (\kappa - \gamma_x)^2 < 0$ and $4g_0^2 - (\kappa - \gamma_x)^2 > 0$, represented in a subfigure. Figure 2.3(a) displays the behavior of a so called over damped system, with $4g_0^2 - (\kappa - \gamma_x)^2 < 0$. We observe that the oscillatory behavior of the state populations from Section 1.3.2 is suppressed. This describes the situation in which the decay of the

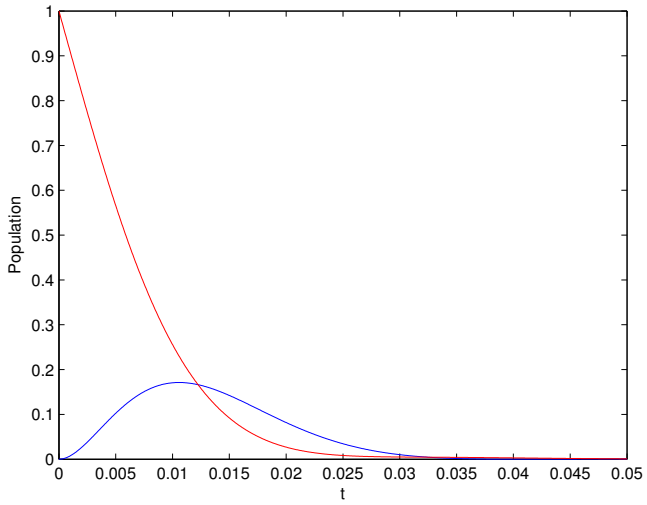

(a) Overdamped system evolution with $\delta = 4g_0^2 - (\kappa - \gamma_x)^2 < 0$ and parameter values $\{g_0, \kappa, \gamma_x\} = 2\pi \times \{15, 20, 3\}$.

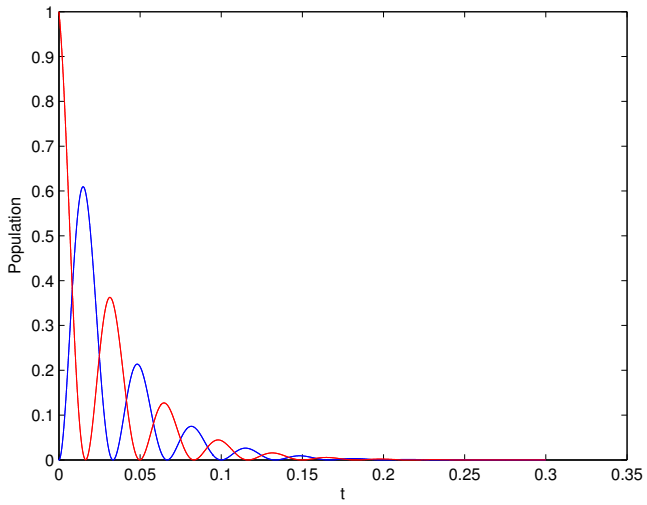

(b) Damped system evolution with $\delta = 4g_0^2 - (\kappa - \gamma_x)^2 > 0$ and parameter values $\{g_0, \kappa, \gamma_x\} = 2\pi \times \{15, 2, 3\}$.

Figure 2.3: The figures show the behavior of the state populations $|c_g|^2$(blue) and $|c_x|^2$(red), in the case of an (a) over damped and (b) damped cavity. The time is given in units of μs, and the atom-field coupling g_0 and the decay rates γ and κ are measured in MHz.

cavity field κ is so fast, that once the atom has de-excited and released a photon into the cavity, it will not have the time to reabsorb it before it escapes entirely. Figure 2.3(b) exhibits the behavior of a system referred to as damped, with $4g_0^2 - (\kappa - \gamma_x)^2 > 0$. Here the atom-field coupling is relatively strong, which causes the Rabi oscillations to occur at a faster rate than the cavity mode decay. This results in the atom having time to

release and reabsorb a photon several times before it is emitted from the cavity, causing the familiar Rabi oscillation of the state population. In both plots the population of $|g,1\rangle$ and $|x,0\rangle$ approaching zero reflect the increasing probability of the cavity having emitted a photon.

2.2.2 The Photon Emission Probability

Imagine being the proud owner a newly purchased, state-of-the-art single photon source. Initiating it according to the pertaining manual you will of course be interested in knowing with what certainty you can actually expect to receive a photon. For most applications the ideal photon source is a deterministic one, which is able to produce a photon on demand with probability close to one. The total emission probability is thus an important characteristic of any single photon source, to which we will devote this subsection.

For cavity-based photon sources a successful photon emission occurs when a cavity photon escapes through one of the cavity walls. This transmission process can only take place whenever there is a photon inside the cavity. In our notation this corresponds to the system being in the state $|g,1\rangle$. To identify the emission rate of our two-level atom-cavity system we examine how the cavity field changes when isolating the effect of decay through the cavity walls. We will thus assume the system starts out in the state $|g,1\rangle$, with no probability of making a transition to the state$|x,0\rangle$. Within the Lindblad formalism lie the assumption that all decaying processes leads to an exponential decay of the dissipating state in question. This means that

$$\tilde{c}_g(t) = \tilde{c}_g(0)e^{-\kappa t}, \tag{2.37}$$

where $\tilde{c}_g$ denotes the coefficient of $|g,1\rangle$, without probability of transition to $|x,0\rangle$. The population of the state will then be given by

$$|\tilde{c}_g(t)|^2 = |\tilde{c}_g(0)|^2 e^{-2\kappa t}. \tag{2.38}$$

The transmission rate is found by taking the derivative of the population

$$\frac{d}{dt}|\tilde{c}_g(t)|^2 = -2\kappa|\tilde{c}_g(t)|^2. \tag{2.39}$$

Now taking the probability of atomic transitions into account, $\tilde{c}_g(t)$ is traded for $c_g(t)$, and the modification in the population of $|g,1\rangle$ due to cavity decay is

$$R(t) = -2\kappa|c_g(t)|^2. \tag{2.40}$$

From integrating the absolute value of (2.40) we finally get the cumulative emission probability at time t

$$P_{\text{emit}}(t) = \int_0^t |R(t)|dt, \tag{2.41}$$

and the total emission probability

$$P_{\text{emit}}^{\text{tot}} = \int_0^\infty |R(t)|dt, \tag{2.42}$$

assuming $t \in [0, \infty]$.

The absolute value of the emission rate $|R(t)|$ describes the probability of detecting a photon outside the cavity as a function of time, assuming we have an ideal detector. The resemblance between $|R(t)|$ and the familiar concept of a particle wavefunction is striking. One should however be extremely careful when drawing parallels between massive particles and photons. The existence of a single photon wavefunction is an intricate and highly disputed subject [25], which we will not dive into the depths of here. Nevertheless, $|R(t)|$ gives a useful description of the temporal qualities associated with our cavity emitted photons. To avoid confusion we will in the following refer to $|R(t)|$ as the photon profile or the temporal shape of the photon, rather than using the term wavefunction. Figure 2.4 displays the photon profiles accompanying the system evolutions in Figures 2.3(a) - 2.3(b) respectively.

If it had not been for the finite decay rate γ_x of the excited atomic state, the outcome of initializing our single photon source would be a successful emission of a cavity photon, with probability $P^{\text{tot}}_{\text{emit}} = 1$. As will be presented in a more detailed manner in Section2.2.3, the decay rate of an excited atom relies mainly on what electromagnetic modes are available for interaction. The effect of emission into non-cavity modes could in principle be prohibited, by totally isolating the atom from available modes. This is however not achievable in practice, as it would also inhibit necessary interactions between the inside of the cavity and its environment, such as an initiating mechanism for the photon production and the laser trap keeping the position of the atom fixed.

From (2.31) and (2.34) we can write out the total emission probability in its entirety

$$P^{\text{tot}}_{\text{emit}}(\kappa) = \frac{4\kappa g_0^2}{4g_0^2 - (\kappa - \gamma_x)^2} \begin{cases} \int_0^\infty e^{-(\kappa+\gamma_x)t}\Big(1 - \cos\Big(\sqrt{4g_0^2 - (\kappa-\gamma_x)^2}t\Big)\Big)dt, & 4g_0^2 - (\kappa-\gamma_x)^2 > 0. \\ \int_0^\infty e^{-(\kappa+\gamma_x)t}\Big(1 - \cosh\Big(\sqrt{(\kappa-\gamma_x)^2 - 4g_0^2}t\Big)\Big)dt, & 4g_0^2(\kappa-\gamma_x)^2 < 0. \end{cases} \tag{2.43}$$

Evaluating the integrals in (2.43) we find that they are equal, and given by

$$I = \frac{4g_0^2 - (\kappa - \gamma_x)^2}{(\kappa + \gamma_x)(4g_0^2 + 4\kappa\gamma_x)}. \tag{2.44}$$

For $4g_0^2 - (\kappa - \gamma_x)^2 \neq 0$ this results in

$$P^{\text{tot}}_{\text{emit}}(\kappa) = \frac{\kappa g_0^2}{(\kappa + \gamma_x)(g_0^2 + \kappa\gamma_x)}. \tag{2.45}$$

Figure 2.5 shows the total emission probability $P^{\text{tot}}_{\text{emit}}$ as a function of the cavity decay rate κ, for selected values of atomic decay rate γ_x and coupling strength g_0. In Figure 2.5(a) the total emission $P^{\text{tot}}_{\text{emit}}(\kappa)$ is shown for different values of atomic decay rate γ_x. We observe how the emission probability is lowered as γ_x is increased, just as one might expect from (2.45). We also note that the maximum emission probability is reached when $\kappa = g_0$. Figure 2.5(b) demonstrates that this appears to be a general tendency.

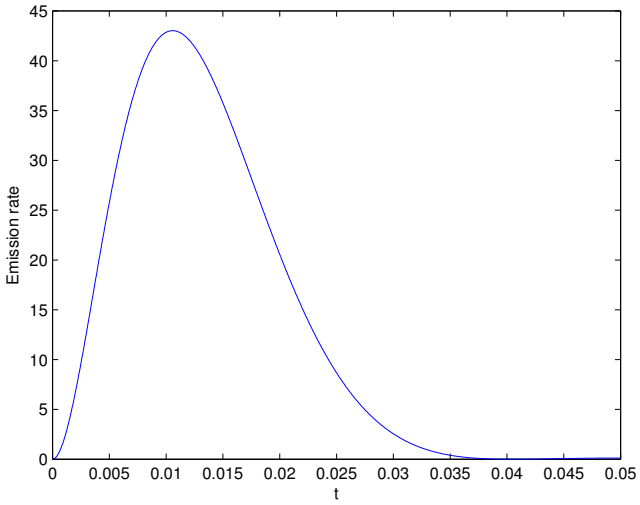

(a) The photon profile resulting from the atom-cavity evolution of Figure 2.3(a), with a corresponding total emission probability $P_{\text{emit}}^{\text{tot}} = 0.68$.

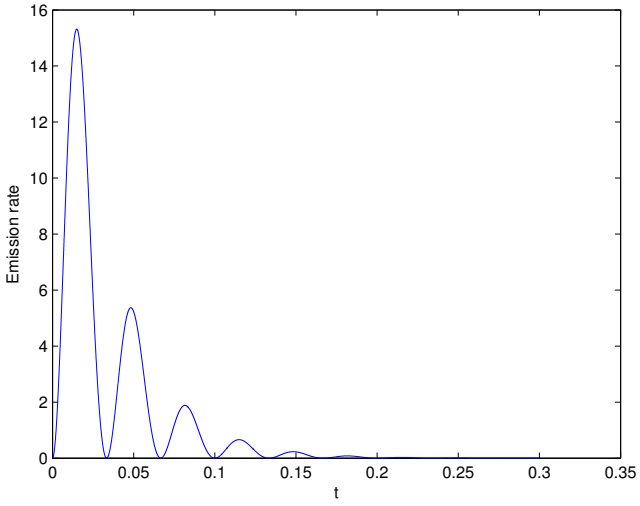

(b) The photon profile resulting from the atom-cavity evolution of Figure 2.3(b), with a corresponding total emission probability $P_{\text{emit}}^{\text{tot}} = 0.39$.

Figure 2.4: The figures show the resulting temporal photon profiles for the cases of over damped and damped system evolution. Time is given in units of μs.

We clearly see how the peak of $P_{\text{emit}}^{\text{tot}}(\kappa)$ is moving as the value of g_0 is changed, keeping in place at $\kappa = g_0$.

Differentiating (2.45) we find the critical κ_c giving the extreme values of the emission

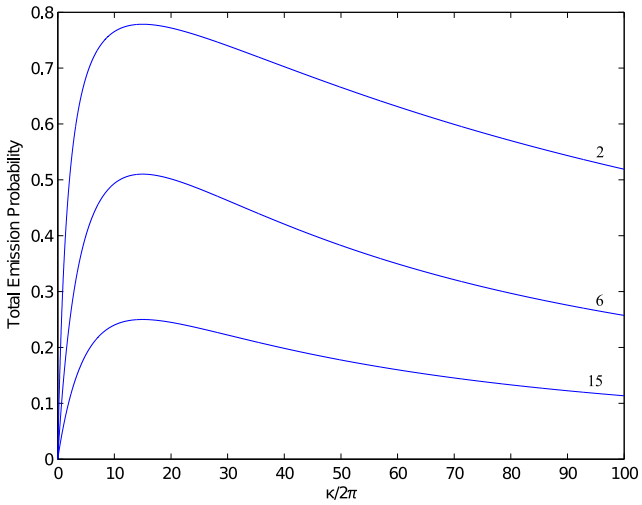

(a) Results for $P^{\text{tot}}_{\text{emit}}(\kappa)$ from varying $\gamma_x = 2\pi \times \{2, 6, 15\}$ as indicated in the figure, while $g_0 = 2\pi \times 15$ is kept constant.

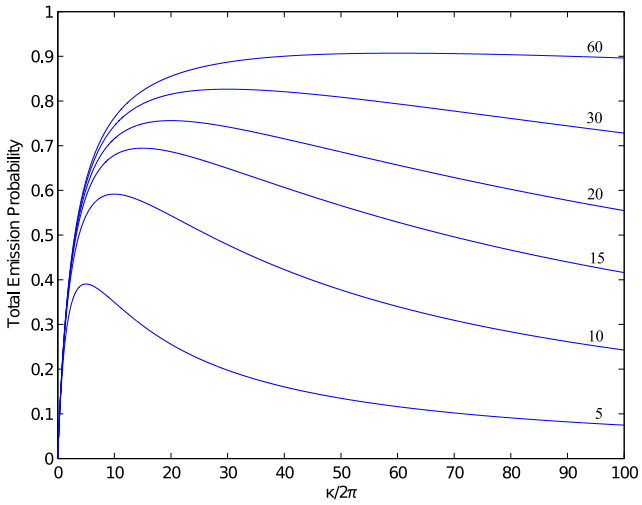

(b) Results for $P^{\text{tot}}_{\text{emit}}(\kappa)$ from varying $g_0 = 2\pi \times \{5, 10, 15, 20, 30, 60\}$ as indicated in the figure, while $\gamma_x = 2\pi \times 3$ is kept constant.

Figure 2.5: The plots show the total emission probability as function of cavity decay rate κ, from varying first the atomic decay rate γ_x and then the strength of the atom-field interaction g_0. g_0, κ and γ_x are given in units of MHz.

probability

$$\left(\frac{\partial}{\partial\kappa}P^{\text{tot}}_{\text{emit}}\right)_{\kappa=\kappa_c} = \frac{g_0^2\gamma_x(g_0^2-\kappa_c^2)}{(\kappa_c+\gamma_x)^2(g_0^2+\kappa_c\gamma_x)^2} = 0 \quad \Rightarrow \quad \kappa_c = \pm g_0. \tag{2.46}$$

The outcome in (2.46) confirms our previous observation. The total emission probability

is maximal when the cavity decay equals the atom-cavity coupling.

More qualitatively, this behavior might be explained by reviewing the results in Section 1.3 on the Jaynes-Cummings model without decay. There we found that the Rabi frequency associated with the system making a complete transition from $|x,0\rangle$ to $|g,1\rangle$ is given by $\Omega_R = 2g_0$. So the time it takes to transfer all the population in $|x,1\rangle$ to $|g,1\rangle$ is about $(2g_0)^{-1}$. We also know that the average lifetime of a cavity photon, and thus the state $|g,1\rangle$, is $(2\kappa)^{-1}$. When these time intervals coincide these two processes are seemingly balancing each other. The population flow from state $|x,0\rangle$ feeds the decaying photon state, at a rate such that the cavity leakage is optimal.

There are situations in which the total emission probability is not the most important success criterion of a photon source. In some cases it could, for instance, be more important for the photon to arrive precisely, than for the total emission probability to be as large as possible. The plot shown in Figure 2.6 indicates that increasing κ slightly, on the expense of the emission probability, results in a more precisely peaked photon profile. This demonstrates that the choice of optimal parameters will depend on what photon specifications we are asking for.

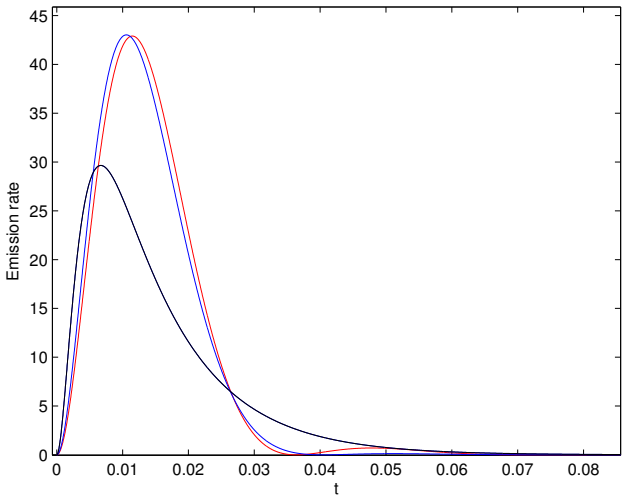

Figure 2.6: Results for the temporal photon profile with parameter values $\{g_0, \gamma_x\} = 2\pi \times \{15, 3\}$, $\kappa = 2\pi \times \{15, 20, 60\}$, in red, blue and black respectively. g_0, γ_x and κ are given in units of MHz, and time is measured in μs.

2.2.3 Cavity Enhanced Emission in the Bad Cavity limit

When the optical cavity was introduced, early in Chapter 1, it was implied that our main reason for resorting to optical cavities is their ability to enhance the interaction between light and matter. Herein lies the atoms ability to emit photons into the electromagnetic mode of our interest.

It has been known for quite some time that the spontaneous emission rate of an excited atom is greatly influenced by its surroundings. Consequently, providing our atom

with the comforts of an optical cavity will affect its emission rate. In the so-called bad cavity limit we are able to find an easily analyzable expression for the emission rate. In this section we will justify and apply the bad cavity limit approximation.

In the previous calculations we have found the system dynamics by solving the energy eigenvalue problem of the Hamiltonian. However, the eigenvalue problem is just an alternative formulation of the time dependent Schödinger equation. It turns out that the Schrödinger coefficients offers a convenient way to implement the bad cavity limit, so we will now turn to look at the atom-cavity system in this notation. After shifting the energy, making $E_0 = \frac{3}{2}\hbar\omega_k + \hbar\omega_g$ the zero energy reference the Schrödinger equation reads

$$\begin{aligned} i\hbar\frac{\partial}{\partial t}|\psi\rangle &= H_T|\psi\rangle \quad \Rightarrow \\ i\hbar\frac{d}{dt}\begin{pmatrix} c_g \\ c_x \end{pmatrix} &= \begin{pmatrix} -i\hbar\kappa & -\hbar g_0 \\ -\hbar g_0 & -i\hbar\gamma_x \end{pmatrix}\begin{pmatrix} c_g \\ c_x \end{pmatrix}. \end{aligned} \tag{2.47}$$

Resulting in the following set of equations

$$\dot{c}_g = -\kappa c_g + ig_0 c_x, \tag{2.48}$$

$$\dot{c}_x = ig_0 c_g - \gamma_x c_x. \tag{2.49}$$

The term *bad cavity* is vaguely defined in the literature, but generally refers to the situation of an extremely leaky cavity. In our case this corresponds to the limit $\kappa \gg \{g_0, \gamma_x\}$, where the cavity-field decays at a rate much faster than the rate at which the atom oscillates between the states $|g,1\rangle$ and $|x,0\rangle$, and the rate at which the excited atomic state decays to produce non-cavity photons. This means that a cavity photon emitted from the atom will leak out from the cavity almost immediately after being emitted. Consequently, if the system starts out in the state $|x,0\rangle$, the population of state $|g,1\rangle$ will remain approximately unaltered throughout the entire system evolution. Thus a zeroth order assumption would be

$$\dot{c}_g \approx 0, \tag{2.50}$$

given the initial conditions $c_g(0) = 0$ and $c_x(0) = 1$. Combining this assumption with Equations (2.48) - (2.49), we find zeroth order approximation for the coefficient c_g and c_x

$$c_g = \frac{ig_0}{\kappa}c_x \quad \Rightarrow \tag{2.51}$$

$$\dot{c}_x = -(\frac{g_0^2}{\kappa} + \gamma_x)c_x \quad \Rightarrow \tag{2.52}$$

$$c_x = e^{-(\frac{g_0^2}{\kappa}+\gamma_x)t}, \tag{2.53}$$

where we in the last step used the initial condition $c_x(0) = 1$.

To determine under what conditions the zeroth order approximations will suffice, we compare it to higher order approximations. For the zeroth order solutions to be satisfactory we must require that they do not deviate appreciably from the higher order solutions. From inserting the expression of (2.51) into (2.53) we get a first order approximation for $\dot{c}_g$

$$\dot{c}_g = \frac{ig_0}{\kappa}\dot{c}_x = -\frac{ig_0}{\kappa}(\frac{g_0^2}{\kappa} + \gamma_x)c_x. \tag{2.54}$$

This can again be used in combination with Equations (2.48) - (2.49) to form first order approximations for the Schödinger coefficients. Calculating the first order approximation for c_g gives

$$c_g = \frac{ig_0}{\kappa}((\frac{g_0^2}{\kappa^2} + \frac{\gamma_x}{\kappa}) + 1)c_x. \tag{2.55}$$

From the expression in (2.55) we conclude that the zeroth and first order solutions will coincide in the limit

$$\frac{g_0^2}{\kappa} + \gamma_x \ll \kappa. \tag{2.56}$$

Presumably any additional terms in solutions of second order or higher will be of even higher order in g_0 and γ_x. As long as (2.56) holds, c_x is described accurately by (2.53).

Notice that the limit in (2.56) agrees well with the bad cavity limit, and confirms that our reasoning on the behavior of the $|g, 1\rangle$ population was correct. It is worth mentioning that (2.53) could also be found from evaluating the energy eigenvalue problem, and approximating the eigenvalues in the limit $\kappa \gg \{g_0, \gamma_x\}$, prior to calculating the state populations.

There are two processes contributing to losses in the excited atomic state population. One is the possible emission of a non-cavity photon due to interaction with non-cavity modes, causing the transition $|x, 0\rangle \rightarrow |g, 0\rangle$. The other is the atom-cavity coupling causing the transition $|x, 0\rangle \rightarrow |g, 1\rangle$. Looking at (2.53) we see that each of these processes can be associated with its own term in the exponent. The γ_x is by definition the representative for the decay rate due to environmental influence. That leaves g_0^2/κ to represent the population loss due to emission into the cavity.

We note that in the bad cavity regime the atom-cavity coupling effectively acts as an additional decay rate on the excited atomic state population. The effect is recognized when looking at the plot in Figure 2.3(a). Since the decay rate of the cavity photon is so large, the atom will never get the chance to reabsorb the photon, and the effect of the atom-cavity coupling will be purely dissipative. This behavior demonstrates a phenomenon known as cavity enhanced spontaneous emission. The atoms ability to emit photons into the cavity mode is increased due to the atom-cavity coupling.

Since we are only interested in the photons that leak out from the cavity modes, it will be to our advantage to amplify this effect as much as possible. This can be accomplished in the limit $g_0^2/\kappa \gg \gamma_x$, where the emission of cavity photons will dominate the atomic decay. Taking this limit into consideration, expression (2.53) transforms

approximately into

$$c_x = e^{-\frac{g_0^2}{\kappa}t}. \tag{2.57}$$

The Purcell Effect

The discovery that the spontaneous emission of an atom is altered by the presence of cavity surroundings is attributed to the work of Edward M. Purcell [18]. For this reason it is commonly referred to as the Purcell effect. In 1946 Purcell found that the enhancement of the spontaneous emission rate of an atom in resonance with a single cavity mode, as compared to the rate in free space, is given by the so-called Purcell factor

$$f = \frac{3Q\lambda^3}{4\pi^2 V}. \tag{2.58}$$

Here λ is the wavelength of the cavity mode in question, V is the cavity mode volume and Q is the so-called quality factor. It is customary to characterize an optical resonator by its quality factor

$$Q = \frac{\omega_k}{2\kappa}. \tag{2.59}$$

Q expresses the number of oscillations of the cavity field during the average life time, $(2\kappa)^{-1}$, of a cavity photon. It is a measure of how effectively the cavity is able to store electromagnetic energy.

An intuitive interpretation of the Purcell effect is found by seeing it as a consequence of a cavity modified density of states. To get an understanding of how these two concepts are connected we start by examining the already familiar concept of spontaneous emission from an excited atom interacting with the free electromagnetic field. Our goal is to show how the associated emission rate is related to the density of states of the emitted photon, and subsequently calculate the emission rate resulting from taking into account the presence of a cavity. In the following derivation of the spontaneous emission rate of an atom we will follow the steps of Leinaas [19].

The transition rate from an initial energy eigenstate $|i\rangle$ to a final energy eigenstate $|f\rangle$ due to a perturbation is, in the interaction picture, given by Fermi's well known golden rule

$$\gamma_{fi} = \frac{2\pi}{\hbar}|\mathcal{T}_{fi}|^2\delta(E_f - E_i), \tag{2.60}$$

$$\mathcal{T}_{fi} = \langle f|\,\hat{H}_I\,|i\rangle - \sum_n \frac{\langle f|\,\hat{H}_I\,|n\rangle\,\langle n|\,\hat{H}_I\,|i\rangle}{\hbar\omega_{ni}} + \ldots \tag{2.61}$$

where $\hat{H}_I$ denotes the perturbation part of the Hamiltonian, which in the case of a decaying atom corresponds to the emission part of the interaction between the atom and the field.

To find the emission rate we look at the case where the atom starts out in an excited state and ends up in a state where a photon is emitted

$$|i\rangle = |x, 0\rangle\,, \quad |f\rangle = |g, 1_{\mathbf{k}a}\rangle\,, \tag{2.62}$$

where $1_{\mathbf{k}a}$ refers to a photon of wave vector $\mathbf{k}$ and a polarization specified by the parameter pair $\mathbf{k}a$. Here a can take two values, and marks the vectors in the set of two arbitrary orthonormal polarization vectors in the plane perpendicular to $\mathbf{k}$.

Making use of Fermi's golden rule and summing over all possible final photon states we get the total emission probability to the first order in perturbation theory

$$\gamma_{gx} = \sum_{\mathbf{k}a} \frac{2\pi}{\hbar} |\langle x, 0| \hat{H}_I |g, 1_{\mathbf{k}a}\rangle|^2 \delta(E_x - E_g - \hbar\omega_k). \tag{2.63}$$

As is customary, we replace the sum over $\mathbf{k}$ by an integral

$$\sum_{\mathbf{k}a} \longrightarrow \frac{1}{4\pi} \int d\Omega \int_0^\infty \rho(k) dk \sum_a, \tag{2.64}$$

where $\rho(k)$ is the density of modes for the emitted photon, and the factor $\frac{1}{4\pi}$ compensates for the fact that the integral $\int d\Omega$ is already accounted for in $\rho(k)$. Performing the replacement results in

$$\begin{aligned}
\gamma_{gx} =& \frac{1}{4\pi} \int d\Omega \int_0^\infty \rho(k) dk \sum_a \frac{2\pi}{\hbar} |\langle x, 0| \hat{H}_I |g, 1_{\mathbf{k}a}\rangle|^2 \delta(E_x - E_g - \hbar\omega_k) \\
=& \frac{1}{2\hbar} \int d\Omega \int_0^\infty \rho(\omega_k) d\omega_k \sum_a |\langle x, 0| \hat{H}_I |g, 1_{\mathbf{k}a}\rangle|^2 \delta(E_x - E_g - \hbar\omega_k) \\
=& \frac{1}{2\hbar^2} \int d\Omega\, \rho(\omega_k) \sum_a |\langle x, 0| \hat{H}_I |g, 1_{\mathbf{k}a}\rangle|^2.
\end{aligned} \tag{2.65}$$

Under the supervision of the δ-function, the emitted photon has no choice but to tune its frequency in accordance with the energy transition, $\omega_k = (E_x - E_g)/\hbar = \omega_{xg}$, of the atom. Now, the result relies on the density of modes for the final photon state $\rho(\omega_k)$, and the matrix element $|\langle x, 0| \hat{H}_I |g, 1_{\mathbf{k}a}\rangle|^2$. Using the above result, we will now go on to calculate the emission rates of the excited atom, first in open space and then confined within a cavity.

For an atom in the free electromagnetic field, the relevant matrix element of the interaction Hamiltonian responsible for emission will be of the form

$$\langle x, 0| \hat{H}_I^{\text{free}} |g, 1_{\mathbf{k}a}\rangle = ie \sqrt{\frac{\hbar\omega_{xg}^2}{2V\epsilon_0\omega_k}} \boldsymbol{\epsilon}_{\mathbf{k}a}^* \cdot \mathbf{r}_{xg} e^{i\omega_k t}, \tag{2.66}$$

and the related density of modes is

$$\rho_{\text{free}}(\omega) = \frac{V\omega^2}{2\pi^2 c^3}. \tag{2.67}$$

(a) (b)

Figure 2.7: (a) An excited atom in open space interacts with a continuum of electromagnetic modes, which causes it to decay at a rate γ_{free}. The resulting photon will have no preferred polarization or direction of emission. (b) An excited atom in resonance with a cavity interacts with a single cavity mode, causing it to decay at a rate γ_{cav}. The atom emits photons into a single well-defined mode with a given linear polarization and direction.

Inserting the matrix element and the density of modes in (2.65) results in

$$\gamma_{\text{free}} = \frac{\omega^3}{8\hbar\epsilon_0\pi^2c^3}\int d\Omega \sum_a |e\boldsymbol{\epsilon}^*_{\mathbf{k}a}\cdot\mathbf{r}_{xg}|^2. \tag{2.68}$$

Since the polarization vectors $\boldsymbol{\epsilon}_{\mathbf{k}a}$ are unit vectors in the plane perpendicular to the wave vector $\mathbf{k}$, we can express

$$|e\boldsymbol{\epsilon}^*_{\mathbf{k}a}\cdot\mathbf{r}_{xg}|^2 = |e\mathbf{r}_{xg}|^2 - \frac{|e\mathbf{r}_{xg}|^2\cdot\mathbf{k}}{\mathbf{k}\cdot\mathbf{k}} = |\mu_{xg}|^2(1-\cos^2\theta). \tag{2.69}$$

Which finally gives us the spontaneous emission rate of the atom in open space

$$\begin{aligned}\gamma_{\text{free}} &= \frac{\omega_{xg}^3|\mu_{xg}|^2}{8\hbar\epsilon_0\pi^2c^3}\int d\Omega(1-\cos^2\theta)\\ &= \frac{\omega_{xg}^3|\mu_{xg}|^2}{8\hbar\epsilon_0\pi^2c^3}\int_0^{2\pi}d\phi\int_0^{\pi}\sin\theta(1-\cos^2\theta)d\theta\\ &= \frac{\omega_{xg}^3|\mu_{xg}|^2}{3\hbar\epsilon_0\pi c^3}.\end{aligned} \tag{2.70}$$

For an atom inside an optical cavity in resonance with a single cavity mode the relevant matrix element of the interaction Hamiltonian takes the simple form of a constant, as verified in Subsection 1.3.1

$$\langle x,0|\,\hat{H}_I^{\text{cav}}\,|g,1_{\mathbf{k}a}\rangle = -\hbar g_0 = \sqrt{\frac{\hbar\omega_{xg}^2|\mu_{xg}|^2}{2\omega_c\epsilon_0 V}}. \tag{2.71}$$

Since the atom is assumed only to interact strongly with a single cavity mode of a given linear polarization, there will only be one possible final photon state available. This is reflected in the independence of $\mathbf{k}$ and a. This assumption is, however, a truth with modifications. Due to the finite lifetime of the cavity mode, its energy is not perfectly sharp. It can be shown that this leads to a broadening mechanism corresponding to a density of modes for the emitted photon [25]

$$\rho_{\text{cav}}(\omega_k) = \frac{1}{\pi}\frac{\frac{\omega_c}{2Q}}{(\omega_c-\omega_k)^2+(\frac{\omega_c}{2Q})^2}. \tag{2.72}$$

Equipped with the cavity-modified density of modes we can make use of (2.65) once again to calculate the cavity induced spontaneous emission rate

$$\begin{aligned}\gamma_{\text{cav}} =& \frac{1}{2\hbar^2}\int d\Omega\, \rho_{\text{cav}}(\omega_k) \sum_a |\, \langle x,0|\, \hat{H}_I\, |g,1_{\mathbf{k}a}\rangle\, |^2 \\ =& \frac{1}{2\hbar^2}\frac{1}{\pi}\frac{2Q}{\omega_k}\frac{\hbar\omega_{xg}^2|\mu_{xg}|^2}{2\omega_c\epsilon_0 V}4\pi \\ =& \frac{2Q|\mu_{xg}|^2}{\hbar\epsilon_0 V}\end{aligned} \tag{2.73}$$

Where we have used that $\omega_c = \omega_{xg} = \omega_k$, since the atom is in resonance with the cavity mode.

Comparing (2.73) to (2.70), we see that the emission of an atom in resonance with a cavity mode is significantly different from that of an atom interacting with the electromagnetic field in open space. As seen from our recent calculations, this is mainly due to the alteration of the density of modes for the emitted photon. It seems intuitively reasonable that an atom interacting with a single isolated mode of the radiation field should behave a bit different from an atom interacting with the whole continuum of electromagnetic modes (see Figure 2.7). The Purcell factor is a measure of the enhancement in the rate of spontaneous emission from introducing a cavity, in terms of the free field value. In terms of γ_{free} the rate enhancement is found to be

$$\frac{\gamma_{\text{cav}}}{\gamma_{\text{free}}} = \frac{2Q|\mu_{xg}|^2}{\hbar\epsilon_0 V}\frac{3\hbar\epsilon_0\pi c^3}{\omega_{xg}^3|\mu_{xg}|^2} = \frac{3Q}{V}\frac{\lambda^3}{4\pi^2}, \tag{2.74}$$

which is exactly the expression presented by Purcell (2.58). From this we see how the Purcell effect can be considered as an effect of the modification of the photon density of modes, caused by the cavity.

Purcell Factor in the Bad Cavity Limit

Now that we have given an intuitive justification of the Purcell effect, we turn back to our decaying Jaynes-Cummings model. How are the results of the bad cavity limit related to the Purcell effect?

Taking the absolute square of (2.57) we get a simple formulation of the emission decay rate caused by the cavity coupling in our decaying Jaynes-Cummings model. In the limits $\kappa \gg \{g_0, \gamma_x\}$ and $g_0^2/\kappa \gg \gamma_x$ it reads

$$\epsilon = 2\frac{g_0^2}{\kappa}. \tag{2.75}$$

Following the track of Kuhn and Ljunggren [14] we identify that dividing (2.75) by the free space decay rate should correspond to the Purcell factor

$$f = 2\frac{g_0^2}{\kappa\gamma_{\text{free}}}. \tag{2.76}$$

From our derivation of the Jaynes-Cummings Hamiltonian we found the strength of the atom-cavity coupling g_0 to be

$$g_0^2 = \frac{\omega_{xg}^2 |\mu_{xg}|^2}{2\omega\epsilon_0 V\hbar}, \tag{2.77}$$

while the spontaneous emission rate of an excited atom interacting with the free electromagnetic field is given in (2.70). Substituting these into (2.76) finally gives

$$f = 2\frac{g_0^2}{\kappa\gamma_{\text{free}}} = \frac{2Q}{V}\frac{3\pi c^3}{\omega_{xg}^3} = \frac{3Q}{V}\frac{\lambda^3}{4\pi^2}, \tag{2.78}$$

which we, as presumed, recognize as the Purcell factor in (2.58). Since the typical solid angle extended by the cavity mirrors are very small, the atomic decay rate into non-cavity modes will be in the same order of magnitude as the rate of atomic decay in free space, $\gamma_x \sim \gamma_{\text{free}}$. This means that the ratio in (2.78) will be much greater than one, and the presence of the cavity leads to a clear enhancement of the atoms ability to emit photons into the cavity mode.

The above result stems from the bad cavity limit. In other coupling regimes simple analytic expression for the Purcell factor is not that easily derived. Nevertheless, the factor will exceed one as long as the cavity mode is in resonance with the atomic energy transition [14]. This means that the atoms ability to emit photons into the cavity mode is indeed be strengthened by the presence of a resonant cavity, in all coupling regimes.

In this chapter we have demonstrated how the plain two-level Jaynes-Cummings model can be manipulated to function as a basic source of single photons. If we had been able to eliminate the atomic decay, initiating the atom-cavity system would lead to an eventual photon emission, with a 100% certainty. For practical reasons this is not possible, and we look instead at how we can, for a given atomic decay rate, adjust the other system parameters in order for our photon source to perform maximally. In Section 2.2.2 we saw how the total photon emission probability reaches a peak for $\kappa = g_0$. We also registered that by increasing κ a little further, what seems to be the most precisely arriving photon is achieved. In the last subsection we have looked into the effect of the cavity on the atomic decay rate, and seen how it may lead to an increase of the atomic decay into the electromagnetic mode of interest. However, the modified Jaynes-Cummings model offers no method for more active control of the temporal shape of the emerging photon. As discussed in the introduction, this is one of the photon characteristics we are eager to have at our command. In Chapter 3 we will investigate an atom-cavity scheme in which manipulation of the photon profile is made possible.

Chapter 3

A New Level of Sophistication

In Chapter 2 we explored the characteristics of the primitive photon source formed from a two-level atom-cavity composition, interacting with its environment. The presented scheme offered a form of passive single photon generation, in the sense that once the photon source had been initiated, there was no mechanism allowing the user to have any further influence on the photon generation process. While this scheme is useful when it comes to demonstrating typical features of cavity based single photon sources, it is often too crude to be of any value in realistic applications.

To make our model a little more sophisticated we will in this chapter add to it another energy level, coupled to the system through the electromagnetic field of a laser. Our motivation for introducing the latter is to enable active user manipulation of the photon manufacturing. The idea is that by adjusting the laser during the system evolution we might be able to influence the system behavior to our advantage.

The first section of the present chapter will give an introduction to the extended system, consisting of three atomic levels, an optical cavity and a laser. Next we introduce interactions between the system and its environment, enabling photon emission. Owing to the newly acquired laser we will no longer be able to produce an analytic solution of the governing Schrödinger equation. Instead we will investigate some interesting limiting areas of the system parameter space, before completing the chapter by conducting a numerical simulation of the full system dynamics.

3.1 The Λ-model

In this section we will extend our two-level atom by adding to it a third energy level $|e\rangle$ of energy $\hbar\omega_e$. Furthermore, we introduce a laser of frequency ω_L, which is assumed to couple to the $|e\rangle \leftrightarrow |x\rangle$ transition, similar to how the cavity mode couples to the $|g\rangle \leftrightarrow |x\rangle$ transition.

In much the same way as we spoke of a two-level atom in the Jaynes-Cummings model, we will in this model speak of a three-level atom. This term will refer to the situation where the fields of the laser and the cavity mode each couples to a single atom transition, such that only three of the atomic levels are effectively involved in field interactions. When this requirement is met, the atom-cavity composition forms a so

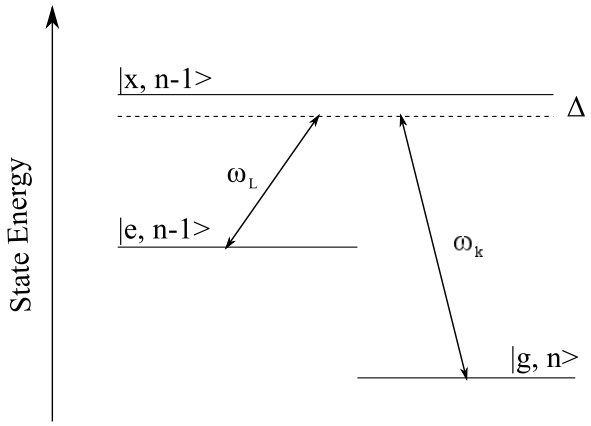

Figure 3.1: A schematic description of a three-level Λ-system. A classical laser field of frequency ω_L drives the $|e, n-1\rangle \leftrightarrow |x, n-1\rangle$ transition, while the quantized cavity mode of frequency ω_k couples to the $|g, n\rangle \leftrightarrow |x, n-1\rangle$ transition. The detunings between the laser and the cavity mode with their respective atomic transitions are here assumed to be equal, and denoted by Δ.

called Λ-configuration, as shown in Figure 3.1. As revealed by the figure, this set-up has been named after its schematic representation, which bears a certain resemblance to the Greek letter Λ. An atomic structure that is commonly used when Λ-dynamics is required is the assembly of hyperfine states of the rubidium isotope ^{85}Rb or ^{87}Rb [6].

3.1.1 The Λ-Hamiltonian

The detuning of the cavity mode and the laser with their respective atom transitions are defined as $\Delta_k = \omega_x - \omega_g - \omega_k$ and $\Delta_L = \omega_x - \omega_e - \omega_L$. We will for the sake of simplicity assume that these detunings are equal, and denoted $\Delta_L = \Delta_k = \Delta$. The transition $|g\rangle \leftrightarrow |e\rangle$ is assumed to be prohibited by the dipole transition rules, and will not be taken into account.

Once again we will use the tactic of splitting a complex system into smaller parts in order to determine the system Hamiltonian. In Subsection 1.3.1 we triumphed over the Jaynes-Cummings system by partitioning out the atom, the cavity field and the atom-field interaction in separate entities. Sticking to this convention, the Hamiltonian will now be enriched with two new entities, the laser field and the atom-laser interaction. In addition the atomic Hamiltonian will get an extra term, on account of the new atomic energy level. With this division the total system is described by the sum of the Hamiltonians of the atom, the cavity field, the atom-cavity interaction and the

atom-laser interaction

$$\hat{H} = \hat{H}_A + \hat{H}_F + \hat{H}_{AF} + \hat{H}_{AL}. \tag{3.1}$$

The laser is considered to be strong, in the sense that adding or subtracting a few photons from its field will not make any significant difference. This means that the strength of the laser field will not be influenced by photon absorption or emission from the atom. The total energy of the laser field can thus be regarded as approximately constant, and its isolated Hamiltonian, $\hat{H}_L$, will be a constant as well. As the only function of a constant term in the total Hamiltonian will be to shift the zero-energy reference of the system, $\hat{H}_L$ will not make any important contributions to the system dynamics. We may thus safely drop the Hamilton operator of the isolated laser field from our description.

With a third energy level in place the atomic Hamiltonian is neatly expressed as a sum

$$\hat{H}_A = \sum_{i\in\{g,e,x\}} \hbar\omega_i \left|i\right\rangle \left\langle i\right| . \tag{3.2}$$

While the Hamilton operators of the cavity field $\hat{H}_F$ and the atom-cavity interaction $\hat{H}_{AF}$ are defined as previously, in Equations (1.31) and (1.44).

Finally, we can find the interaction between the atom and the laser can be found from slightly modifying the procedure followed when determining the atom-field interaction Hamiltonian (1.44), in Subsection 1.3.1. Since we have already been through a similar calculation in detail, we will here only give a short version of the story.

Starting with the electromagnetic field under consideration, the quantized cavity mode is in the present case traded for the monochromatic, plane polarized, classical field of a laser

$$\mathbf{A} = (A_0 e^{-i\omega_L t} + A_0^* e^{i\omega_L t})\boldsymbol{\epsilon}. \tag{3.3}$$

Here the amplitude A_0 will in general be position dependent, ω_L is the laser frequency and $\boldsymbol{\epsilon}$ is the laser polarization vector. Expressing the atom-laser interaction (1.33) in terms of the electron position operator $\hat{\mathbf{r}}$, like we did for the atom-cavity interaction, we get an expression of the form

$$\hat{H}_{AL} = -\hbar\omega_{xe}|\mu_{xe}|\Big(A_0 e^{-i\omega_L t} + A_0^* e^{i\omega_L t}\Big)\Big(\left|e\right\rangle \left\langle x\right| + \left|x\right\rangle \left\langle e\right|\Big), \tag{3.4}$$

with $\omega_{xe} = \omega_x - \omega_e$ and $\mu_{xe} = e\boldsymbol{\epsilon}\cdot\hat{\mathbf{r}}$. Just as in Section 1.3.1, we can now apply the rotating wave approximation. The resulting Hamilton operator associated with the interaction of the laser and the atomic transition $|e\rangle \leftrightarrow |x\rangle$ can then be formulated

$$\hat{H}_{AL} = -\frac{\hbar\Omega}{2}\Big(\left|x\right\rangle \left\langle e\right| e^{-i\omega_L t} + \left|e\right\rangle \left\langle x\right| e^{i\omega_L t}\Big), \tag{3.5}$$

with

$$\Omega = 2\omega_{xe}|\mu_{xe}||A_0|. \tag{3.6}$$

Along the way we have written $A_0 = |A_0|e^{i\chi}$, and absorbed the phase factor into the new state $|e\rangle$, to arrive at the last expression. The quantity Ω denotes the Rabi frequency of the laser-induced oscillation in the state populations. In analogy with the Rabi frequency of the Jaynes-Cummings model, which is dominated by the coupling strength between the atom and the cavity mode, Ω will be a measure of the strength of the atom-laser interaction. To enable the previously mentioned active laser manipulation of the system evolution, we will allow for a time dependent coupling strength between the laser and the atom, so $\Omega = \Omega(t)$.

With all the Hamilton operators of the partial systems in place, only one little thing remains to make the total system Hamiltonian fully operable. It is convenient to have the Hamiltonian in the simplest possible form. The time dependence of the laser $\Omega(t)$ is hard to get rid of, but there is a way to remove the time varying exponential terms in (3.4). Applying the unitary transformation $\hat{T}(t)$, will cause all states and operators to be mapped

$$|\alpha\rangle \to \hat{T}\,|\alpha\rangle\,, \qquad \hat{A} \to \hat{T}\hat{A}\hat{T}^\dagger, \qquad \hat{H} \to \hat{T}\hat{H}\hat{T}^\dagger - i\hbar\hat{T}\frac{d\hat{T}^\dagger}{dt}, \tag{3.7}$$

but preserve all observable quantities. To get rid of the impractical time dependence it suffices to use the transformation $\hat{T} = e^{-i\omega_L|e\rangle\langle e|t}$. Exploiting the identity

$$e^{\hat{B}}\hat{A}e^{-\hat{B}} = \hat{A} + [\hat{B},\hat{A}] + \frac{1}{2}[\hat{B},[\hat{B},\hat{A}]] + \ldots, \tag{3.8}$$

gives

$$\begin{aligned} |\alpha\rangle\langle\beta|\,e^{i\omega t} &= e^{i\omega|\alpha\rangle\langle\alpha|t}\,|\alpha\rangle\langle\beta|\,e^{-i\omega|\alpha\rangle\langle\alpha|t}, \\ |\beta\rangle\langle\alpha|\,e^{-i\omega t} &= e^{i\omega|\alpha\rangle\langle\alpha|t}\,|\beta\rangle\langle\alpha|\,e^{-i\omega|\alpha\rangle\langle\alpha|t}. \end{aligned} \tag{3.9}$$

The transformed Hamiltonian of the total system is then

$$\begin{aligned} \hat{H}_T =& \hbar\Big(\omega_g\,|g\rangle\langle g| + (\omega_e+\omega_L)\,|e\rangle\langle e| + \omega_x\,|x\rangle\langle x|\Big) + \hbar\omega_k(\hat{a}\hat{a}^\dagger + \frac{1}{2}) \\ & - g_0\hbar(\hat{a}\,|x\rangle\langle g| + \hat{a}^\dagger\,|g\rangle\langle x|) - \frac{\hbar\Omega(t)}{2}(|x\rangle\langle e| + |e\rangle\langle x|). \end{aligned} \tag{3.10}$$

Since we are assuming there are no transitions between the levels $|g\rangle$ and $|e\rangle$, the Hamiltonian couples only the states $|g,n\rangle$, $|e,n-1\rangle$ and $|x,n-1\rangle$ for a given photon number n. Expressing the Hamiltonian in this basis we get

$$H_T = \begin{pmatrix} \hbar\omega_k(n+\frac{1}{2}) + \hbar\omega_g & 0 & -\hbar g_0\sqrt{n} \\ 0 & \hbar\omega_k(n-\frac{1}{2}) + \hbar\omega_e + \hbar\omega_L & -\frac{\hbar\Omega}{2} \\ -\hbar g_0\sqrt{n} & -\frac{\hbar\Omega}{2} & \hbar\omega_x + \hbar\omega_k(n-\frac{1}{2}) \end{pmatrix}. \tag{3.11}$$

For convenience we define $\alpha = \hbar\omega_k(n-\frac{1}{2})$, $\beta = -\hbar g_0\sqrt{n}$ and $\gamma = -\frac{\hbar\Omega}{2}$, simplifying H_T to

$$
\begin{aligned}
H_T &= \begin{pmatrix} \hbar\omega_k + \hbar\omega_g + \alpha & 0 & \beta \\ 0 & \hbar\omega_e + \hbar\omega_L + \alpha & \gamma \\ \beta & \gamma & \hbar\omega_x + \alpha \end{pmatrix} \\
&= \begin{pmatrix} -\hbar\Delta & 0 & \beta \\ 0 & -\hbar\Delta & \gamma \\ \beta & \gamma & 0 \end{pmatrix} + (\alpha + \hbar\omega_x)\mathbb{I} \\
&= A + (\alpha + \hbar\omega_x)\mathbb{I}. \qquad (3.12)
\end{aligned}
$$

The Energy Eigenstates

As recently mentioned, allowing for a time varying laser will introduce a time dependence in the system Hamiltonian that can not be transformed away. This complicates the process of finding exact analytical solutions to the Schrödinger equation, since the straightforward method of finding the evolution of the eigenstates will no longer suffice. Nevertheless, it turns out determining the eigenstates of the Hamiltonian for a constant laser interaction $\Omega = \text{const.}$ is still worthwhile.

The eigenvalues of the Hamiltonian can be found by first identifying the eigenvalues of the matrix A of (3.12), and then adding the diagonal terms $\alpha + \hbar\omega_x$. The eigenvalue equation of A reads

$$
\begin{aligned}
&(-\hbar\Delta - \lambda)\Big(- \lambda(-\hbar\Delta - \lambda) - \gamma^2\Big) - \beta^2(-\hbar\Delta - \lambda) = 0 \quad \Rightarrow \\
&\lambda_0 = -\hbar\Delta, \\
&\lambda_\pm = -\frac{\hbar\Delta}{2} \pm \frac{1}{2}\sqrt{\hbar^2\Delta^2 + 4(\beta^2 + \gamma^2)}. \qquad (3.13)
\end{aligned}
$$

The eigenvalues of the total Hamiltonian are given by $E = \lambda + \alpha + \hbar\omega_x$, resulting in

$$
\begin{aligned}
E_0 &= \hbar\omega_g + \hbar\omega_k(n + \frac{1}{2}), \\
E_\pm &= \hbar\omega_g + \hbar\omega_k(n + \frac{1}{2}) + \frac{\hbar\Delta}{2} \pm \frac{1}{2}\sqrt{\hbar^2\Delta^2 + 4(\beta^2 + \gamma^2)}. \qquad (3.14)
\end{aligned}
$$

With the corresponding eigenstates

$$
\begin{aligned}
\left|\psi_n^0\right\rangle &= -\sin\theta\left|g, n\right\rangle + \cos\theta\left|e, n-1\right\rangle, \\
\left|\psi_n^-\right\rangle &= \sin\phi\cos\theta\left|g, n\right\rangle + \sin\phi\sin\theta\left|e, n-1\right\rangle + \cos\phi\left|x, n-1\right\rangle, \\
\left|\psi_n^+\right\rangle &= \cos\phi\cos\theta\left|g, n\right\rangle + \cos\phi\sin\theta\left|e, n-1\right\rangle - \sin\phi\left|x, n-1\right\rangle. \qquad (3.15)
\end{aligned}
$$

Here

$$
\cos\theta = -\frac{\beta}{\sqrt{\beta^2 + \gamma^2}}, \quad \sin\theta = -\frac{\gamma}{\sqrt{\beta^2 + \gamma^2}}, \qquad (3.16)
$$

and

$$\cos\phi = -\frac{K}{\sqrt{\beta^2+\gamma^2+K^2}}, \quad \sin\phi = -\frac{\sqrt{\beta^2+\gamma^2}}{\sqrt{\beta^2+\gamma^2+K^2}},$$
$$K = -\frac{\hbar\Delta}{2} - \frac{1}{2}\sqrt{\hbar^2\Delta^2 + 4(\beta^2+\gamma^2)}. \tag{3.17}$$

These eigenstates will prove very useful in Section 3.2.3, where they will serve as instantaneous eigenstates, in the so called strong coupling limit.

3.2 The Λ-model with Decay

In the former section we identified the Hamiltonian of the plain Λ-model and its corresponding eigenstates. We are now able to dynamically describe our new and extended system, consisting of a three-level atom inside an optical cavity, with one atomic transition in resonance with a cavity mode, and another in resonance with a classical laser field. But this set-up cannot yet be utilized as a single photon source. As in the case of the plain Jaynes-Cummings model, we need to introduce interactions with the environment, to enable the system to emit photons.

In the current section we will proceed to discuss the three-level Λ-system with decay. We will open with a brief description of the slightly modified governing equations, followed by an analytic investigation of selected parameter limits and finally an exploration of numerical solutions.

3.2.1 The Effective Schödinger Equation

As in the two-level case we will assume the cavity modes to leak out of the cavity at a rate κ, and the excited atom state $|x\rangle$ to decay at a rate γ_x. We will in the remainder of this chapter assume that the excited atomic state $|x\rangle$ can only decay to the atomic ground state $|g\rangle$. This supplies our system with two decay channels, $|x,0\rangle \to |g,0\rangle$ and $|g,1\rangle \to |g,0\rangle$. These incoherent transition are exactly the ones we encountered in the decaying Jaynes-Cummings model, causing the system to strand in the state $|g,0\rangle$, which is not included in the effective Hamiltonian. The system can then be described through the modified Schrödinger equation, as demonstrated in Section 2.1. In Chapter 4 we will investigate how to describe transitions that are not in this category.

Following the same procedure as in the case of a two-level system we find the effective Hamiltonian

$$\hat{H} = \hat{H}_T - i\hbar\kappa\hat{a}^\dagger\hat{a} - i\hbar\gamma_x |x\rangle\langle x|. \tag{3.18}$$

Where $\hat{H}_T$ is the transformed Hamilton operator of the plain Λ-model, given in (3.10).

As we are mainly interested in the Λ-model for its single photon manufacturing properties we will set the photon number of the eigenstates to $n = 1$ from now on. A general state may then be expressed as a superposition of the basis states

$$|\psi\rangle = c_g |g,1\rangle + c_e |e,0\rangle + c_x |x,0\rangle. \tag{3.19}$$

Assuming zero detuning between the $|g\rangle \leftrightarrow |x\rangle$ transition and the cavity field, as well as between the $|e\rangle \leftrightarrow |x\rangle$ transition and the laser, we have $\Delta = 0$. After shifting the energy, making $E_0 = \frac{3}{2}\hbar\omega_k + \hbar\omega_g$ the zero energy reference, the corresponding effective Scrödinger equation reads

$$\begin{aligned} i\hbar\frac{\partial}{\partial t}|\psi\rangle = H|\psi\rangle \quad \Rightarrow \\ i\hbar\begin{pmatrix}\dot{c}_g\\ \dot{c}_e\\ \dot{c}_x\end{pmatrix} = \begin{pmatrix}-i\hbar\kappa & 0 & \beta\\ 0 & 0 & \gamma\\ \beta & \gamma & -i\hbar\gamma_x\end{pmatrix}\begin{pmatrix}c_g\\ c_e\\ c_x\end{pmatrix}, \end{aligned} \tag{3.20}$$

with $\beta = -\hbar g_0$ and $\gamma = -\frac{\hbar\Omega}{2}$. From this we get the equations

$$\dot{c}_g = -\kappa c_g + ig_0 c_x, \tag{3.21}$$

$$\dot{c}_e = i\frac{\Omega}{2}c_x, \tag{3.22}$$

$$\dot{c}_x = ig_0 c_g + i\frac{\Omega}{2}c_e - \gamma_x c_x. \tag{3.23}$$

Since the dynamical equations (3.21)-(3.23) of the three-level system contain the time dependent laser parameter $\Omega(t)$, it is not obvious that it will be possible to find an exact analytic solution. In the following we will instead look into some extreme limits for which the system is more easily analyzed, leaving the full system dynamics to a numerical simulation at the end of the chapter.

3.2.2 Photon Emission Probability in The Bad Cavity Limit

With the introduction of cavity mode decay in the previous subsection, our Λ-model is all set to start photon production. As discussed in Section 2.2.2, the temporal photon profile along with the total photon emission probability are useful quantities, when the quality of a single photon source is to be evaluated. In this subsection we aim to develop analytic expressions for these benchmarks in the bad cavity regime, as carried out by Law and Kimble [11].

In Section 2.2.3 we witnessed how interesting dynamical features of the decaying Jaynes-Cummings model could be studied analytically in the so called bad cavity limit $\kappa \gg \{g_0, \gamma_x\}$. We found that the state population of $|g,1\rangle$ would stay approximately constant, $\dot{c}_g \approx 0$, during the system evolution, given that the system was initialized in the state $|x,0\rangle$. We also concluded that adding the condition $g_0^2/\kappa \gg \gamma_x$ caused the dominating decay rate of state $|x,0\rangle$ to be given by g_0^2/κ. With this in mind we can similarly argue that within the Λ-model, in the limits $\kappa \gg g_0^2/\kappa \gg \gamma_x$ and $\gamma_x^2/\kappa \gg \Omega$, the populations of both $|g,1\rangle$ and $|x,0\rangle$ will stay approximately constant, given that the system starts out in the state $|e,0\rangle$. So a zeroth order assumption would in this case be

$$\dot{c}_g \approx \dot{c}_x \approx 0, \tag{3.24}$$

given the initial conditions $c_g(0) = c_x(0) = 0$ and $c_e(0) = 1$. In combination with Equations (3.21) - (3.23) these give zeroth order approximations for the coefficients c_g, c_x and c_e. From (3.21) we have

$$c_g = \frac{ig_0}{\kappa} c_x. \tag{3.25}$$

Combining this with (3.23) we find

$$c_x = \frac{i\Omega}{2(\frac{g_0^2}{\kappa} + \gamma_x)} c_e = \frac{i\alpha}{2}\Omega c_e, \quad \text{with} \quad \alpha = \frac{1}{\frac{g_0^2}{\kappa} + \gamma_x}. \tag{3.26}$$

At last, inserting the expression for c_x in (3.26) into (3.22) gives a solvable equation for c_e

$$\begin{aligned} &\dot{c}_e = -\frac{\alpha}{4}\Omega^2 c_e \quad \Rightarrow \\ &c_e = \exp\Big(-\frac{\alpha}{4}\int_0^t \Omega^2\, dt\Big). \end{aligned} \tag{3.27}$$

Before we can draw any conclusions about our system on the basis of these zeroth order results, we need to know under what conditions they are satisfactory. As in our evaluation of the two-level system we will determine this by comparing them to higher order approximations. In the regimes where the zeroth order expressions are approximately equal to those of higher order, they can be said to give a fairly accurate description of the system dynamics. We will set off with the evaluation of c_g, before moving on to c_x. Given that both of these are described accurately to the lowest order, the same will automatically hold for c_e.

From Equations (3.25) and (3.26) we get first order approximations for $\dot{c}_g$ and $\dot{c}_x$

$$\dot{c}_g = \frac{ig_0}{\kappa}\dot{c}_x, \tag{3.28}$$

$$\dot{c}_x = \frac{i\alpha}{2}(\dot{\Omega}c_e + \Omega\dot{c}_e) = \frac{i\alpha}{2}(\dot{\Omega}c_e + \frac{i\Omega^2}{2}c_x). \tag{3.29}$$

Using (3.28) and (3.21) yields

$$\frac{ig_0}{\kappa}\dot{c}_x = -\kappa c_g + ig_0 c_x = \frac{ig_0}{\kappa}(c_x - \frac{1}{\kappa}\dot{c}_x). \tag{3.30}$$

Which in combination with (3.29) gives

$$c_g = = \frac{ig_0}{\kappa}\Big((1 + \frac{\alpha\Omega^2}{4\kappa})c_x - \frac{i\alpha\dot{\Omega}}{2\kappa}c_e\Big). \tag{3.31}$$

Comparing the zeroth order solution for c_g (3.25) with the first order solution (3.31), we observe that for the zeroth order approximation to suffice we must require

$$\{\Omega^2, \dot{\Omega}\} \ll \frac{\kappa}{\alpha} = \kappa\Big(\frac{g_0^2}{\kappa} + \gamma_x\Big). \tag{3.32}$$

Given that the zeroth order approximation for c_g is correct, we can use (3.23) and (3.29) to find the first order approximation for c_x

$$c_x = i\frac{\alpha\Omega - \alpha^2\dot{\Omega}}{2 - \frac{\alpha^2\Omega^2}{2}}c_e \tag{3.33}$$

For this to coincide with the zeroth order solution for c_x (3.26) we must have

$$\Omega \ll \frac{1}{\alpha} = \frac{g_0^2}{\kappa} + \gamma_x \quad \text{and} \quad \dot{\Omega} \ll \frac{\Omega}{\alpha} = \Omega(\frac{g_0^2}{\kappa} + \gamma_x). \tag{3.34}$$

By inspection we see that in the limit $\kappa \gg g_0^2\kappa \gg \gamma_x$, whenever (3.34) is satisfied, so is (3.32). Thus we conclude that as long as (3.34) holds, the Schrödinger coefficients are accurately described by Equations (3.25) - (3.27).

With the analytic approximations for the state coefficients c_g, c_x and c_e in Equations (3.25) - (3.27), we can find a formula for the temporal photon profile

$$R(t) = -2\kappa|c_g|^2 = -\frac{g_0^2\alpha^2\Omega^2}{2\kappa}\exp\Big(-\frac{\alpha}{2}\int_0^t \Omega^2 dt\Big), \tag{3.35}$$

and the total photon emission probability

$$\begin{aligned} P_{\text{emit}}^{\text{tot}} &= \frac{g_0^2\alpha^2}{2\kappa}\int_0^\infty \Omega^2(t')\exp\Big(-\frac{\alpha}{2}\int_0^{t'} \Omega^2(t'')dt''\Big)dt' \\ &= -\frac{g_0^2\alpha}{\kappa}\Big[\exp\Big(-\frac{\alpha}{2}\int_0^{t'} \Omega^2(t'')dt''\Big)\Big]_{t'=0}^{t'=\infty} \\ &= \frac{g_0^2\alpha}{\kappa}(1 - \exp\Big(-\frac{\alpha}{2}\int_0^\infty \Omega^2(t')dt'\Big)), \end{aligned} \tag{3.36}$$

in the bad cavity regime of the Λ-model.

The expression in (3.36) tells us that in this regime the total emission probability will not dependent on the shape of the atom-laser coupling function $\Omega(t)$, but only on its integral. When the area under $\Omega(t)$ is large, the total emission probability approaches

$$P_{\text{emit}}^{\text{tot}} \to \frac{g_0^2\alpha}{\kappa} = \frac{g_0^2/\kappa}{g_0^2/\kappa + \gamma_x}. \tag{3.37}$$

Our results are valid in the limit $g_0^2/\kappa \gg \gamma_x$. In this limit, when $\int_0^\infty \Omega^2(t)dt$ is large, the emission probability will be close to one.

3.2.3 Adiabatic Population Transfer in The Strong Coupling Limit

In the former subsection we worked out an analytic expression for the photon profile and the total photon emission probability, in the bad cavity regime. Here we will dive into the dynamics of another regime, known as the *strong coupling limit*. The strong coupling limit describes the situation where the atom-field and atom-laser couplings dominate the system evolution, while the environmental interactions are considered to

be small in comparison. It is more formally defined by $\{g_0, \Omega(t)\} >> \{\kappa, \gamma_x\}$.

In the analytical examination that now follows, we will consider the case where the decay terms of the system Hamiltonian are completely neglected. This is where our work of finding the energy eigenstates for constant Ω, in Section 3.1, finally pays off. Since the Hamiltonian is time dependent through the laser parameter $\Omega(t)$, the energy eigenstates will also vary with time. The evolution of the eigenstates is not necessarily trivial to determine. However, if we consider the Hamilton operator at a specific moment in time, the corresponding eigenstates can be found in the usual manner. These states are then referred to as instantaneous eigenstates. Not taking the decay rates into account the instantaneous system eigenstates of the Λ-model are then given by the results in (3.15), with $n = 1$ and $\Delta = 0$.

Inspecting the eigenstate

$$\left|\psi_1^0\right\rangle = -\sin\theta\,|g,1\rangle + \cos\theta\,|e,0\rangle\,, \tag{3.38}$$

with the trigonometric coefficients written out in their entirety

$$\cos\theta = \frac{g_0}{\sqrt{g_0^2 + \frac{\Omega^2}{4}}}, \quad \sin\theta = \frac{\Omega}{2\sqrt{g_0^2 + \frac{\Omega^2}{4}}}, \tag{3.39}$$

we discover that this state has some noteworthy features. For $\Omega << 2g_0$, the state $\left|\psi_1^0\right\rangle$ coincides with $|e,0\rangle$, while for $\Omega >> 2g_0$, it coincides with $|g,1\rangle$. We will soon see how this provides an interesting opportunity for producing single cavity photons, with minimal decay loss. The method makes use of the so-called *adiabatic theorem*.

The Adiabatic Theorem and Criterion

The adiabatic theorem states that for a slowly varying Hamiltonian, the instantaneous eigenstates of the Hamiltonian evolve continuously into the corresponding eigenstates at a later time.

It means that a quantum mechanical system under the influence of gradually changing external conditions, will adjust its wavefunction accordingly, provided that the changes happen slowly enough. On the other hand, a sudden change in the external conditions will prevent the system from adapting during the process, and the functional form of the Hamiltonian will not in general be preserved. In this regard David J. Griffiths [9] has an illustrative example, which we will recite here. Imagine we prepare a particle in the ground state of an infinite square well of width a

$$\psi_i(x) = \sqrt{\frac{2}{a}}\sin\Big(\frac{\pi}{a}x\Big), \tag{3.40}$$

as illustrated in Figure 3.2(a). Suppose then, that we expand the well to have twice the initial width. What final state $\psi_f(x)$ the particle will end up in, will depend on how

fast the expansion is carried out. If we make the expansion slow enough, the adiabatic theorem states that the system will end up in the ground state of the expanded well,

$$\psi_f(x) = \sqrt{\frac{1}{a}} \sin\Big(\frac{\pi}{2a}x\Big), \tag{3.41}$$

which is an eigenstate of the new Hamiltonian. The situation is illustrated in Figure 3.2(b). If we instead expand the well with a sudden jerk, the particle wavefunction will not have the time to adapt, and the system will no longer end up in an eigenstate of the Hamiltonian, but in some linear combination of eigenstates, as seen in Figure 3.2(c).

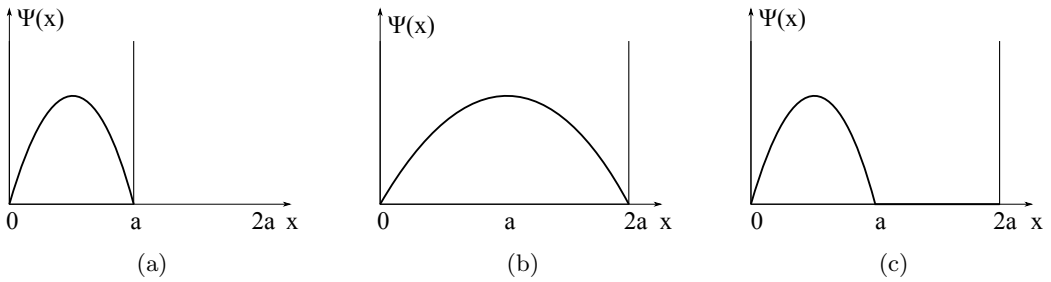

Figure 3.2: The figure illustrates how the wavefunction of a particle in an infinite well behaves when the well is expanded. Figure (*a*) shows the particles wavefunction as it is prepared in the ground state of a well of width a. In Figure (*b*) the result of a slow adiabatic expansion is displayed, while Figure (*c*) shows the result of a sudden diabatic expansion.

So, under what conditions is the Hamiltonian considered to vary slowly enough for the adiabatic theorem to apply? To answer this question we will closely follow the derivation given by Leinaas in [19]. We consider a quantum mechanical system described by the Hamiltonian $H = H(x(t))$ that depends on a set of continuous time-dependent parameters $x(t) = \{x_1(t), x_2(t), \ldots, x_k(t)\}$. The parameters are assumed to vary slowly with time. Let the states $|\chi_x^n\rangle$ with $x = x(t)$ be the instantaneous eigenstates of the Hamiltonian at time t. Then

$$H(x)\,|\chi_x^n\rangle = E_n(x)\,|\chi_x^n\rangle\,, \tag{3.42}$$

and the time evolution of the system is given by the time-dependent Schrödinger equation

$$i\hbar\frac{d}{dt}\,|\psi(t)\rangle = H(x(t))\,|\psi(t)\rangle\,. \tag{3.43}$$

An arbitrary state can then be expressed

$$\begin{aligned} |\psi(t)\rangle &= \sum_n c_n(t)\,\Big|\chi^n_{x(t)}\Big\rangle \quad \Rightarrow \\ \frac{d}{dt}\,|\psi\rangle &= \sum_n \frac{dc_n}{dt}\,|\chi_x^n\rangle + \sum_n c_n\,|\dot{\chi}_x^n\rangle\,. \end{aligned} \tag{3.44}$$

Substituting into the time-dependent Schrödinger equation gives

$$
\begin{aligned}
i\hbar(\sum_n \frac{dc_n}{dt}\left|\chi_x^n\right\rangle + \sum_n c_n\left|\dot{\chi}_x^n\right\rangle) &= H(x(t))\sum_n c_n(t)\left|\chi_x^n\right\rangle, \\
i\hbar\sum_n\Big(\frac{dc_n}{dt}\left|\chi_x^n\right\rangle + c_n\left|\dot{\chi}_x^n\right\rangle\Big) &= \sum_n E_n\left|\chi_x^n\right\rangle. \qquad (3.45)
\end{aligned}
$$

Multiplying through by $\langle\chi_x^m|$ gives

$$
i\hbar\dot{c}_m + i\hbar\sum_n c_n\left\langle\chi_x^m\right|\left.\dot{\chi}_x^n\right\rangle = E_m c_m. \qquad (3.46)
$$

It is convenient to factor out the usual energy-dependent term from the coefficients c_n

$$
c_n = v_n e^{-\frac{i}{\hbar}\int_0^t E_n(t')dt'}. \qquad (3.47)
$$

Inserting this into (3.46) results in the following

$$
\begin{aligned}
&\dot{v}_m e^{-\frac{i}{\hbar}\int_0^t E_m(t')dt'} + v_m(-\frac{i}{\hbar}E_m)e^{-\frac{i}{\hbar}\int_0^t E_m(t')dt'} + \sum_n v_n e^{-\frac{i}{\hbar}\int_0^t E_n(t')dt'}\left\langle\chi_x^m\right|\left.\dot{\chi}_x^n\right\rangle \\
&= -\frac{i}{\hbar}E_m v_m e^{-\frac{i}{\hbar}\int_0^t E_m(t')dt'} \quad \Rightarrow \\
&\dot{v}_m e^{-\frac{i}{\hbar}\int_0^t E_m(t')dt'} = -\sum_n v_n e^{-\frac{i}{\hbar}\int_0^t E_n(t')dt'}\left\langle\chi_x^m\right|\left.\dot{\chi}_x^n\right\rangle \quad \Rightarrow \\
&\dot{v}_m = -\sum_n v_n\left\langle\chi_x^m\right|\left.\dot{\chi}_x^n\right\rangle e^{\frac{i}{\hbar}\int_0^t E_m(t')-E_n(t')dt'}. \qquad (3.48)
\end{aligned}
$$

We assume that the system is initialized in its k'th eigenstate at $t = 0$.

$$
\begin{aligned}
dv_m &= -\sum_n v_n\left\langle\chi_x^m\right|\left.\dot{\chi}_x^n\right\rangle e^{\frac{i}{\hbar}\int_0^t E_m(t')-E_n(t')dt'}dt, \\
v_m(t) - v_m(0) &= -\int_0^t\sum_n v_n\left\langle\chi_x^m\right|\left.\dot{\chi}_x^n\right\rangle e^{\frac{i}{\hbar}\int_0^{t''} E_m(t')-E_n(t')dt'}dt'', \\
v_m(t) &= \delta_{mk} - \sum_n\int_0^t v_n\left\langle\chi_x^m\right|\left.\dot{\chi}_x^n\right\rangle e^{\frac{i}{\hbar}\int_0^{t''} E_m(t')-E_n(t')dt'}dt''. \qquad (3.49)
\end{aligned}
$$

Assume the parameter x makes a finite change in a time interval T. Then consider the evolution of the system in a time interval $\delta t << T$. For a sufficiently small δt the parameter x as well as the energies E_n and coefficients c_n can be considered constant. Applying these assumptions in equation (3.49) gives the following approximation

$$
\begin{aligned}
v_m(t+\delta t) &= \delta_{mk} - \sum_n \int_0^{t+\delta t} v_n \langle \chi_x^m | \dot{\chi}_x^n \rangle \, e^{\frac{i}{\hbar}\int_0^{t''} E_m(t') - E_n(t') dt'} dt'' \\
&= \delta_{mk} - \sum_n \int_0^{t} v_n \langle \chi_x^m | \dot{\chi}_x^n \rangle \, e^{\frac{i}{\hbar}\int_0^{t''} E_m(t') - E_n(t') dt'} dt'' - \sum_n \int_t^{t+\delta t} v_n \langle \chi_x^m | \dot{\chi}_x^n \rangle \, e^{\frac{i}{\hbar}\int_0^{t''} E_m(t') - E_n(t') d} \\
&= v_m(t) - \sum_n \int_t^{t+\delta t} v_n \langle \chi_x^m | \dot{\chi}_x^n \rangle \, e^{\frac{i}{\hbar}\int_0^{t''} E_m(t') - E_n(t') dt'} dt'' \\
&\approx v_m(t) - \sum_n v_n \langle \chi_x^m | \dot{\chi}_x^n \rangle \int_t^{t+\delta t} e^{\frac{i}{\hbar}(E_m - E_n)t''} dt'' \\
&= v_m(t)(1 - \langle \chi_x^m | \dot{\chi}_x^m \rangle \, \delta t) + i\hbar \sum_{n \neq m} v_n \frac{\langle \chi_x^m | \dot{\chi}_x^n \rangle}{E_m - E_n} e^{\frac{i}{\hbar}(E_m - E_n)t} \Big(e^{\frac{i}{\hbar}(E_m - E_n)\delta t} - 1 \Big).
\end{aligned}
\tag{3.50}
$$

The last expression shows that the system will stay in the initial eigenstate as long as

$$
\hbar \left| \frac{\langle \chi_x^m | \dot{\chi}_x^n \rangle}{E_m - E_n} \right| = \left| \frac{\langle \chi_x^m | \dot{\chi}_x^n \rangle}{\omega_m - \omega_n} \right| << 1. \tag{3.51}
$$

This is the so-called *adiabatic criterion*. It defines the validity range of the adiabatic theorem.

Adiabatic Population Transfer

Equipped with the adiabatic theorem, we now head back to take a another glance at the eigenstate $|\psi_1^0\rangle$ in (3.38). Assume that our three-level atom is prepared in the intermediate state $|e\rangle$ and placed inside an empty optical cavity. The total atom-cavity system is then initially in the state $|e, 0\rangle$, coinciding with $|\psi_1^0\rangle$ in the case of no laser, $\Omega(0) = 0$. The laser driving the transition $|e, n-1\rangle \leftrightarrow |x, n-1\rangle$, with a Rabi frequency $\Omega(t)$, is then turned on, and $\Omega(t)$ is slowly increased until $\Omega(t) >> 2g_0$. According to the adiabatic theorem the system will then evolve continuously from $|e, 0\rangle$ to $|g, 1\rangle$, through the process that is called *adiabatic population transfer* or *STIRAP*(stimulated Raman adiabatic passage). STIRAP is a highly valued technique within quantum optics, and is widely studied both theoretical and experimentally, as seen in for instance [12] or [13].

The recently described procedure is particularly interesting, since the eigenstate $|\psi_1^0\rangle$ contains no contribution from the state $|x, 0\rangle$, which in a realistic setting would be subject to non-negligible decay. Thus, by adiabatically evolving this eigenstate, we can produce a cavity photon, and at the same time ensure that practically no population is lost via the decay channel of $|x, 0\rangle$.

Having a method that enables us to nearly eliminate the effect of atomic decay will of course be beneficial to the photon emission efficiency of our Λ-model photon source. As the STIRAP-scheme of evolution is potentially very useful to us, we will take some time to compute the adiabatic criterions, for this process. According to (3.51) they can be found from

$$\left|\frac{\left\langle \psi_1^0\right| \dot{\psi}_1^+\right\rangle}{\omega_0-\omega_+}\right| << 1, \quad \left|\frac{\left\langle \psi_1^0\right| \dot{\psi}_1^-\right\rangle}{\omega_0-\omega_-}\right| << 1. \tag{3.52}$$

For $\Delta = 0$ and $n = 1$ we have

$$\cos\phi = \frac{1}{\sqrt{2}}, \quad \sin\phi = -\frac{1}{\sqrt{2}}, \tag{3.53}$$

and

$$\omega_0 - \omega_\pm = \frac{1}{\hbar}(E_0 - E_\pm) = \mp\frac{1}{\hbar}\sqrt{\beta^2+\gamma^2}. \tag{3.54}$$

This gives

$$\begin{aligned}\left\langle \psi_n^0\right| \dot{\psi}_n^+\right\rangle &= \left\langle \psi_n^0\right| \frac{d}{dt}\left|\psi_n^+\right\rangle \\ &= -\sin\theta\frac{d}{dt}\Big(\cos\phi\cos\theta\Big) + \cos\theta\frac{d}{dt}\Big(\cos\phi\sin\theta\Big) \\ &= \frac{1}{\sqrt{2}}\Big(-\sin\theta\frac{d}{dt}\Big(\cos\theta\Big) + \cos\theta\frac{d}{dt}\Big(\sin\theta\Big)\Big) \\ &= -\left\langle \psi_n^0\right| \dot{\psi}_n^-\right\rangle. \end{aligned} \tag{3.55}$$

Which means that the two inequalities in (3.52) are equivalent.
Calculating the derivatives

$$\begin{aligned}\frac{d}{dt}\sin\theta &= \frac{d}{dt}\Big(-\frac{\gamma}{\sqrt{\beta^2+\gamma^2}}\Big) = \dot{\gamma}\Big(-(\beta^2+\gamma^2)^{-\frac{1}{2}} + \gamma^2(\beta^2+\gamma^2)^{-1}\Big), \\ \frac{d}{dt}\cos\theta &= \frac{d}{dt}\Big(-\frac{\beta}{\sqrt{\beta^2+\gamma^2}}\Big) = \beta\gamma\dot{\gamma}(\beta^2+\gamma^2)^{-1}. \end{aligned} \tag{3.56}$$

and inserting these into (3.55) gives

$$\begin{aligned}\left\langle \psi_n^+\right| \dot{\psi}_n^0\right\rangle &= -\frac{1}{\sqrt{2}}(-\frac{\beta}{\sqrt{\beta^2+\gamma^2}})\dot{\gamma}\Big(-(\beta^2+\gamma^2)^{-\frac{1}{2}} + \gamma^2(\beta^2+\gamma^2)^{-1}\Big) + \frac{1}{\sqrt{2}}(-\frac{\gamma}{\sqrt{\beta^2+\gamma^2}})\beta\gamma\dot{\gamma}(\beta^2+\gamma^2)^{-1} \\ &= \frac{1}{\sqrt{2}}\Big(\frac{\beta\dot{\gamma}}{\sqrt{\beta^2+\gamma^2}}\Big(-(\beta^2+\gamma^2)^{-\frac{1}{2}} + \gamma^2(\beta^2+\gamma^2)^{-1}\Big) - \frac{\gamma\beta\gamma\dot{\gamma}}{\sqrt{\beta^2+\gamma^2}}(\beta^2+\gamma^2)^{-1}\Big) \\ &= -\frac{1}{\sqrt{2}}\frac{\beta\dot{\gamma}}{\beta^2+\gamma^2}. \end{aligned} \tag{3.57}$$

This finally results in the criterion for adiabatic evolution of the eigenstate $\left|\psi_1^0\right\rangle$

$$\left|\frac{\left\langle \psi_1^0\right| \dot{\psi}_1^+\right\rangle}{\omega_0-\omega_+}\right| = \left|\frac{\hbar}{\sqrt{2}}\frac{\beta\dot{\gamma}}{(\beta^2+\gamma^2)^{\frac{3}{2}}}\right| = \frac{g_0|\dot{\Omega}|}{(2g_0^2+\frac{\Omega^2}{2})^{\frac{3}{2}}} << 1. \tag{3.58}$$

Examining (3.58) we see that the rate of change of the atom-laser interaction $|\dot{\Omega}|$ must be kept under close surveillance. This should come as no surprise, as we are aiming for an adiabatic process, which will not allow for any sudden external changes. Additionally there is a relation between $|\dot{\Omega}|$ and Ω that must be preserved, in order to keep the evolution adiabatic. We observe that the stronger the atom-laser interaction Ω, the faster its allowed rate of change $|\dot{\Omega}|$. This means that when switching on the laser we must increase its strength extremely slow, but as Ω grows we are allowed to speed up the rate of change.

3.2.4 Numerical Simulations of STIRAP

Having seen how STIRAP can be applied to the Λ-model to produce a single cavity photon, while excluding the effect of atomic decay, we are now eager to study the system behavior during this procedure. This means that we must solve the Schrödinger equation in (3.21) - (3.23), with the initial conditions $c_g(t_i) = c_x(t_i) = 0$ and $c_e(t_i) = 1$, and a laser interaction $\Omega(t)$ that is turned on as the system is initialized, and then slowly rises during the system evolution.

As pointed out previously, the time varying laser profile $\Omega(t)$ undermines our prospects of finding an exact analytic solution describing the three-level system. We will therefore have to settle for numerical simulations. In our recent investigation of the STIRAP-procedure we considered the case where the decay of the excited atomic state and cavity mode are neglected altogether. This was necessary to enable an analytic analysis, but does not give a complete description of the system behavior. In the numerical simulations we are about to conduct we will take the effects of decay into account. This will cause less optimal circumstances for the STIRAP-scheme, but we will soon see that within realistic decay rate values, the destructive effects of including the decay channels will be small.

Before we can simulate the STIRAP-procedure we have to choose a specific laser profile $\Omega(t)$. We will begin this subsection with a presentation of the characteristics of a selected Gaussian profile $\Omega(t)$, followed by a short introduction to the fourth order Runge-Kutta method. Finally, we conclude this chapter with a discussion of numerical results.

A Gaussian Laser

There will be a number of different Ωs satisfying the inequality in (3.58). We will in the following assume that we are equipped with a laser for which $\Omega(t)$ is a Gaussian function of the form

$$\Omega(t) = \Omega_0 e^{-(\frac{t}{\Delta\tau})^2}, \quad \Omega_0 = kg_0, \quad k = \text{const.} \tag{3.59}$$

We will now take a closer look at the properties of this specific laser profile, and investigate the corresponding adiabatic criterion (3.58).

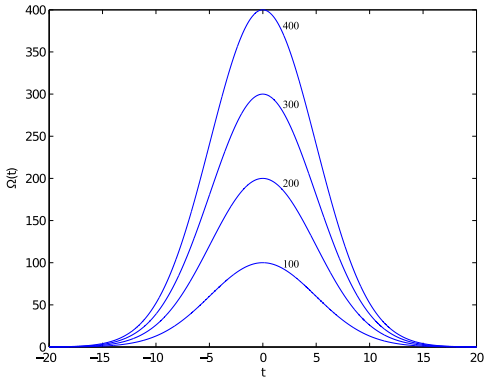

(a) The effect of varying Ω_0. Ω_0 is seen to equal the amplitude of $\Omega(t)$. Both $\Omega(t)$ and Ω_0 are measured in units of MHz.

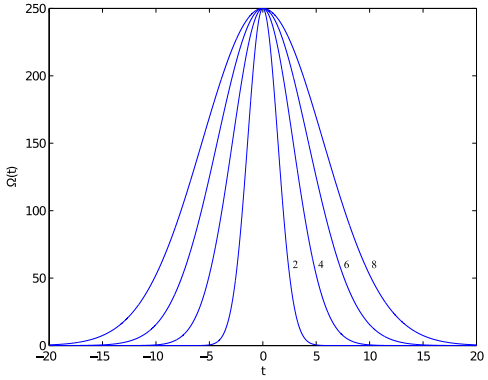

(b) The effect of varying $\Delta\tau$. Decreasing $\Delta\tau$ narrows the laser profile. $\Omega(t)$ is measured in units of MHz, while $\Delta\tau$ is measured in units of μs.

Figure 3.3: Figures demonstrating how the Gaussian-shaped laser pulse $\Omega(t)$ responds to changes in the parameters Ω_0 and $\Delta\tau$.

For a laser described by (3.59) we have essentially two laser parameters at our disposal, namely Ω_0 and $\Delta\tau$. Figure 3.3 shows how the laser profile is affected by variations in the above-mentioned quantities. From the expression in (3.59) it is clear that Ω_0 corresponds to the maximum strength of the laser pulse, and in Figure 3.3(a) we see how the peak of the function drops as Ω_0 decreases. $\Delta\tau$ determines the width of the laser pulse, and is related to the full width at half maximum through

$$\text{FWHM} = 2\sqrt{\ln 2\Delta\tau}. \tag{3.60}$$

Figure 3.3(b) shows how the laser pulse narrows as $\Delta\tau$ is decreased.

With the laser profile specified we can calculate the corresponding adiabatic criterion

on a more detailed level. For a Gaussian laser the inequality in (3.58) transforms into

$$\begin{aligned} g_0|\dot{\Omega}| &<< (2g_0^2 + \frac{\Omega^2}{2})^{\frac{3}{2}} \quad \Rightarrow \\ kg_0^2\Big| - \frac{2t}{\Delta\tau^2}\Big|e^{-(\frac{t}{\Delta\tau})^2} &<< \Big(2g_0^2 + \frac{k^2g_0^2}{2}e^{-2(\frac{t}{\Delta\tau})^2}\Big)^{\frac{3}{2}} \quad \Rightarrow \\ \frac{2k}{\Delta\tau^2}te^{-(\frac{t}{\Delta\tau})^2} &<< g_0\Big(2 + \frac{k^2}{2}e^{-2(\frac{t}{\Delta\tau})^2}\Big)^{\frac{3}{2}}. \end{aligned} \tag{3.61}$$

Let

$$g(t) = \frac{2k}{\Delta\tau^2}te^{-(\frac{t}{\Delta\tau})^2} \quad \text{and} \quad f(t) = g_0\Big(2 + \frac{k^2}{2}e^{-2(\frac{t}{\Delta\tau})^2}\Big)^{\frac{3}{2}}. \tag{3.62}$$

It is easily seen that

$$f(t) > 2^{\frac{3}{2}}g_0 \quad \text{for all } t. \tag{3.63}$$

Let $g(t_m)$ be the maximum value of $g(t)$. If we can see to it that

$$g(t_m) << 2^{\frac{3}{2}}g_0, \tag{3.64}$$

then (3.61) surely holds. Taking the derivative of $g(t)$ gives

$$g'(t) = \frac{2k}{\Delta\tau^2}e^{-(\frac{t}{\Delta\tau})^2}\Big(1 - \frac{2t^2}{\Delta\tau^2}\Big). \tag{3.65}$$

Setting $g'(t_m) = 0$ and solving for t_m leads to

$$t_m = \frac{\Delta\tau}{\sqrt{2}} \quad \Rightarrow \quad g(t_m) = \frac{\sqrt{2}k}{\Delta\tau}e^{-\frac{1}{2}}. \tag{3.66}$$

This finally leads to the adiabatic evolution criterion for a laser with Ω as given in (3.59)

$$\frac{g_0\Delta\tau}{k} >> \frac{1}{2\sqrt{e}}. \tag{3.67}$$

The inequality (3.67) tells us that for the process to be adiabatic, there has to be a certain relationship between the width $\Delta\tau$ and the amplitude $\Omega_0 = kg_0$ of the laser. For a given coupling g_0 between the atom and the cavity field, we get a lower limit on the size of $\Delta\tau$, compared to k. $\Delta\tau$, in turn, characterizes the profile amplitude Ω_0. Larger amplitude requires larger width. This reflects that for great changes in the Hamiltonian, the system will require more time in order to adjust adiabatically.

The Fourth Order Runge-Kutta Method

Having analytically examined the features of the Gaussian laser, and determined its criterion for adiabatic population transfer, we are ready to move on to the actual system dynamics. The solutions of the Schrödinger equation for the three-level system, as given in Equations (3.21) - (3.23), will be found numerically from the well-known fourth order Runge-Kutta method. We will here present the main features of the Runge-Kutta procedure for a set of two coupled ordinary differential equations. The generalization

to sets consisting of more than two equations should be obvious. A more thorough introduction to Runge-Kutta methods can be found in most introductory literature concerning differential equations, such as [7] and [5].

The fourth order Runge-Kutta method can be seen as an advanced version of Simpson's method, which in its turn stems from the very basic techniques of the midpoint and trapezoidal rules of numerical integration. Consider the two coupled ordinary differential equations

$$\frac{dy}{dt} = f(t, y, z), \qquad \frac{dz}{dt} = g(t, y, z), \tag{3.68}$$

with two simultaneous initial conditions

$$y(t_0) = y_0, \qquad z(t_0) = z_0. \tag{3.69}$$

Our objective is to solve the above problem for some finite time interval $t \in [a, b]$. We start by defining a step length, which is used to divide the region of interest into N subintervals

$$h = \frac{b-a}{N}. \tag{3.70}$$

The functions $y(t)$ and $z(t)$ may then be discretized

$$y_n = y(t_n) = y(t_0 + nh), \qquad z_n = z(t_n) = z(t_0 + nh). \tag{3.71}$$

Given the simultaneous function values at time t_n, their values at the next time step is approximated according to the fourth order Runge-Kutta algorithm as follows

$$\begin{aligned} y_{n+1} &= y_n + \frac{h}{6}(k_1 + 2k_2 + 2k_3 + k_4), \\ z_{n+1} &= z_n + \frac{h}{6}(l_1 + 2l_2 + 2l_3 + l_4). \end{aligned} \tag{3.72}$$

Where

$$\begin{aligned} k_1 &= f(t_n, y_n, z_n) & l_1 &= g(t_n, y_n, z_n) \\ k_2 &= f\Big(t_n + \frac{1}{2}h, y_n + \frac{1}{2}k_1, z_n + \frac{1}{2}l_1\Big) & l_2 &= g\Big(t_n + \frac{1}{2}h, y_n + \frac{1}{2}k_1, z_n + \frac{1}{2}l_1\Big) \\ k_3 &= f\Big(t_n + \frac{1}{2}h, y_n + \frac{1}{2}k_2, z_n + \frac{1}{2}l_2\Big) & l_3 &= g\Big(t_n + \frac{1}{2}h, y_n + \frac{1}{2}k_2, z_n + \frac{1}{2}l_2\Big) \\ k_4 &= f\Big(t_n + h, y_n + k_3, z_n + l_3\Big) & l_4 &= g\Big(t_n + h, y_n + k_3, z_n + l_3\Big). \end{aligned} \tag{3.73}$$

The idea is to estimate the desired function values for each time step using the function values from the previous time step and a weighted average of approximated slopes. We define k_1 and l_1 to be the slopes of respectively $y(t)$ and $z(t)$ at time t_n. We then use k_1 and l_1 to estimate the slopes at the midpoint $t_n + \frac{1}{2}h$ as given by k_2 and l_2. Next, we use these to make an even better forecast of the midpoint slopes given by k_3 and l_3. At last, equipped with the improved estimates of the midpoint slopes, k_3 and l_3, we

predict the slopes at t_{n+1} as described by k_4 and l_4. The slope approximations for each function are then weighted and summed up to form a sort of mean slope. Equation (3.72) shows the expressions $\frac{1}{6}(k_1 + 2k_2 + 2k_3 + k_4)$ and $\frac{1}{6}(l_1 + 2l_2 + 2l_3 + l_4)$ serves as approximated averages of the function slopes in the interval $[t_n, t_{n+1}]$.

The error of the fourth order Runge-Kutta method is, as the name suggests, bound by the the step size h to the fourth power,

$$|y(t_n) - y_n| \leq Ch^4, \quad C = \text{const.} \tag{3.74}$$

It should be emphasized that the classical Runge-Kutta method, as described above, is a brute force algorithm in terms of computational efficiency. There certainly exists other methods, such as predictor-corrector schemes, that would do the job more efficiently. These will however come at a considerably larger implementation cost than the standard Runge-Kutta. There are also several ways of improving the classical Runge-Kutta method by introducing some form of adaptive step control. These are procedures which, in a fairly intelligent manner, adjusts the step size of the computations according to how well behaved the functions are. In regions where the functions are well mannered we can leap through with a few steps, while in regions with a lot of action we need to slow down in order to capture the details. Such a method could lessen the computation time substantially without diminishing the accuracy.

The primary intentions of our numerical efforts are to give a qualitative description of a quantum mechanical system interacting with its environment. We will therefore not concern our selves with the technicalities of numerical algorithms. The brute force method is sufficient for our purposes. An implementation of the fourth order Runge-Kutta method for the three-level Λ-system can be found in Appendix B.

Numerical Results

In the remainder of Chapter 3 we will concentrate on the results from the numerical simulations of the Scrödinger equation, using a Gaussian laser to perform the STIRAP evolution. We will present plots, showing how the populations of the three levels $|g, 1\rangle, |e, 0\rangle$ and $|x, 0\rangle$ behave as functions of time, for different areas of parameter space. We emphasize that while realistic values of the atom-cavity coupling and the various decay rates are usually in the order of 10 MHz, we will for the sake of demonstration allow the typical parameter values to be greatly exceeded.

To get an idea of how the STIRAP-scheme will look under ideal circumstances, we will start by looking into the system behavior without influence from the environment. Subsequently we will study the isolated effects of both atomic decay and cavity mode decay, before both decay processes are set to work simultaneously.

Neglecting Environmental Interaction We first consider the case where the effects of system decay are entirely neglected, so $\kappa = \gamma_x = 0$. This coincides with the situation for which we derived the adiabatic population transfer, from state $|e, 0\rangle$ to $|g, 1\rangle$. Of course, turning off the environmental interaction will inhibit the model from emitting photons, so in this part of parameter space we do not have a single photon source.

However, the setting is well suited for investigating how the STIRAP-scheme behaves under ideal circumstances.

As discussed in the previous section, the Gaussian laser has two parameters which we are free to control, namely the amplitude $\Omega_0 = kg_0$ and the width of the laser pulse $\Delta\tau$. The latter is directly related to the adiabatic criterion (3.67), as it controls how rapidly the laser pulse $\Omega(t)$ increases with time. Making $\Delta\tau$ large corresponds to a slowly rising laser pulse, which agrees well with an adiabatic evolution. This means that the larger we make $\Delta\tau$ the less transient population will be found in the undesirable excited state $|x, 0\rangle$.

As can be concluded from the expression for $|\psi_1^0\rangle$ in (3.38), the ratio of the trigonometric coefficients in (3.39) is equivalent to the ratio of the populations in the contributing states $|e, 0\rangle$ and $|g, 1\rangle$

$$\frac{|\langle e, 0| \psi^0\rangle|^2}{|\langle g, 1| \psi^0\rangle|^2} = \frac{4g_0^2}{\Omega^2}. \tag{3.75}$$

From the expression in (3.75) we see that the population transfer from $|e, 0\rangle$ to $|g, 1\rangle$ will be at its maximum when Ω reaches its maximum value Ω_0. It is evident that the transfer can be made arbitrarily good by increasing Ω_0. This is confirmed by the simulations.

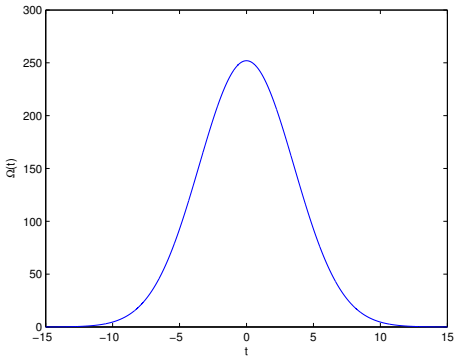

(a) Laser profile.

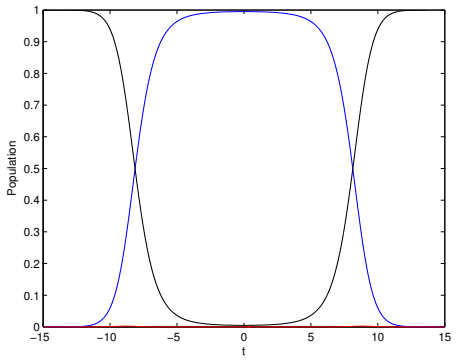

(b) The population evolution without any form of decay.

Figure 3.4: (a) The laser profile $\Omega(t) = kg_0e^{-(t/\Delta\tau)^2}$, with parameter values $k = 28$, $g_0 = 9\pi$, $\Delta\tau = 5$. (b) The resulting behavior of the state populations during the STIRAP-procedure. Time is measured in units of μs, while g_0 and Ω are given in MHz. The black, blue and red graphs describe the populations of the states $|e, 0\rangle$, $|g, 1\rangle$ and $|x, 0\rangle$, respectively.

Figure 3.4(b) shows the results for selected values of the parameters Ω_0 and $\Delta\tau$. It demonstrates how the population in $|x, 0\rangle$ is kept inferior during the whole process, peaking at the order of 10^{-3}, as predicted by the adiabatic criterion. As expected, the amount of population transferred to state $|g, 1\rangle$ reaches a maximum at $\Omega(t) = \Omega_0$. The strength of the atom-laser interaction then slowly starts to fall off. Since the laser profile is symmetric in time, this will reverse the STIRAP-process, adiabatically leading the

population back to the initial state $|e,0\rangle$.

We can imagine that by rapidly turning off the laser when the population transfer is at its peak, we could trap the system in the state $|g,1\rangle$, preventing it from adiabatically evolving back into the initial state. Repeating this process we could in theory produce states of arbitrary photon number.

Including Environmental Decay The time has come to look at more realistic set-ups, where effects on the system from its environment are taken into account. We will start by letting the decay of the excited atomic state make its entrance, closely followed by a solo act from the decay of the cavity mode. Our investigation will end in a duet, where both decaying channels are at work.

With the incorporation of a final lifetime of the atomic state $|x\rangle$, our atom-cavity system will still not constitute a single photon source. Nevertheless, a characterization of how this decay channel affects the system behavior can be very useful. The numerical results from STIRAP-evolution including only atomic decay are displayed in Figure 3.6 on page 63, for increasing decay rate γ_x. Enhancing γ_x is seen to cause a loss of population from the system. The peak in the population profile of $|g,1\rangle$ is lowered, but is otherwise not dramatically affected. We also register that the population of $|x,0\rangle$ is kept at a minimum, so the adiabatic scheme is still working efficiently. At first glance, it might therefore seem strange that the decay of state $|x,0\rangle$ could possibly have a significant effect on the population of $|g,1\rangle$. We must then keep in mind, that the trick of the adiabatic population transfer is not really to transfer population directly from $|e,0\rangle$ to $|g,1\rangle$. No matter what we do, there is no physical coupling between these to states, which means that when population is transferred between the two, it must go via the state $|x,0\rangle$. The adiabatic scheme however, utilizes the fact that the decay of $|x,0\rangle$ depends on the size of the state population. By making the transition from $|e,0\rangle$ via $|x,0\rangle$ to $|g,1\rangle$ very slowly, this population can be kept at a minimum, almost eliminating the atomic decay. We note that due to the efficiency of the STIRAP-procedure, the decay rate γ_x must reach unrealistically large values, before significant losses are seen.

The results of isolating the impact of a leaking cavity mode are displayed in Figure 3.7 on page 64, for decreasing decay rate κ. We see that the population of $|g,1\rangle$ is relatively sensitive to changes in κ as opposed to changes in γ_x. This is as we should expect, since the adiabatic evolution serves to nearly decouple the state $|x,0\rangle$ from the system. Having turned on the cavity mode decay, the Λ-system is finally transformed into a single photon source. In order to get a high photon emission probability, we must get the decay rate high enough for the photon to escape before the Gaussian laser strength starts to recede, adiabatically transferring the system back to the initial state $|e,0\rangle$. Since the possibility of population loss through atomic decay is not considered here, the amount of population sitting in the state $|e,0\rangle$ at the end of the evolution, is a direct measure of the total photon emission probability. From the plots in Figure 3.7 we observe that for increasing κ, the final population of $|e,0\rangle$ quickly approaches zero, giving a photon emission probability close to one.

Figure 3.5(a) shows the temporal photon profile $R(t)$, corresponding to the different evolutions displayed in Figure 3.7. We see how the photon profile changes shape as the

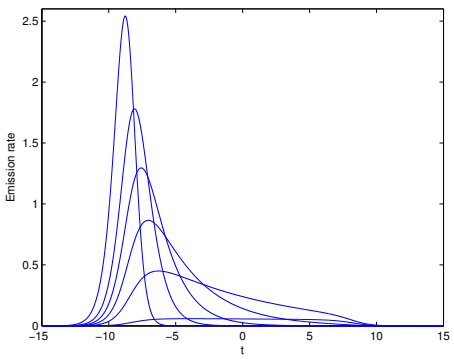

(a) The temporal photon profiles resulting from the evolutions displayed in Figure 3.7.

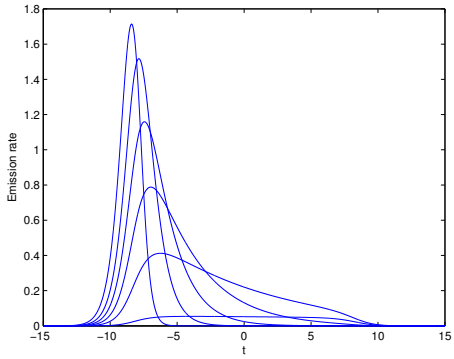

(b) The temporal photon profiles resulting from the evolutions displayed in Figure 3.8.

Figure 3.5: The plots show the temporal photon profile $R = 2\kappa|c_g|^2$, resulting from the STIRAP-evolutions shown in Figures 3.7 and 3.8. (a) The photon shape resulting from isolating the cavity decay. (b) The photon profile resulting from including both cavity decay and atomic decay. In both (a) and (b) the profile is seen to rise, narrow and shift towards earlier times, for increasing values of the decay rate κ. Time is measured in units of μs.

cavity mode decay rate increases. The peak of the profile, where photon emission is at its most probable, shifts toward earlier times for larger decay rates. This matches our intuition; the time of photon emission should be sooner for higher cavity mirror transparency.

In the derivation of the STIRAP-evolution, all system decay was neglected. When introducing the different decaying channels in the numerical simulations, we should therefore expect that the adiabatic population transfer from state $|e,0\rangle$ to $|g,1\rangle$, nearly avoiding the state $|x,0\rangle$, will possibly not be as successful as in the case of no decay. For larger values of κ, this is reflected in a slight increase in the state population of the undesired state $|x,0\rangle$. This hints that in the case where both atomic and cavity mode decay are included, the best result in terms of photon emission probability will be found when κ is large enough for the cavity photon to escape before the system population is adiabatically reversed, but still small enough not to cause a significant population in the decaying state $|x,0\rangle$.

Finally activating both decay channels, we will have a look at the complete system behavior. Figures 3.8 on page 65 shows selected results of including both decay channels $|x,0\rangle \rightarrow |g,0\rangle$ and $|g,1\rangle \rightarrow |g,0\rangle$, for a constant value of γ_x and increasing values of κ. The separate effects of each of the decay channels are still clearly recognizable, which indicates that these two processes are not influenced by each other. The accompanying temporal photon profiles for the simulations of Figure 3.8 are seen in Figure 3.5(b). Comparing with the profiles of pure cavity decay in Figure 3.5(a), we observe that about the only consequence of introducing the additional effect of atomic decay, is to overall lower the photon emission probability, but otherwise leaving the photon profiles unchanged.

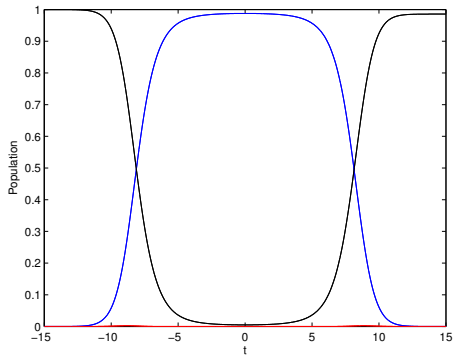

(a) $\kappa = 0$, $\gamma_x = \pi$

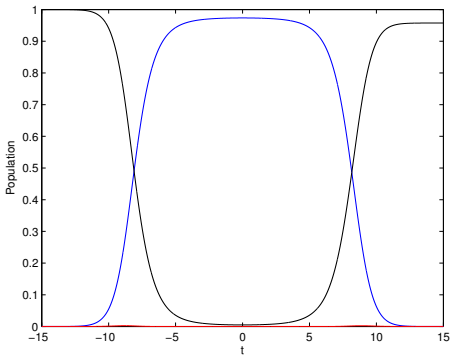

(b) $\kappa = 0$, $\gamma_x = 3\pi$

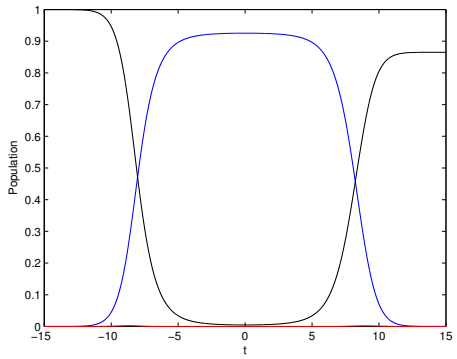

(c) $\kappa = 0$, $\gamma_x = 10\pi$

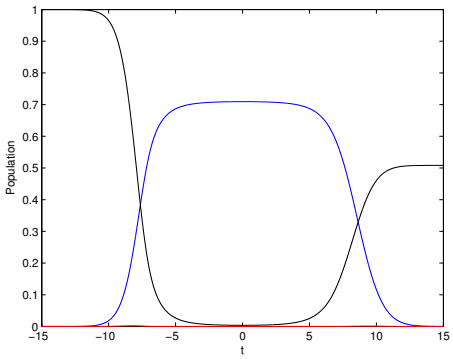

(d) $\kappa = 0$, $\gamma_x = 50\pi$

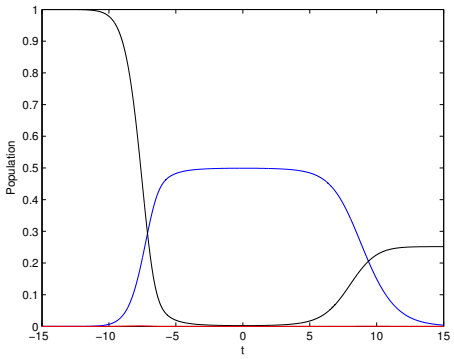

(e) $\kappa = 0$, $\gamma_x = 120\pi$

Figure 3.6: The list of figures show the isolated effect of atomic decay, for increasing decay rate γ_x. The applied laser profile is given by $\Omega(t) = kg_0e^{-(t/\Delta\tau)^2}$, with parameter values $k = 28$, $g_0 = 9\pi$, $\Delta\tau = 5$. Time is measured in units of μs, while g_0, Ω and γ_x are given in MHz. The black, blue and red graphs describe the populations of the states $|e, 0\rangle$, $|g, 1\rangle$ and $|x, 0\rangle$, respectively.

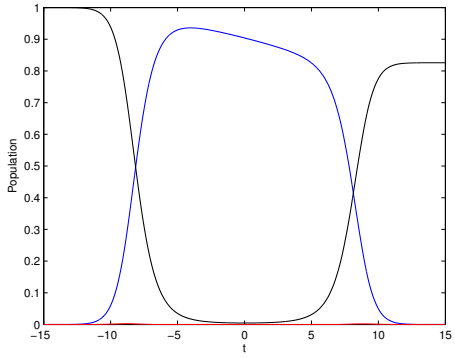

(a) $\kappa = 0.01\pi$, $\gamma_x = 0$

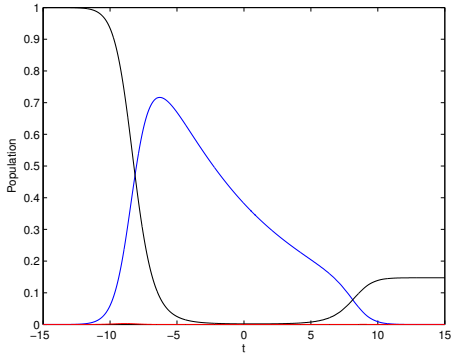

(b) $\kappa = 0.1\pi$, $\gamma_x = 0$

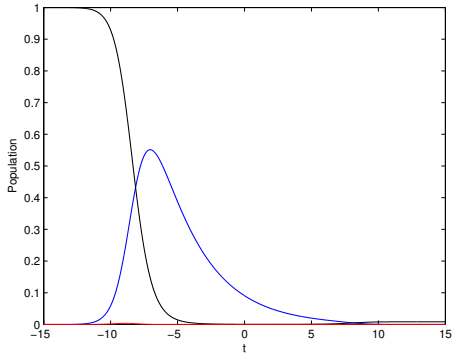

(c) $\kappa = 0.25\pi$, $\gamma_x = 0$

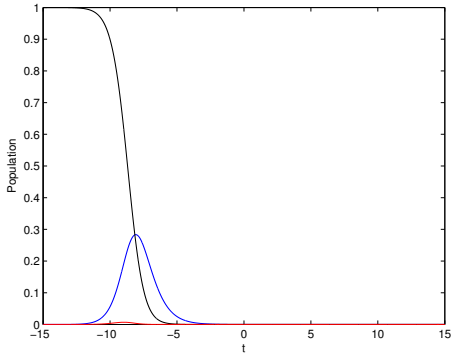

(d) $\kappa = \pi$, $\gamma_x = 0$

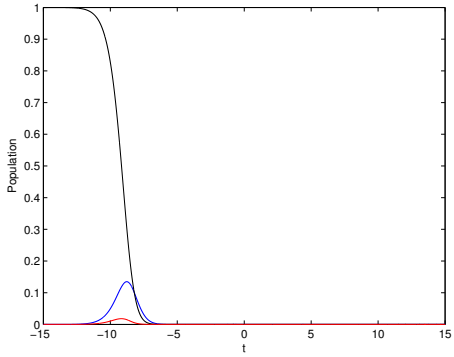

(e) $\kappa = 3\pi$, $\gamma_x = 0$

Figure 3.7: The list of figures show the isolated effect of a decaying cavity mode, for increasing values of decay rate κ. The applied laser profile is given by $\Omega(t) = kg_0 e^{-(t/\Delta\tau)^2}$, with parameter values $k = 28$, $g_0 = 9\pi$, $\Delta\tau = 5$. Time is measured in units of μs, while g_0, Ω and κ are given in MHz. The black, blue and red graphs describe the populations of the states $|e, 0\rangle$, $|g, 1\rangle$ and $|x, 0\rangle$, respectively.

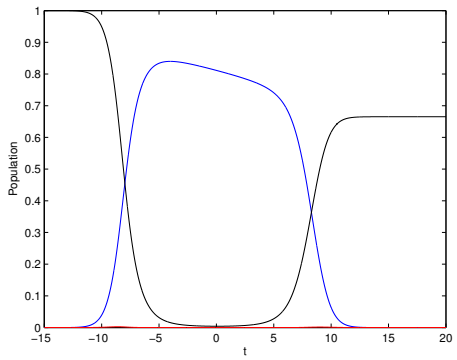

(a) $\kappa = 0.01\pi$, $\gamma_x = 15\pi$

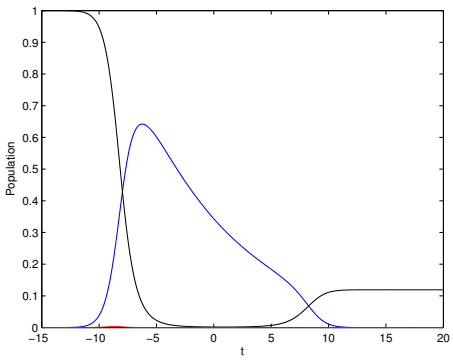

(b) $\kappa = 0.1\pi$, $\gamma_x = 15\pi$

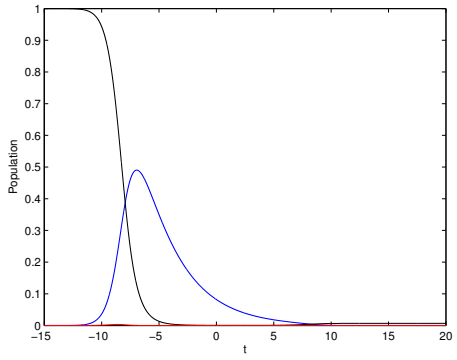

(c) $\kappa = 0.25\pi$, $\gamma_x = 15\pi$

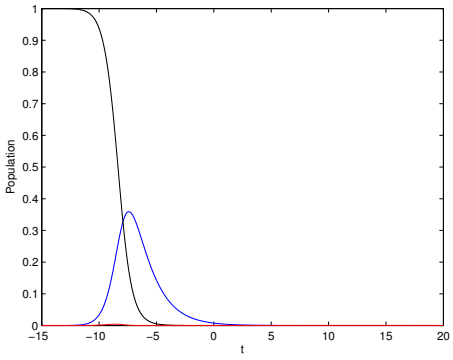

(d) $\kappa = 0.5\pi$, $\gamma_x = 15\pi$

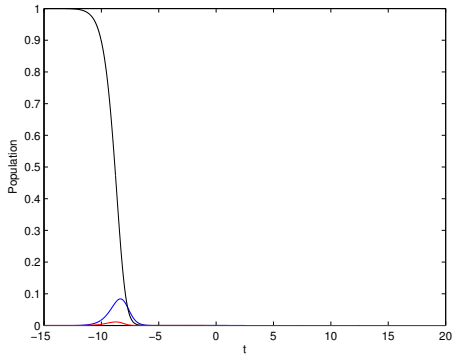

(e) $\kappa = 3\pi$, $\gamma_x = 15\pi$

Figure 3.8: The list of figures displays the results from including both atomic decay and decay of the cavity mode, for increasing values of the cavity decay rate κ. The atomic decay rate is kept content at $\gamma_x = 15\pi$. The applied laser profile is given by $\Omega(t) = kg_0e^{-(t/\Delta\tau)^2}$, with parameter values $k = 28$, $g_0 = 9\pi$, $\Delta\tau = 5$. Time is measured in units of μs, while g_0, Ω, γ_x and κ are given in MHz. The black, blue and red graphs describe the populations of the states $|e, 0\rangle$, $|g, 1\rangle$ and $|x, 0\rangle$, respectively.

With this discussion of numerical results we consider Chapter 3 to be completed. Within its pages we have introduced new system features, in the form an additional atomic energy level and the effect of an adjustable laser. We have seen how the temporal photon profile and the total emission probability can be analytically described in the bad-cavity limit, giving high emission probability for large laser exposure $\int_0^\infty \Omega(t)dt$. Thereafter we demonstrated how the Λ-system can be evolved according to the so called STIRAP-procedure, producing a cavity photon and at the same time nearly eliminating population loss from atomic decay. Finally, we have presented a numerical study of the STIRAP-evolution, solving the Schrödinger equation with a Gaussian laser profile.

In the next chapter we expand our Λ-model even further, and explore the consequences of incorporating new a kind of incoherent transitions. A kind that we have not yet encountered.

Chapter 4

The Full Master Equation and Monte Carlo Simulations

In Chapter 3 we studied a three-level Λ-system, consisting of three atomic levels, coupling to the electromagnetic mode of an optical cavity, and a laser. Interactions between the system and its environment were included through the decay of the excited atomic level and the cavity mode, respectively. However, we only allowed for the system to decay to a state $|g, 0\rangle$, a state which is not, through the effective Hamiltonian, actively participating in the system evolution. As was demonstrated in Chapter 2, the system evolution described by the effective Schrödinger equation (2.15) will then suffice. If we want to include incoherent transitions to states whose evolution is in fact described by $\hat{H}_{\text{eff}}$, we must turn to the systems full master equation.

We will in this chapter take another look at the decaying Λ-system, this time allowing the excited atomic state to decay to both $|g, 0\rangle$ and $|e, 0\rangle$, as depicted in Figure 4.1. The system dynamics is then be described by the full master equation in the so called Lindblad form

$$\frac{\partial}{\partial t}\hat{\rho}^S = -\frac{i}{\hbar}(\hat{H}_{\text{eff}}\hat{\rho}^S - \hat{\rho}^S\hat{H}_{\text{eff}}^\dagger) + \hat{\mathcal{L}}_j\hat{\rho}^S, \tag{4.1}$$

instead of the effective Schrödinger equation. This equation can be solved numerically by means of standard integration methods, such as Runge-Kutta methods. There is, however, another possibility which offers more physical insight: the Monte Carlo wavefunction method. The idea of using a Monte Carlo approach to solve dissipative problems in quantum optics was introduced in several different articles in the early 1990's, see for instance [17], [3].

In the following we will present a procedure for simulating the dynamics of an open quantum system using a Monte Carlo method, as suggested by Mølmer, Castin and Dalibard [17] . We will start with a short introduction to the concept of Monte Carlo algorithms, followed by a description of the procedure and a justification of the validity of the method. We will then go on to discuss the specifics of how to simulate our three-level system, the physical significance of the Monte Carlo method, and finish with a discussion of the final results.

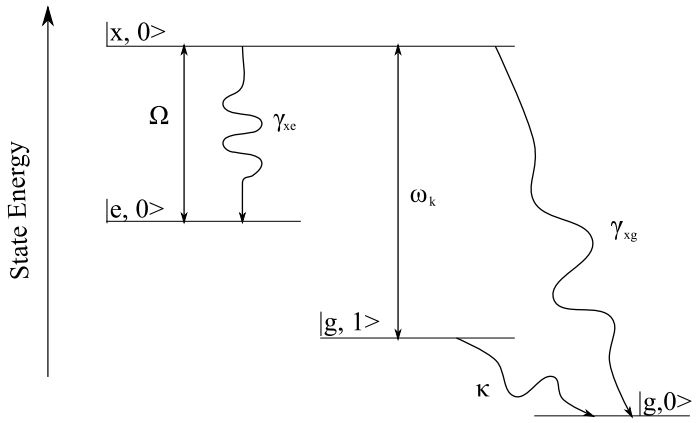

Figure 4.1: Three-level system interacting with its environment, here represented by the state $|g, 0\rangle$. The rippled arrows indicate incoherent transitions due to effects of the environment, while the straight arrows indicate coherent transitions driven by the laser and the cavity field.

4.1 Monte Carlo Methods

Monte Carlo methods are a class of numerical algorithms for simulating stochastic processes, such as the evolution of thermo dynamical or economical systems. The methods aim to give a numerical estimate of probability distributions and corresponding expectation values. The concept was developed in the 1940's by Ulam and Metropolis [21]. The basic idea of all Monte Carlo methods is to numerically generate a large number of independent realizations of the stochastic process in question, with the help of a random number generator. Expectation values are then estimated from these samples. The method relies upon a theorem in probability theory, known as the *strong law of large numbers*.

Let X be a random variable with expectation value $A = E(X)$. We generate a sample of n independents random variables $X_1, X_2, \ldots, X_n$, with equal distributions. The strong law of large numbers states that

$$\langle A \rangle_n = \frac{1}{n} \sum_{i=1}^{n} X_i \to A \quad \text{for} \quad n \to \infty. \tag{4.2}$$

The quantities A and $\langle A \rangle_n$ are often referred to as the population mean and sample mean. For large n we can approximate the population mean with the sample mean

$$A \approx \langle A \rangle_n . \tag{4.3}$$

Most numerical simulations are of little or no use without knowledge of the accuracy of their results. In the case of Monte Carlo methods we are interested in how well the estimated sample mean $\langle A \rangle_n$ (4.2) approximates the actual mean of the population A. The sample mean can in itself be regarded as a random variable, with a corresponding

probability distribution. The standard deviation of this distribution if often referred to as the *standard error*, and is a common measure of the error in a Monte Carlo simulation. The standard error is given by

$$\Delta_{STD} = \frac{\sigma}{\sqrt{n}} \approx \frac{s}{\sqrt{n}}, \qquad s^2 = \frac{1}{n-1}\sum_{i=1}^{n}(X_i - \langle A \rangle_n)^2. \tag{4.4}$$

Where σ is the true standard deviation of the population, s is the standard deviation of the sample and n is the number of observations in the sample. Since we hardly ever know the true standard deviation of the population σ, it is commonly approximated by the standard deviation of the sample s. One should however note that the above estimate for the standard error is not a very precise one, and will often not suffice in cases where the used sample is even moderately correlated. A derivation of the standard error and further reading on more sophisticated methods for error analysis in Monte Carlo methods can be found in [7].

The applications for Monte Carlo methods are vast; multidimensional integration, random walks and variational methods, to mention some. It is therefore difficult to give a very specific description of the typical Monte Carlo algorithm without specifying what system is being modeled. Still, most of the methods tend to follow a certain recipe

1. Define a domain of possible inputs.

2. Generate inputs with the help of a random number generator according to a probability distribution over the domain.

3. Use the average properties of the samples as an estimate for the quantity of interest.

Physicists tend to be found of the Monte Carlo concept, as it in many cases gives associations to the process of doing physical experiments. Imagine wanting to measure an observable, for instance the average energy of the particles in a gas. In dealing with large systems it will rarely be possible to actually measure the true average. What we do is measure the energy of a fairly large sample of the particles, and say that if the sample is large enough, then the sample average will be a good estimate of the actual average energy. This largely resembles the principles behind a Monte Carlo simulation. Instead of simulating the dynamics of the total system deterministically, we make due with a sample of the possible realizations of the system, and approximate the actual means of the system with the means of the sample. Monte Carlo methods are widely applied in the world of physics. They make a powerful tool for dealing with systems of great complexity, when more standard numerical methods become to time-consuming or to cumbersome.

4.2 Monte Carlo Wavefunctions and The Lindblad Equation

We will now try to get an understanding of how the Monte Carlo concept can be useful in the case of simulating the evolution described by the Lindblad equation (4.1). It turns out that this equation can be assigned a stochastic interpretation. The Lindblad equation describes the piecewise deterministic evolution of a pure normalized quantum state, undergoing a stochastic time evolution. The first term of Equation (4.1) is associated with a continuous time evolution, governed by the effective Hamiltonian, while the last term is associated with an incoherent jumping behavior. It is in this regard the jump superoperator has earned its name. This interpretation opens for the possibility of using Monte Carlo simulations. By generating a large number of realizations of the system evolution, we can estimate any desired observable by calculating the average of the observable from the generated realizations. Each distinct realization is referred to as a *Monte Carlo wavefunction*. In the following we will outline an approach for how to model a large number of Monte Carlo wavefunctions, which will on average result in a process coinciding with the one described by Equation (4.1).

4.2.1 The Procedure

Assume that at time t the system is in the normalized state $|\Psi(t)\rangle$. In order to evolve the system state to the next time step $|\Psi(t+\delta t)\rangle$ we have to decide between two different types of evolution.

1. The state $|\Psi(t)\rangle$ evolves continuously with the effective Hamiltonian, according to the Schrödinger equation.
2. The state $|\Psi(t)\rangle$ makes an incoherent quantum jump as described by one of the Lindblad operators.

To determine which of the two paths to choose we start by calculating the evolved state $|\psi(t+\delta t)\rangle$ that would result from the evolution of the effective Hamiltonian. From first order perturbation theory the time evolution operator is

$$\hat{U}_{\text{eff}} = 1 - \frac{i}{\hbar}\int_{t}^{t+\delta t} \hat{H}_{\text{eff}}(t')dt'. \tag{4.5}$$

Thus for sufficiently small δt the effective Hamiltonian gives the time evolution

$$|\psi(t+\delta t)\rangle = \left(1 - \frac{i\delta t}{\hbar}\hat{H}_{\text{eff}}(t)\right)|\psi(t)\rangle\,. \tag{4.6}$$

As mentioned in Section 2.1, the non-hermiticity of the effective Hamiltonian will cause the norm of the state to decrease with time. The squared norm of the state in (4.6) gives a measure of the probability for the system to make at jump at time $t+\delta t$

$$\delta p = 1 - \langle\psi(t+\delta t)|\,\psi(t+\delta t)\rangle\,. \tag{4.7}$$

This is where the Monte Carlo idea is used. We choose the system evolution path in accordance with the jumping probability δp, by the help of a random number generator. We simply draw a random number $\eta \in [0,1]$ from a uniform distribution. If the system does not jump we renormalize before iterating further.

If $\eta > \delta p$ the state is evolved according to the Schödinger equation with the effective Hamilton operator, here denoted by the use of the corresponding effective time evolution operator $\hat{U}_{\text{eff}}$

$$|\psi(t+\delta t)\rangle = \hat{U}_{\text{eff}} |\psi(t)\rangle . \tag{4.8}$$

Resulting in the system state

$$|\Psi(t+\delta t)\rangle = \frac{|\psi(t+\delta t)\rangle}{\sqrt{\langle\psi(t+\delta t)|\ \psi(t+\delta t)\rangle}}. \tag{4.9}$$

If $\eta < \delta p$ a quantum jump occurs, and the system decays through one of the possible decay channels. Given that the system has more than one decay channel, we must now decide through which channel the jump is going to happen. The probability for a jump to occur through channel i at time $t+\delta t$ is

$$\delta p_i = 2\gamma_i \langle\Psi(t)| \hat{\alpha}_i^\dagger \hat{\alpha}_i |\Psi(t)\rangle \, \delta t. \tag{4.10}$$

The term $\langle\psi(t)| \hat{\alpha}_i^\dagger \hat{\alpha}_i |\psi(t)\rangle$ picks out the population of the decaying system state, while the factor $2\gamma_i$ originates from the exponential decay of the state. Taking the sum over all the possible decay channels i gives a second expression for the total probability for having a jump at $t+\delta t$

$$\delta p = \sum_i \delta p_i = \sum_i 2\gamma_i \langle\Psi(t)| \hat{\alpha}_i^\dagger \hat{\alpha}_i |\Psi(t)\rangle \, \delta t. \tag{4.11}$$

The conditional probability that the system will decay through channel i given that a jump actually occurs at time $t+\delta t$ is

$$\delta p(i|t+\delta t) = \frac{\delta p_i}{\delta p}. \tag{4.12}$$

In order to determine through which channel i the system will decay we divide the interval $[0,1]$ into subintervals with lengths $\delta p(i|t+\delta t)$, one for each possible decay channel. Then a new random number $\rho \in [0,1]$ is drawn. The interval containing ρ will be the one corresponding to the chosen decay. Assuming that the i'th channel is chosen, the state $|\Psi(t)\rangle$ will make a sudden transition to $\hat{\alpha}_i |\Psi(t)\rangle$. This results in the normalized system state

$$|\Psi(t+\delta t)\rangle = \frac{\hat{\alpha}_i |\Psi(t)\rangle}{\sqrt{\langle\Psi(t)| \hat{\alpha}_i^\dagger \hat{\alpha}_i |\Psi(t)\rangle}}. \tag{4.13}$$

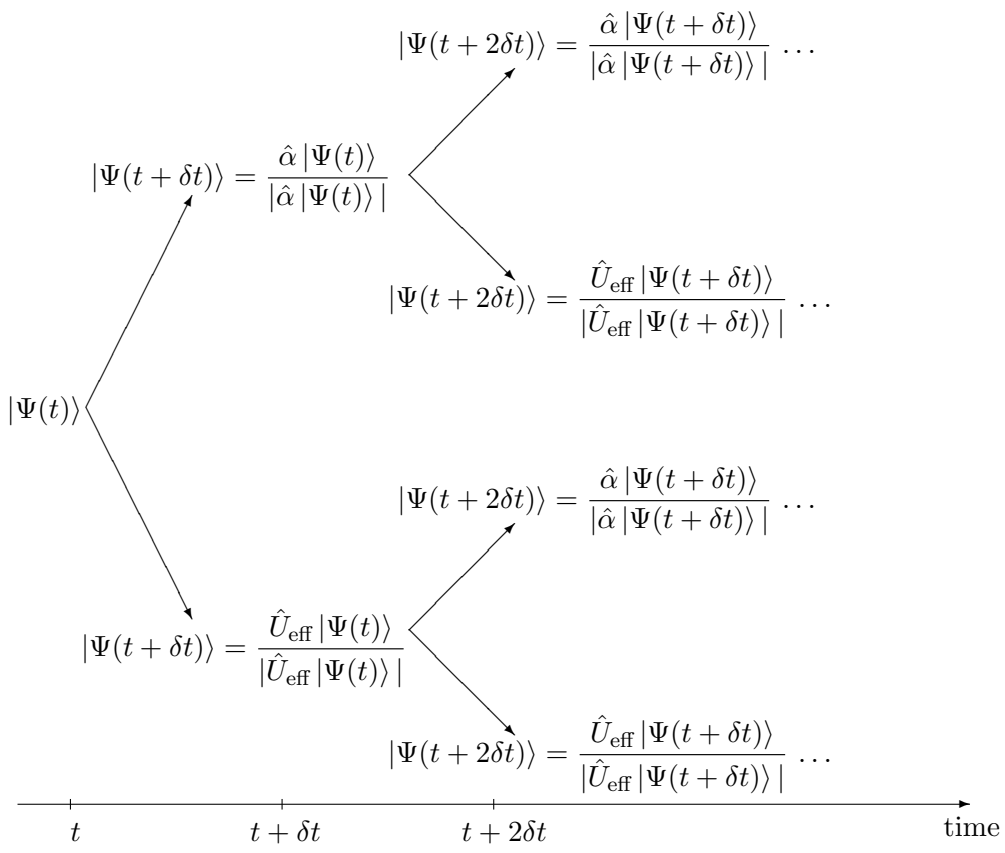

Figure 4.2: The figure illustrates the stochastic time evolution of a single Monte Carlo wavefunction.

The above procedure will be repeated until the chosen final time $t_{\max}$ has been reached. A schematic presentation of the process is given in Figure 4.2. It shows the evolution of a Monte Carlo wavefunction of a system starting out in the state $|\Psi(t)\rangle$, with only one possible decay channel described by the operator $\hat{\alpha}$. At time $t_{\max}$ we have completed a Monte Carlo wavefunction. The system is then reinitialized and the process repeated until the desired number of wavefunction samples has been realized.

Finally, when the required collection of wavefunctions have been constructed, we are ready to calculate the system observables. The density operator is determined by

$$\rho^S(t) = \frac{1}{N}\sum_{n=1}^{N} |\Psi_n(t)\rangle\,\langle\Psi_n(t)|\,, \tag{4.14}$$

where n indexes the different Monte Carlo simulations. The expectation values of all the system observables can then be found from

$$\langle A(t)\rangle = Tr(\rho^S \hat{A}) = \frac{1}{N}\sum_{n=1}^{N} \langle \Psi_n(t)|\, \hat{A}\, |\Psi_n(t)\rangle\,. \tag{4.15}$$

We have in this description taken the system to be initialized in a pure state. In the most general case the system would start out in a statistical mixture of pure states

$$\hat{\rho}(0) = \sum_j p_j\, |\Psi_j\rangle\, \langle\Psi_j|\,. \tag{4.16}$$

In this case the initial system state must be chosen by the help of random numbers in the beginning of each Monte Carlo cycle, according to the probabilities p_j.

4.2.2 Unravelling of the Master Equation

To prove that the procedure described in the previous subsection is actually equivalent to a process described by the master equation we will closely follow the steps of the proof [17]. We must show that the expectation value of the computed density operator coincides with $\hat{\rho}^S(t)$ at all times t. That is, it must satisfy the Lindblad master equation (4.1).

In Section 4.2.1 we described how to calculate all system observables by first generating a large number of Monte-Carlo wavefunctions, each representing a distinct realization of the system dynamics, within the given time interval. The different physical quantities are then computed as functions of time by averaging over all the realizations. It seems reasonable to assume that for a very large number of realizations, the generated Monte Carlo wavefunctions will eventually map out the whole sample space of the system evolution. The number of occurrences found for each possible outcome, at each time step, will reflect that outcomes probability. Trusting this assumption, the Monte Carlo algorithm described in Section 4.2.1 will be equivalent to calculating the average of the observables from all possible outcomes, at each time step.

Let $|\Psi(t)\rangle$ be one particular Monte Carlo realization of the system state at time t, and denote the corresponding realization of the system density operator as $\hat{\sigma}(t) = |\Psi(t)\rangle\,\langle\Psi(t)|$. Let $\langle\hat{\sigma}(t)\rangle$ denote the averaging over many Monte Carlo realizations. Relying on the assumption above, the Monte Carlo procedure corresponds to propagating the density operator according to

$$\overline{\hat{\sigma}(t+\delta t)} = (1-\delta p)\frac{|\psi(t+\delta t)\rangle\,\langle\psi(t+\delta t)|}{\langle\psi(t+\delta t)|\,\psi(t+\delta t)\rangle} + \delta p \sum_i \delta p_i(i|t+\delta t)\frac{\hat{\alpha}_i\,|\Psi(t)\rangle\,\langle\Psi(t)|\,\hat{\alpha}_i^\dagger}{\langle\Psi(t)|\,\hat{\alpha}_i^\dagger\hat{\alpha}_i\,|\Psi(t)\rangle}, \tag{4.17}$$

where the bar denotes the expectation value of $\hat{\sigma}(t+\delta t)$ from one Monte Carlo realization.

This can be simplified by using the following relations from the previous subsection

$$\begin{aligned}
&\langle\psi(t+\delta t)|\,\psi(t+\delta t)\rangle = 1-\delta p,\\
&\delta p_i(i|t+\delta t) = \frac{\delta p_i}{\delta p},\\
&\langle\Psi(t)|\,\hat{\alpha}_i^\dagger\hat{\alpha}_i\,|\Psi(t)\rangle = \frac{1}{2\gamma_i}\frac{\delta\rho_i}{\delta t}.
\end{aligned} \tag{4.18}$$

Which gives

$$\begin{aligned}
\overline{\hat{\sigma}(t+\delta t)} &= |\psi(t+\delta t)\rangle\langle\psi(t+\delta t)| + \sum_i 2\gamma_i\hat{\alpha}_i\,|\Psi(t)\rangle\langle\Psi(t)|\,\hat{\alpha}_i^\dagger\delta t\\
&= \Big(1-\frac{i\delta t}{\hbar}\hat{H}_{\text{eff}}(t)\Big)\,|\Psi(t)\rangle\langle\Psi(t)|\,\Big(1+\frac{i\delta t}{\hbar}\hat{H}_{\text{eff}}^\dagger(t)\Big) + \sum_i 2\gamma_i\hat{\alpha}_i\,|\Psi(t)\rangle\langle\Psi(t)|\,\hat{\alpha}_i^\dagger\delta t\\
&= \Big(1-\frac{i\delta t}{\hbar}\hat{H}_{\text{eff}}(t)\Big)\Big(\hat{\sigma}(t)+\frac{i}{\hbar}\hat{\sigma}(t)\hat{H}_{\text{eff}}^\dagger(t)\delta t\Big) + \sum_i 2\gamma_i\hat{\alpha}_i\hat{\sigma}(t)\hat{\alpha}_i^\dagger\delta t\\
&= \hat{\sigma}(t) + \frac{i}{\hbar}\hat{\sigma}(t)\hat{H}_{\text{eff}}^\dagger(t)\delta t - \frac{i}{\hbar}\hat{H}_{\text{eff}}(t)\hat{\sigma}(t)\delta t + \sum_i 2\gamma_i\hat{\alpha}_i\hat{\sigma}(t)\hat{\alpha}_i^\dagger\delta t + \mathcal{O}(\delta t^2)
\end{aligned} \tag{4.19}$$

Resulting in the equation

$$\frac{\overline{\hat{\sigma}(t+\delta t)}-\hat{\sigma}(t)}{\delta t} = -\frac{i}{\hbar}\Big(\hat{H}_{\text{eff}}^\dagger(t)\hat{\sigma}(t)-\hat{\sigma}(t)\hat{H}_{\text{eff}}^\dagger(t)\Big) + \sum_i 2\gamma_i\hat{\alpha}_i\hat{\sigma}(t)\hat{\alpha}_i^\dagger, \tag{4.20}$$

Averaging (4.20) over many Monte Carlo realizations results in

$$\frac{d\,\langle\hat{\sigma}(t)\rangle}{dt} = -\frac{i}{\hbar}\Big(\hat{H}_{\text{eff}}^\dagger(t)\,\langle\hat{\sigma}(t)\rangle - \langle\hat{\sigma}(t)\rangle\,\hat{H}_{\text{eff}}^\dagger(t)\Big) + \sum_i 2\gamma_i\hat{\alpha}_i\,\langle\hat{\sigma}(t)\rangle\,\hat{\alpha}_i^\dagger, \tag{4.21}$$

which is the master equation of interest. Thus, assuming $\hat{\rho}^S(0) = |\Psi(0)\rangle\langle\Psi(0)|$ the calculated $\langle\hat{\sigma}(t)\rangle$ of our Monte-Carlo method and the true reduced system density operator $\hat{\rho}^S(t)$ will coincide at all times t.

4.2.3 An Alternative Approach

The description and proof for the Monte Carlo method given in Subsections 4.2.1 and 4.2.2 gives a lucid explanation of the concept. But there is another way of implementing the algorithm, which is more practical from a numerical point of view [16], [17].

In the previous description we used first order perturbation theory to determine the probability δp, for the system to decay within each time step δt. We then described how to evolve the system state by, for each time step, generating a random number $\eta \in [0,1]$ from a uniform distribution, and comparing it to δp. Another possible procedure is

to use the cumulative distribution function $P(t)$, often referred to as the waiting time distribution, describing the collected probability for the system to decay at some time $\tau < t$

$$P(t) = 1 - \langle \Psi(t) | \, \Psi(t) \rangle \, . \tag{4.22}$$

Where the state has not been renormalized in each step. Assume you want to produce samples from a random variable Y, with probability distribution function $f_Y(y)$, and corresponding cumulative distribution function $F_Y(y)$. Let X be a uniformly distributed random variable in the interval $[0, 1]$. To get a random sample from the variable Y, simply generate a random number from the uniform distribution X. Then a sample from the variable of distribution $f_Y(y)$ is given by $Y = F^{-1}(X)$. This is a well-known statistical result, and proof can be found in most standard introductions to statistics, such as [15]. Equipped with the cumulative distribution function $P(t)$, we can employ this method to produce a random waiting time τ, giving the time for the system to make a jump, as follows

1. Generate a random number $\eta \in [0, 1]$, from the uniform distribution.

2. Determine the waiting time $\tau(\eta)$ for a jump to occur by solving the equation

$$P(\tau) = \eta. \tag{4.23}$$

To evolve the system state we start by generating a random number η_1 from a uniform distribution. The system state is then evolved in a continuous manner according to the effective Hamiltonian, until the time $t = \tau_1$, where $P(\tau_1) = \eta_1$, is reached. This is where the first jump occurs, and the system decays through one of the possible decay channels. Which decay channel is used is determined in the same manner as described in Section 4.2.1, by use of the conditional probabilities. Immediately after the first jump a new random number is generated, determining the time τ_2 for the second jump to occur, and so on.

This procedure is more practical than the one described previously, since it allows for the use of higher order methods to solve the coherent part of the time evolution, such as Runge-Kutta methods. Another advantage is that we do not have to draw by far as many random numbers, which makes it a slightly more efficient method and prevents exhaustion of the random number generator.

4.3 Simulating the Three-level Λ-system

We will now return to the analysis of the decaying Λ-system from Chapter 3, this time adding the possibility of having incoherent transitions from the state $|x, 0\rangle$ to the state $|e, 0\rangle$, as well as to $|g, 0\rangle$. The situation is visualized in Figure 4.1 on page 68. Our aim is to simulate the system dynamics, using the recently studied Monte Carlo wavefunction method.

As mentioned at the beginning of this chapter, the Monte Carlo approach has a physical interpretation. Imagine having an ideal detector completely encapsulating our atom-cavity system. Under these circumstances each quantum jump corresponds to the detection of a photon, either from the atom or from the cavity. The measurement will project the system onto one of the pure states $|e,0\rangle$ or $|g,0\rangle$, depending on the characteristics of the photon. In the Monte Carlo method this process is represented by determining the waiting time for a photon to be measured, and then resetting the wavefunction in either of the above states, depending on which decay process was realized. In between jumps, the system evolution is modeled through the Schrödinger equation with the effective non-Hermitian Hamiltonian.

4.3.1 The Effective Hamiltonian and Decay Probabilities

To be able to implement the procedure of Section 4.2.3, we need to identify the effective Hamiltonian, the cumulative distribution function $P(t)$, and the conditional probabilities associated with the different decay channels, given that a jump occurs.

The system now has three different decay channels. The decay of the state $|x,0\rangle$, causing a transition to either of the states $|g,0\rangle$ and $|e,0\rangle$, represents two distinct channels. The process of the cavity photons escaping into the environment, causing the state $|g,1\rangle$ to decay to $|g,0\rangle$, adds a third channel. The corresponding Lindblad operators for each of these mechanisms are respectively

$$\begin{aligned}\hat{\alpha}_{xg} &= |g,0\rangle\langle x,0|\,,\\ \hat{\alpha}_{xe} &= |e,0\rangle\langle x,0|\,,\\ \hat{\alpha}_{10} &= |g,0\rangle\langle g,1|\,.\end{aligned} \tag{4.24}$$

$\hat{\alpha}_{xg}$ corresponds to the transition $|x,0\rangle \to |g,0\rangle$, $\hat{\alpha}_{xe}$ to $|x,0\rangle \to |e,0\rangle$ and $\hat{\alpha}_{10}$ to $|g,1\rangle \to |g,0\rangle$. We will stick to our previous notation for the decay rates, letting γ_x denote the total decay rate of the atom, and κ denote the decay rate of the cavity mode. We will in addition let the rate of the two separate atomic decay channels be noted by γ_{xg} and γ_{xe}. The indices xj, $j \in \{g,e\}$ referring to a transition from $|x\rangle$ to $|j\rangle$. Obviously, we must have $\gamma_x = \gamma_{xg} + \gamma_{xe}$. With all the Lindblad operators at hand the effective Hamiltonian is found to be

$$\begin{aligned}\hat{H}_{\text{eff}} &= \hat{H}_T - i\hbar\sum_i \gamma_i \hat{\alpha}_i^\dagger \hat{\alpha}_i\\ &= \hat{H}_T - i\hbar\gamma_{xg}\,|x,0\rangle\langle g,0|\,|g,0\rangle\langle x,0| - i\hbar\gamma_{xe}\,|x,0\rangle\langle e,0|\,|e,0\rangle\langle x,0| - i\hbar\kappa\,|1,g\rangle\langle g,0|\,|g,0\rangle\langle g,1|\\ &= \hat{H}_T - i\hbar(\gamma_{xg}+\gamma_{xe})\,|x,0\rangle\langle x,0| - i\hbar\kappa\,|g,1\rangle\langle g,1|\\ &= \hat{H}_T - i\hbar\gamma_x\,|x,0\rangle\langle x,0| - i\hbar\kappa\hat{a}^\dagger\hat{a}.\end{aligned} \tag{4.25}$$

Here $\hat{H}_T$ is the Hamiltonian of the plain Λ-model found in (3.10), and $\hat{a}^\dagger\hat{a} = n\,|g,n\rangle\langle g,n| = |g,1\rangle\langle g,1|$, in the case of $n = 1$. Equation (4.25) is, not surprisingly, recognized as the Hamiltonian from the earlier study of the decaying three-level Λ-system. The continuous system evolution of the Monte Carlo procedure is thereby determined by the

corresponding Schrödinger equation (3.20).

Having worked out the effective Hamilton operator, we now need to determine the conditional probabilities associated with the different decay processes and the accumulated probability decay function. The probability for decay through a channel must correspond to the amount of population leaking through that channel. Having already worked out the rate of change for the decaying state populations in Chapter 2, we have

$$\begin{aligned}
\frac{dp_{xg}}{dt} &= 2\gamma_{xg} \langle \psi(t)| \, x,0\rangle \langle x,0| \, \psi(t)\rangle = 2\gamma_{xg}|c_x(t)|^2, \\
\frac{dp_{xe}}{dt} &= 2\gamma_{xe} \langle \psi(t)| \, x,0\rangle \langle x,0| \, \psi(t)\rangle = 2\gamma_{xg}|c_x(t)|^2, \\
\frac{dp_{10}}{dt} &= 2\kappa \langle \psi(t)| \, g,1\rangle \langle g,1| \, \psi(t)\rangle = 2\kappa|c_g(t)|^2.
\end{aligned} \tag{4.26}$$

These sum up to give the total probability per time of the system decaying

$$\frac{dp_{\text{tot}}}{dt} = \sum_i p_i(t) = 2(\gamma_{xg} + \gamma_{xe})|c_x(t)|^2 + 2\kappa|c_g(t)|^2. \tag{4.27}$$

The conditional probabilities that the system decays through channel i given it decays at time τ is then found from dividing the expressions of (4.26) by (4.27)

$$\begin{aligned}
p(xg|\tau) &= \frac{\gamma_{xg}|c_x(\tau)|^2}{(\gamma_{xg} + \gamma_{xe})|c_x(\tau)|^2 + \kappa|c_g(\tau)|^2}, \\
p(xe|\tau) &= \frac{\gamma_{xg}|c_x(\tau)|^2}{(\gamma_{xg} + \gamma_{xe})|c_x(\tau)|^2 + \kappa|c_g(\tau)|^2}, \\
p(10|\tau) &= \frac{\kappa|c_g(\tau)|^2}{(\gamma_{xg} + \gamma_{xe})|c_x(\tau)|^2 + \kappa|c_g(\tau)|^2}.
\end{aligned} \tag{4.28}$$

Finally, the cumulative distribution function for the system to have decayed at some time $\tau < t$ is

$$P(t) = 1 - \langle \psi(t)| \, \psi(t)\rangle = 1 - (|c_g(t)|^2 + |c_e(t)|^2 + |c_x(t)|^2). \tag{4.29}$$

4.3.2 Results From Numerical Simulations

We now wish to study the effect of including incoherent transitions from $|x,0\rangle$ to $|e,0\rangle$ in the STIRAP-method of Chapter 3. Thus, we look at a scheme for producing single cavity photons through adiabatic population transfer, using the Gaussian laser defined in (3.59). The results will be presented through plots, describing how the populations of the system states $|g,1\rangle$, $|e,0\rangle$ and $|x,0\rangle$ evolve with time, within different regions of parameter space. We point out that while the various system decay rates are realistically in the order of 10 megahertz, we will here allow the realistic parameter values to be greatly exceeded, with the intention of demonstrating various effects.

We will once again conduct our investigation in a systematic manner, starting with isolating the effect of letting $|x,0\rangle$ decay to $|e,0\rangle$. We will then add the processes of the

previous decay channels $|x,0\rangle \to |g,0\rangle$ and $|g,1\rangle \to |g,0\rangle$, in turn. A short description and schematic visualization of the used program, along with the program C++-code, is found in Appendix C.

Results from isolating the effects of incoherent transitions from $|x,0\rangle$ to $|e,0\rangle$, for increasing decay rate γ_{xe}, are displayed in Figure 4.3 on page 80. First of all we note that as compared to the previously encountered decay channels (see pages 63 - 65), the channel $|x,0\rangle \to |e,0\rangle$ requires a very high decay rate for any noticeable impact on the state populations to be seen. This probably has to do with the fact that this decay channel causes no loss of state population.

Nevertheless, for very large values of decay rate γ_{xe} significant changes in the population profiles of both $|e,0\rangle$ and $|g,1\rangle$ emerge. We observe how the decay channel $|x,0\rangle \to |e,0\rangle$ seems to work against the STIRAP-procedure, pushing population back into the initial state. For increasing values of γ_{xe}, an increasing amount of population is prevented from ever reaching the target state $|g,1\rangle$. The laser withdraws to soon, transporting all the population back to the initial state $|e,0\rangle$.

Results from letting the excited atomic state $|x,0\rangle$ decay to both $|e,0\rangle$ and $|g,0\rangle$ are shown in Figure 4.4 on page 81, together with corresponding plots including only the process $|x,0\rangle \to |g,0\rangle$. As we see no apparent reason why one of the decay channels should dominate the other, we have chosen to study situations in which the two decay rates γ_{xg} and γ_{xe} are equal. Comparing the plots in Figure 4.4, it seems introducing the additional incoherent system transitions to the state $|e,0\rangle$ lowers and broadens the population profile of state $|g,1\rangle$. This reflects that it now takes longer to transport the population of $|e,0\rangle$ to $|g,1\rangle$, since the decay $|x,0\rangle \to |e,0\rangle$ keeps forcing it back to start. Glancing back at the plots in to Figure 4.3 we see that introducing the decay channel $|x,0\rangle \to |g,0\rangle$ in addition to $|x,0\rangle \to |e,0\rangle$, makes the latter decay channel less efficient, in the sense that population is no longer seen to be stuck in the initial state throughout the entire evolution.

Results for decay from channels $|x,0\rangle \to |g,0\rangle$, $|x,0\rangle \to |e,0\rangle$ and $|g,1\rangle \to |g,0\rangle$ are displayed in Figure 4.5 on page 82, together with corresponding plots without the new channel $|x,0\rangle \to |e,0\rangle$. Within reasonable values of the decay rates, the effect of γ_{xe} is hardly visible.

The Purity of The Photon

From our numerical results we see that under realistic conditions, the decay channel $|x,0\rangle \to |e,0\rangle$, has little significant impact on the population of $|g,1\rangle$, during the STIRAP-evolution. Thus it is reasonable to assume that this channel will cause no great changes to the photons emitted from the cavity. If the only thing we cared about were the time dependent probability associated with detecting a photon emission, this would certainly be true.

For quantum processing and networking purposes, we need the single photon resulting from the STIRAP-scheme to be in a pure state. When we introduce incoherent transition from $|x,0\rangle$ to the active state $|e,0\rangle$, the system evolution may continue after

a decay incident. This allows for the possibility of producing a cavity photon in more than one way, causing the final emitted photon to be in a mixed state. This matter was of no concern in the case for the incoherent transitions resulting in the state $|g,0\rangle$. Once such a transition has occurred, the system will evolve no further, and there is no chance of producing a subsequent cavity photon. The same cannot be said in the case of our most recently acquired decay channel.

Imagine initializing the system in state $|e,0\rangle$, and turning on the laser to start the STIRAP-magic. Since we have activated a variety of decay channels, the STIRAP-scheme will not be at its optimal, and there will always be a small finite chance that the system makes a transition to the state $|x,0\rangle$ during the evolution. Once in this state, there is a chance the system may make a transition back to the initial state, caused by the decay channel $|x,0\rangle \rightarrow |e,0\rangle$. This process might repeat several times, before the system reaches the state $|g,1\rangle$, and eventually emits a photon. The number of times the system makes an incoherent transition from $|x,0\rangle$ to $|e,0\rangle$, prior to emitting a cavity photon, will change the state of the emitted photon. The final photon will be in a mixed state, with all the distinct ways of producing a cavity photon, contributing with its own pure state to the final mixture.

The questions of how to determine the actual mixed state of the final photon and the degree of its purity are indeed interesting. One way of conducting such an examination could be to perform dynamical simulations through the Monte Carlo wavefunction method, collecting the probabilities for each distinct way for the system to produce a single photon, along with their corresponding photon profile. The probabilities would then represent the weight given to each distinct pure photon state, in the final mixed state. The final photon entropy could then be calculated, giving a measure of the purity of the resulting photon. An implementation of such a procedure will be too extensive to be included in this thesis.

4.3.3 Testing the Program

The behavior of the three-level system coupled to a reservoir is not necessarily easy to predict. Tests need to be conducted, if we are to be able to trust the results from the above program simulations. The test case should include incoherent transitions between internal system states and be as simple as possible. Hopefully it will enable us to find a closed form solution to the Shcrödinger equation. We will show that the driven two-level atom is a well-suited test subject in this regard.

Two-level System with Internal Incoherent Transitions

Imagine a two-level atom with ground state $|g\rangle$ and an excited state $|x\rangle$, with accompanying energies $\hbar\omega_g$ and $\hbar\omega_x$. The two levels are coupled through a classical laser, and the laser frequency corresponds perfectly with the energy transition between the two atomic levels. The Hamiltonian will be similar to the one found for the three-level Λ-system in the beginning of Chapter 3, but without the contributions from the ground state and the cavity field.

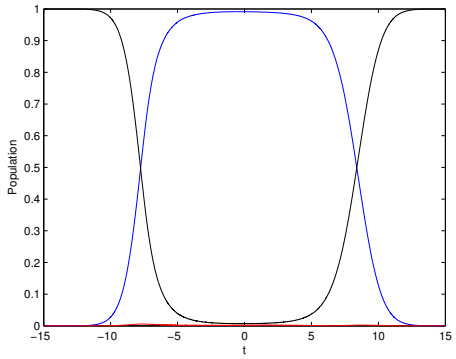

(a) $\kappa = 0$, $\gamma_{xe} = 30\pi$, $\gamma_{xg} = 0$

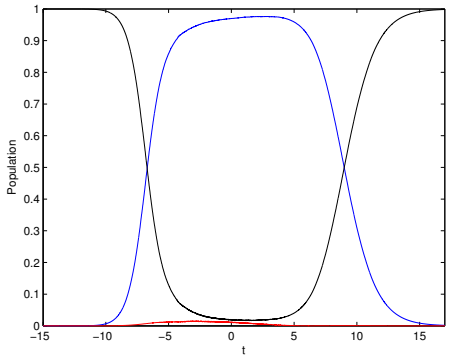

(b) $\kappa = 0$, $\gamma_{xe} = 120\pi$, $\gamma_{xg} = 0$

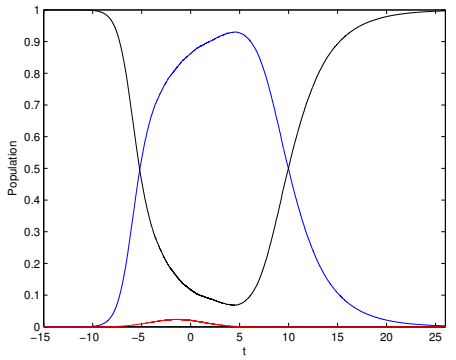

(c) $\kappa = 0$, $\gamma_{xe} = 300\pi$, $\gamma_{xg} = 0$

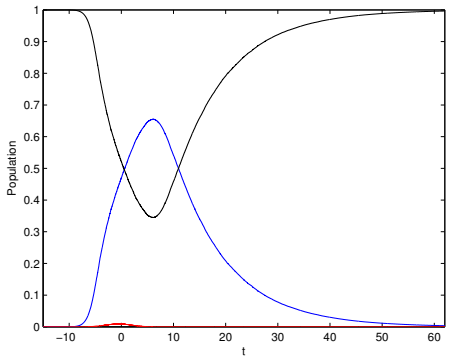

(d) $\kappa = 0$, $\gamma_{xe} = 1000\pi$, $\gamma_{xg} = 0$

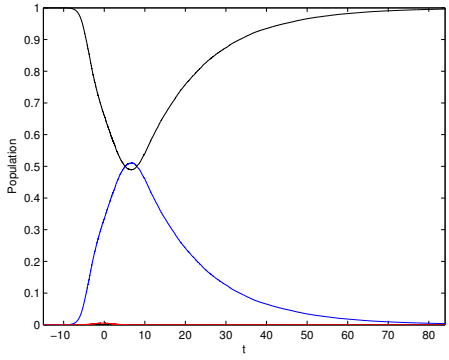

(e) $\kappa = 0$, $\gamma_{xe} = 1500\pi$, $\gamma_{xg} = 0$

Figure 4.3: The list of figures shows the isolated effect of incoherent decay from $|x, 0\rangle$ to $|e, 0\rangle$, for increasing values of decay rate γ_{xe}. The applied laser profile is given by $\Omega(t) = kg_0 e^{-(t/\Delta\tau)^2}$, with parameter values $k = 28$, $g_0 = 9\pi$, $\Delta\tau = 5$. Time is measured in units of μs, while g_0, Ω and γ_{xe} are given in MHz. The black, blue and red graphs describe the populations of the states $|e, 0\rangle$, $|g, 1\rangle$ and $|x, 0\rangle$, respectively.

$$\begin{aligned}
\hat{H}_A &= \sum_{i \in \{g,x\}} \hbar\omega_i \left|i\right\rangle \left\langle i\right|, \\
\hat{H}_L &= -\frac{\hbar\Omega}{2}(\hat{\sigma}_{xg} e^{-i\omega_L t} + \hat{\sigma}_{gx} e^{i\omega_L t}), \\
\hat{H} &= \hat{H}_A + \hat{H}_L. \qquad (4.30)
\end{aligned}$$

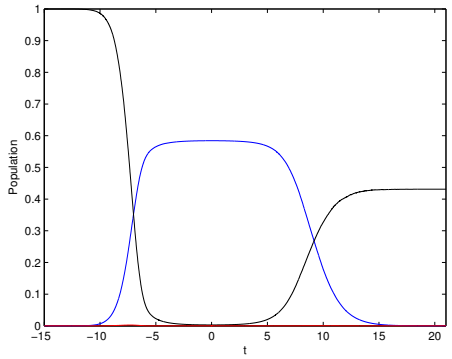

(a) $\kappa = 0$, $\gamma_{xe} = 60\pi$, $\gamma_{xg} = 60\pi$

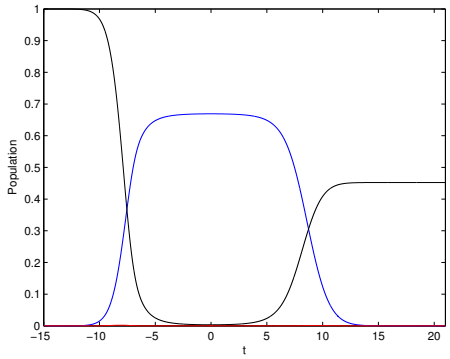

(b) $\kappa = 0$, $\gamma_{xe} = 0$, $\gamma_x = 60\pi$

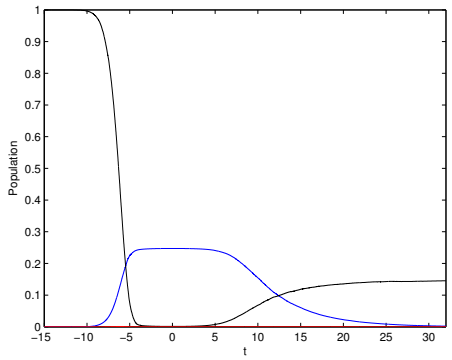

(c) $\kappa = 0.0$, $\gamma_{xe} = 250\pi$, $\gamma_{xg} = 250\pi$

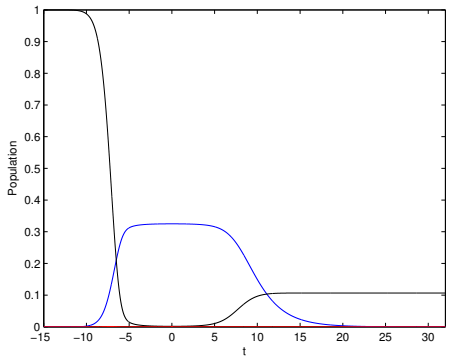

(d) $\kappa = 0$, $\gamma_{xe} = 0$, $\gamma_x = 250\pi$

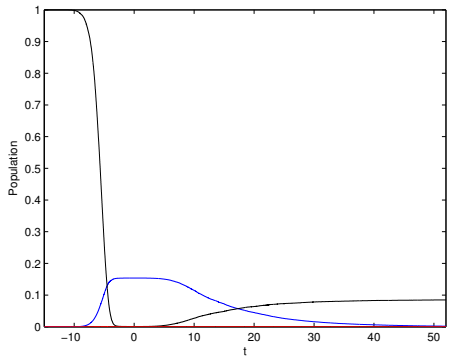

(e) $\kappa = 0.0$, $\gamma_{xe} = 500\pi$, $\gamma_{xg} = 500\pi$

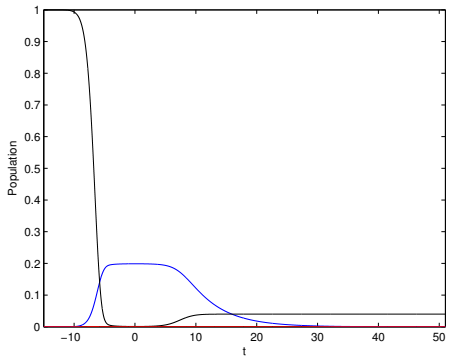

(f) $\kappa = 0$, $\gamma_{xe} = 0$, $\gamma_x = 500\pi$

Figure 4.4: The list of figures shows the effect of including both incoherent transitions $|x, 0\rangle \to |g, 0\rangle$ and $|x, 0\rangle \to |e, 0\rangle$ in the left column, compared to the case including only $|x, 0\rangle \to |g, 0\rangle$ in the right column. The results are displayed for increasing decay rates γ_{xg} and γ_{xe}. The applied laser profile is given by $\Omega(t) = kg_0 e^{-(t/\Delta\tau)^2}$, with parameter values $k = 28$, $g_0 = 9\pi$, $\Delta\tau = 5$. Time is measured in units of μs, while g_0, Ω, γ_{xg} and γ_{xe} are given in MHz. The black, blue and red graphs describe the populations of the states $|e, 0\rangle$, $|g, 1\rangle$ and $|x, 0\rangle$, respectively.

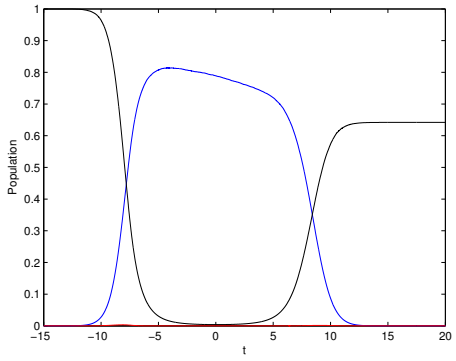

(a) $\kappa = 0.01\pi$, $\gamma_{xe} = 15\pi$, $\gamma_{xg} = 15\pi$

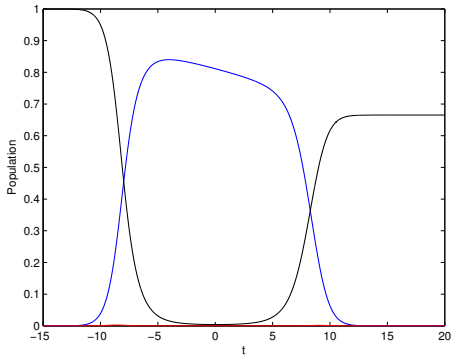

(b) $\kappa = 0.01\pi$, $\gamma_{xe} = 0$, $\gamma_x = 15\pi$

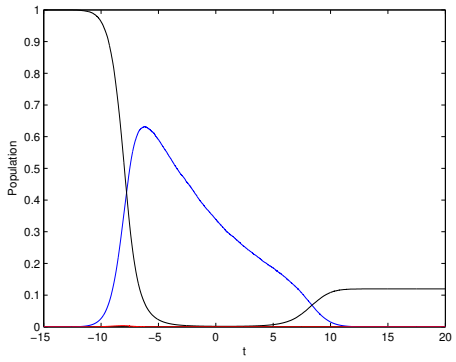

(c) $\kappa = 0.1\pi$, $\gamma_{xe} = 15\pi$, $\gamma_{xg} = 15\pi$

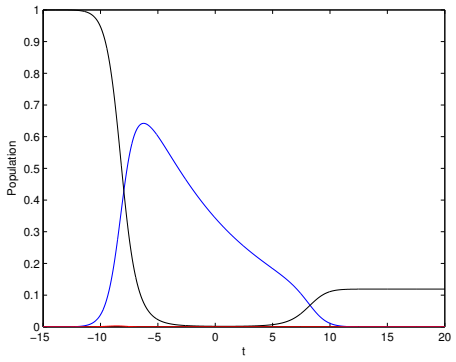

(d) $\kappa = 0.1\pi$, $\gamma_{xe} = 0$, $\gamma_x = 15\pi$

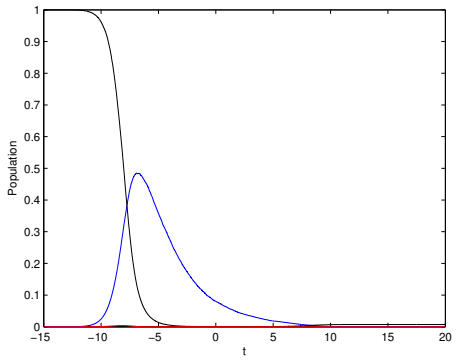

(e) $\kappa = 0.25\pi$, $\gamma_{xe} = 15\pi$, $\gamma_{xg} = 15\pi$

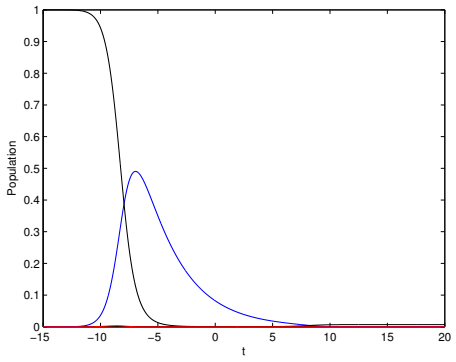

(f) $\kappa = 0.25\pi$, $\gamma_{xe} = 0$, $\gamma_x = 15\pi$

Figure 4.5: The list of figures shows the effect of including all three decay channels $|x,0\rangle \to |e,0\rangle$, $|x,0\rangle \to |g,0\rangle$ and $|g,1\rangle \to |g,0\rangle$ in the left column, compared to the case including only $|x,0\rangle \to |g,0\rangle$ and $|g,1\rangle \to |g,0\rangle$ in the right column. The results are displayed for a selected values for the decay rates γ_{xg} and γ_{xe}, and increasing values of decay rate κ. The applied laser profile is given by $\Omega(t) = kg_0 e^{-(t/\Delta\tau)^2}$, with parameter values $k = 28$, $g_0 = 9\pi$, $\Delta\tau = 5$. Time is measured in units of μs, while g_0, Ω, γ_{xg}, γ_{xe} and κ are given in MHz. The black, blue and red graphs describe the populations of the states $|e,0\rangle$, $|g,1\rangle$ and $|x,0\rangle$, respectively.

The time dependence is removed by applying the transformation described by

$$\hat{T} = e^{-i\omega_L \hat{\sigma}_{gg} t}, \tag{4.31}$$

leading to

$$\hat{H}_T = \hbar\Big((\omega_g + \omega_L)\hat{\sigma}_{gg} + \omega_x \hat{\sigma}_{xx}\Big) - \frac{\hbar\Omega}{2}(\hat{\sigma}_{xg} + \hat{\sigma}_{gx}). \tag{4.32}$$

Now, introducing an exponential decay with a rate γ_x of the excited level gives the effective Hamiltonian

$$\hat{H}_{\text{eff}} = \hat{H}_T - i\hbar\gamma_x \left|x\right\rangle \left\langle x\right|. \tag{4.33}$$

The corresponding Lindblad operator is

$$\hat{\alpha} = \left|g\right\rangle \left\langle x\right|. \tag{4.34}$$

Giving rise to the jump superoperator

$$\hat{\mathcal{L}}_j \hat{\rho}^S = \sum_i 2\gamma_i \hat{\alpha}_i \hat{\rho}^S \hat{\alpha}_i^\dagger = 2\gamma_x \left|g\right\rangle \left\langle x\right| \hat{\rho}^S \left|x\right\rangle \left\langle g\right|,$$

and the Master equation

$$\begin{aligned}
\frac{\partial}{\partial t}\hat{\rho}^S =& -\frac{i}{\hbar}(\hat{H}_{\text{eff}}\hat{\rho}^S - \hat{\rho}^S \hat{H}_{\text{eff}}^\dagger) + \hat{\mathcal{L}}_j \hat{\rho}^S \qquad (4.35)\\
=& -i\Bigg(\Big((\omega_g + \omega_L)\left|g\right\rangle \left\langle g\right| + (\omega_x - i\gamma_x)\left|x\right\rangle \left\langle x\right| - \frac{\Omega}{2}(\left|x\right\rangle \left\langle g\right| + \left|g\right\rangle \left\langle x\right|)\Big)\hat{\rho}^S\\
&- \hat{\rho}^S\Big((\omega_g + \omega_L)\left|g\right\rangle \left\langle g\right| + (\omega_x + i\gamma_x)\left|x\right\rangle \left\langle x\right| - \frac{\Omega}{2}(\left|x\right\rangle \left\langle g\right| + \left|g\right\rangle \left\langle x\right|)\Big)\Bigg) + 2\gamma_x \left|g\right\rangle \left\langle x\right| \hat{\rho}^S \left|x\right\rangle \left\langle g\right|.
\end{aligned}$$

This gives the equations for the four different elements of the density matrix

$$\frac{\partial}{\partial t}\hat{\rho}^S_{gg} = i\frac{\Omega}{2}(\hat{\rho}^S_{xg} - \hat{\rho}^S_{gx}) + 2\gamma_x \hat{\rho}^S_{xx}, \tag{4.36}$$

$$\frac{\partial}{\partial t}\hat{\rho}^S_{xx} = i\frac{\Omega}{2}(\hat{\rho}^S_{gx} - \hat{\rho}^S_{xg}) - 2\gamma_x \hat{\rho}^S_{xx}, \tag{4.37}$$

$$\frac{\partial}{\partial t}\hat{\rho}^S_{gx} = -\gamma_x \hat{\rho}^S_{gx} + i\frac{\Omega}{2}(\hat{\rho}^S_{xx} - \hat{\rho}^S_{gg}), \tag{4.38}$$

$$\frac{\partial}{\partial t}\hat{\rho}^S_{xg} = -\gamma_x \hat{\rho}^S_{xg} - i\frac{\Omega}{2}(\hat{\rho}^S_{xx} - \hat{\rho}^S_{gg}). \tag{4.39}$$

The solutions of Equations (4.36) - (4.39) for given values of the parameters Ω and γ_x can be obtained by using the command DSolve() in Mathematica. The exact solutions for $\Omega = 2$, $\gamma_x = 1$, and $\Omega = 10$, $\gamma_x = 1$, with initial conditions $\hat{\rho}^S_{xx}(0) = 1, \hat{\rho}^S_{gg}(0) = \hat{\rho}^S_{gx}(0) = \hat{\rho}^S_{xg}(0) = 0$, are displayed in expression (4.40) and (4.41).

$$\begin{aligned}
\hat{\rho}^S_{gg} =& \frac{2}{15}e^{-3t/2}\Big(5e^{3t/2} - 5\cos\Big(\frac{\sqrt{15}t}{2}\Big) + \sqrt{15}\sin\Big(\frac{\sqrt{15}t}{2}\Big)\Big),\\
\hat{\rho}^S_{xx} =& \frac{1}{15}e^{-3t/2}\Big(5e^{3t/2} + 10\cos\Big(\frac{\sqrt{15}t}{2}\Big) - 2\sqrt{15}\sin\Big(\frac{\sqrt{15}t}{2}\Big)\Big),\\
\hat{\rho}^S_{gx} =& -\frac{i}{15}e^{-3t/2}\Big(5e^{3t/2} - 5\cos\Big(\frac{\sqrt{15}t}{2}\Big) - 3\sqrt{15}\sin\Big(\frac{\sqrt{15}t}{2}\Big)\Big),\\
\hat{\rho}^S_{gx} =& \frac{i}{15}e^{-3t/2}\Big(5e^{3t/2} - 5\cos\Big(\frac{\sqrt{15}t}{2}\Big) - 3\sqrt{15}\sin\Big(\frac{\sqrt{15}t}{2}\Big)\Big).
\end{aligned} \tag{4.40}$$

$$\begin{aligned}
\hat{\rho}^S_{gg} =& \frac{2}{969}e^{-3t/2}\Big(247e^{3t/2} - 247\cos\Big(\frac{\sqrt{399}t}{2}\Big) + 3\sqrt{399}\sin\Big(\frac{\sqrt{399}t}{2}\Big)\Big),\\
\hat{\rho}^S_{xx} =& \frac{1}{969}e^{-3t/2}\Big(475e^{3t/2} + 494\cos\Big(\frac{\sqrt{399}t}{2}\Big) - 6\sqrt{399}\sin\Big(\frac{\sqrt{399}t}{2}\Big)\Big),\\
\hat{\rho}^S_{gx} =& -\frac{5i}{969}e^{-3t/2}\Big(19e^{3t/2} - 19\cos\Big(\frac{\sqrt{399}t}{2}\Big) - 5\sqrt{399}\sin\Big(\frac{\sqrt{399}t}{2}\Big)\Big),\\
\hat{\rho}^S_{gx} =& \frac{5i}{969}e^{-3t/2}\Big(19e^{3t/2} - 19\cos\Big(\frac{\sqrt{399}t}{2}\Big) - 5\sqrt{399}\sin\Big(\frac{\sqrt{399}t}{2}\Big)\Big).
\end{aligned} \tag{4.41}$$

This system can be realized numerically by turning off the coupling between the ground state $|g,1\rangle$ and excited state $|x,0\rangle$, in the program describing the three-level system. That is, setting $g_0 = 0$. This leaves two levels coupled by a laser. Simulation results are plotted together with the analytic solutions in Figure 4.6. Our program seems to do its job rather well.

The Statistical Error

In Subsection 4.1 a rather crude estimate of the standard error of a Monte Carlo simulation is given. It states that the error of a properly working Monte Carlo algorithm should go as $\frac{1}{\sqrt{n}}$, where n is the number of Monte Carlo trials. A final test that our program works the way it should is to test that this is actually the case.

In order to test this we calculate the maximum deviation of the Monte Carlo simulation from the exact solution of (4.40) for selected values of n. A plot of the results together with the function $\frac{1}{\sqrt{n}}$ is found in Figure 4.7. Everything seems to be in order.

Throughout this chapter we have introduced the possibility of incoherent transitions to an active system state, with the consequence that the effective Schrödinger equation had to be traded for the full Lindblad master equation. Furthermore, we have thoroughly studied a Monte Carlo wavefunction procedure for modeling the Lindblad equation, which was later implemented to simulate the dynamics of the three-level Λ-system, including decay channels resulting in both static and active system states. The

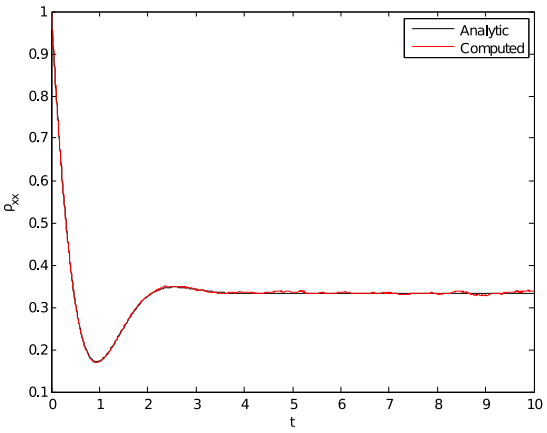

(a) Plot of analytic and numerical Monte Carlo solution of equation (4.37), with $\Omega = 2$ and $\gamma_x = 1$, and initial conditions $\hat{\rho}^S_{xx}(0) = 1, \hat{\rho}^S_{gg}(0) = \hat{\rho}^S_{gx}(0) = \hat{\rho}^S_{xg}(0) = 0$.

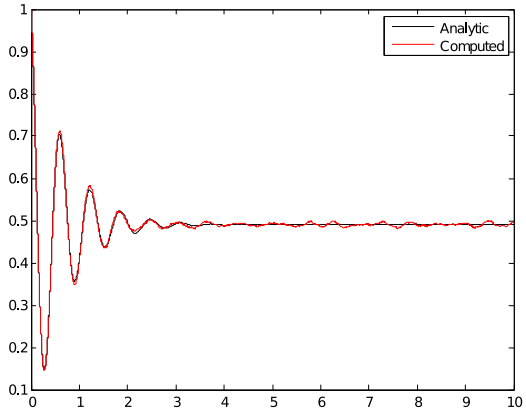

(b) Plot of analytic and numerical Monte Carlo solution of equation (4.37), with $\Omega = 10$ and $\gamma_x = 1$, and initial conditions $\hat{\rho}^S_{xx}(0) = 1, \hat{\rho}^S_{gg}(0) = \hat{\rho}^S_{gx}(0) = \hat{\rho}^S_{xg}(0) = 0$.

Figure 4.6: Plot of analytic and numerical Monte Carlo solution of equation (4.37). In the program simulation time steps $\delta t = 10^{-3}$ and the number og Monte Carlo samples $n = 10^3$ were used.

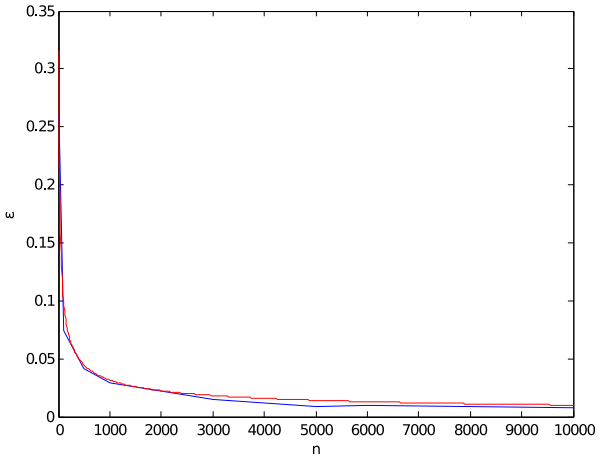

Figure 4.7: Blue line: The absolute error $\epsilon = \max_t(|\rho_{xx}^{\text{exact}}(t) - \rho_{xx}^{\text{MC}}(t)|)$ between the analytic solution (4.40) and the MC-calculated solution. Red line: Plot of the function $\frac{1}{\sqrt{n}}$. Generally, the constant of proportionality may be different form one.

chapter was ended with a discussion of numerical results, and a crude error analysis of our Monte Carlo implementation.

In the last two chapters we have seen indication of how the laser profile can be used to manipulate the population profile of the cavity mode, and thereby also the temporal photon profile. In the preceding chapter we look into how this effect can be exploited in photon design.

Chapter 5

Custom-made Photons

In previous sections we have presented a scheme for how single photons can be generated by the use of a three-level atom-cavity system and a laser, and how the photon probability amplitude will rely on the laser profile. In the two previous chapters we used a laser, with a Gaussian laser profile $\Omega(t)$, to perform the so called STIRAP-scheme, producing a photon while nearly eliminating the decaying excited atomic state. As was pointed out in Subsection 3.2.4, there are an infinite number of different laser profiles that meets the requirements of the STIRAP-procedure. We will in this section pursue the idea presented by Vasilev et al. [29]. If we want a specific photon profile, what kind of laser profile must be used in order to produce it?

It turns out that within quantum processing there are certain photon shapes that are preferable to others. The ability to produce any preferred predefined photon profile would therefore be a valuable attribute for a single photon source. We will devote this chapter to the study of a scheme for producing custom-made photons, using laser manipulation in the decaying Λ-model. We will begin by calculating a general expression for the required laser profile $\Omega(t)$, for the manufacturing of a given photon shape. Next we will solve the problem explicitly for some selected temporal photon profiles.

5.1 Calculating The Laser Profile

As discussed in Section 4.3.2, the only Λ-model transition causing decoherence of different photon states is the incoherent transition between $|x,0\rangle$ and $|e,0\rangle$. Imagine we construct a setup that in some way is able to register the photon emission from such a transition, and at the moment of detection immediately puts a stop the to the system evolution. Then the $|x,0\rangle \rightarrow |e,0\rangle$ transition could be considered a total loss, like the incoherent transitions to the passive state $|g,0\rangle$. The system evolution will be governed by the effective Hamiltonian, found in Chapter 3. The differential equations describing the corresponding dynamics were found in Section 3.2.1

$$\dot{c}_g = -\kappa c_g + i g_0 c_x, \tag{5.1}$$

$$\dot{c}_e = i\frac{\Omega}{2} c_x, \tag{5.2}$$

$$\dot{c}_x = i g_0 c_g + i\frac{\Omega}{2} c_e - \gamma_x c_x. \tag{5.3}$$

Here all the symbols have their usual meaning. c_g, c_e and c_x are the time dependent Schrödinger state coefficients. κ and γ_x are the decay rates of the cavity mode and the excited atomic level. g_0 and $\Omega(t)$ each represent the coupling strength of the cavity mode and the laser with their respective atomic transitions. In the this section we will work out an analytic expression for the time dependent atom-laser coupling $\Omega(t)$, based on the above equations.

Given the recently described setup, the photon emerging from the cavity should be in a pure state, and its temporal shape can be described by a function

$$\psi_{\mathrm{ph}}(t) = \sqrt{\eta}\psi_0(t). \tag{5.4}$$

Assuming ψ_0 describes a sort of normalized photon wavefunction, we have

$$\int |\psi_0(t)|^2 dt = 1. \tag{5.5}$$

η then corresponds to the total photon emission probability.

In order to find an analytic solution for $\Omega(t)$, we need to express the coefficients c_g, c_e and c_x in terms of the given photon profile (5.4). From previous argumentation we know that the temporal photon probability amplitude is

$$|\psi_{\mathrm{ph}}(t)|^2 = 2\kappa |c_g(t)|^2. \tag{5.6}$$

Assuming ψ_{ph} is real, we get a known expression for the coefficient $c_g(t)$

$$c_g(t) = \frac{\psi_{\mathrm{ph}}(t)}{\sqrt{2\kappa}}. \tag{5.7}$$

From Equation (5.1) we can then express the coefficient $c_x(t)$ in terms of the known coefficient c_g and its derivative

$$c_x(t) = -\frac{i}{g_0}(\dot{c}_g(t) + \kappa c_g(t)). \tag{5.8}$$

To find the missing formula for c_e we turn to the effective master equation

$$\frac{\partial}{\partial t}\hat{\rho}^S = -\frac{i}{\hbar}(\hat{H}_{\mathrm{eff}}\hat{\rho}^S - \hat{\rho}^S \hat{H}_{\mathrm{eff}}^\dagger). \tag{5.9}$$

From this we get the following equations for the populations of the combined atom-cavity states

$$\dot{\rho}^S_{gg} = -2\kappa\rho^S_{gg} + ig_0(\rho^S_{xg} - \rho^S_{gx}), \tag{5.10}$$

$$\dot{\rho}^S_{ee} = i\frac{\Omega}{2}(\rho^S_{xe} - \rho^S_{ex}), \tag{5.11}$$

$$\dot{\rho}^S_{xx} = -ig_0(\rho^S_{xg} - \rho^S_{gx}) - i\frac{\Omega}{2}(\rho^S_{xe} - \rho^S_{ex}) - 2\gamma_x\rho^S_{xx}. \tag{5.12}$$

Combining (5.10) - (5.12) gives

$$\dot{\rho}^S_{ee} = -(\dot{\rho}^S_{gg} + \dot{\rho}^S_{xx}) - 2(\kappa\rho^S_{gg} + \gamma_x\rho^S_{xx}). \tag{5.13}$$

With initial conditions $c_e(0) = 1, c_g(t) = c_x(t) = 0$ required by the STIRAP-procedure we then have

$$\rho^S_{ee} = 1 - \rho^S_{gg} - \rho^S_{xx} - 2\int_0^t \kappa\rho^S_{gg} + \gamma_x\rho^S_{xx}dt. \tag{5.14}$$

Now, we know that $\rho^S_{ee}(t) = |c_e|^2$. From the assumption that ψ_{ph} is real we then find

$$\psi_{\text{ph}} \in \mathbb{R} \Rightarrow c_g \in \mathbb{R} \Rightarrow c_x \in \mathbb{C} \Rightarrow c_e \in \mathbb{R}, \tag{5.15}$$

so

$$c_e = \sqrt{\rho_{ee}}. \tag{5.16}$$

Finally we get an expression for the required laser profile from (5.2)

$$\Omega = -2i\frac{\dot{c}_e}{c_x} = -i\frac{\dot{\rho}_{ee}}{c_x\sqrt{\rho_{ee}}}. \tag{5.17}$$

From the look of Equation (5.17) it may seem like the decaying Λ-model can produce any photon of our choice. This is however, not quite true. On our way to revealing (5.17), we have made assumptions about the initial conditions that sets limits to the validity range of our expression for $\Omega(t)$.

$$c_g(0) = 0 \quad \Rightarrow \quad \psi_{\text{ph}}(0) = 0 \tag{5.18}$$

$$c_x(0) = 0 \quad \Rightarrow \quad \dot{c}_g(0) = 0, \quad \Rightarrow \quad \dot{\psi}_{\text{ph}}(0) = 0. \tag{5.19}$$

So both the photon profile $\psi_{\text{ph}}(t)$ and its derivative $\dot{\psi}_{\text{ph}}(t)$ must be zero at the time the system evolution is initialized. From a physical point of view this means the photon emission rate must build up continuously from zero, which seems a very reasonable requirement.

5.2 Results for Specific Photon Shapes

The above solution for $\Omega(t)$ is surprisingly simple and beautiful. So simple in fact, that for a given reasonably well behaved $\psi_{\text{ph}}(t)$ the system can be solved directly in Mathematica. In this section we will numerically determine the laser profiles for some

selected photon shapes. We will first look at time symmetric photons, because of their desirable qualities in regard to quantum network set-ups, before taking the liberty to treat a more exotic photon profile of our choice.

All result will be presented through plots. Although analytical expressions for $\Omega(t)$ could in principle be extracted, the solutions are of little interest, as they in general are to complicated for meaningful analysis.

5.2.1 Time Symmetric Photons

In 1996 Cirac et. al [10] proposes a scheme of ideal quantum state transfer between nodes in a quantum network, using the methods of STIRAP in cavity based Λ-systems of the kind studied throughout this thesis.

The article is based on the idea of using atom-cavity Λ-systems to form the nodes of a quantum network, while the cavity produced photons function as information carriers between nodes. By laser manipulation at an initial atom-cavity node, the quantum state of the atom is transferred to the cavity photon, encoded in, for instance, two of the photon polarization states. The photon then leaks out from the initial cavity, and propagates to the next. At the second cavity the photon wavepacket will, under the right circumstances, enter through the cavity wall, once again playing the role of a cavity photon. Finally, the state of the photon is transferred to the atom of the second node. If this process is carried out, a quantum state transfer between distant systems has been successfully realized.

It is shown in [10] that the above scheme works optimally when the information carrying photons are symmetric in time. The explanation for this result is rather intuitive. An ideal quantum mechanical system evolves in a unitary manner, meaning that all processes are in theory reversible. We can imagine time reversing the cavity emitted photon, making it return to the initial cavity. This would then restore the initial state of the atom-cavity system. The same process will be at work if we instead produce photons that are symmetric in time, and send them toward a second, correctly prepared atom-cavity node. The described method was recently realized in a quantum network prototype by Ritter and coworkers, reported in [28].

The above conclusions motivate the study of producing photons of symmetric temporal shape. We will in the following treat two different time symmetric photon profiles. A sinusoidal variant

$$\psi_{\mathrm{ph}}(t) = \sqrt{\eta}\sqrt{\frac{8}{3T}}\sin^2\left(\frac{\pi t}{T}\right), \tag{5.20}$$

and a Gaussian one

$$\psi_{\mathrm{ph}}(t) = \sqrt{\eta}\,\pi^{-\frac{1}{4}}e^{-\frac{(t-a)^2}{b}}, \quad a, b = const. \tag{5.21}$$

The first one is also studied in [29]. An example of the sinusoidal photon profile, accompanied by its required laser shape, is found in Figure 5.1 on page 92. An example of the Gaussian photon profile is found in Figure 5.2 on page 93. In both figures, $\Omega(t)$ is plotted for different values of photon emission probability.

Apart from their specific shapes, the laser profiles show similar behavior for variation in the photon emission efficiency η. For small efficiencies, the laser profiles are seen to be very similar i shape to their photon profile. We observe that as we increase η, the strength of the laser is also required to increase. This might be explained by the fact that higher photon emission probability requires the cavity mode to leak out at a faster rate, demanding the laser to work harder to maintain the optimal feed of population from the initial state $|e,0\rangle$, to the cavity mode state $|g,1\rangle$.

For large values of η, $\Omega(t)$ starts to deviate appreciably from the photon shape. Its peak is seen to narrow and shift toward later times. This is can be seen as a consequence of the continuously decreasing population of the initial state $|e,0\rangle$, making it increasingly harder for the laser to maintain a population flow to the state $|g,1\rangle$.

Figure 5.1 demonstrates that when we request efficiencies larger than one, the laser profile will diverge, reflecting the physical impossibility this represents.

5.2.2 An Exotic Creature

At last we chose to include a somewhat more unusual photon profile, given by

$$\psi(t) = \sqrt{\eta}\frac{1}{N}(\sin(bt) + t)e^{-at}, \quad a, b = const. \tag{5.22}$$

Where N is a normalization constant, given by

$$N = \sqrt{\frac{b^2}{4a(a^2+b^2)} + \frac{8ab}{(4a^2+b^2)^2} + \frac{1}{4a^3}}. \tag{5.23}$$

The photon profile for $a = 0.5$ and $b = 2.1$, and the required laser profile are found in Figure 5.3 on page 94. The behavior of this laser profile is very similar to the one of the two symmetric profiles studied in the previous subsection. The strength of $\Omega(t)$ increases for increasing efficiency η, and increasing strength is required when the state $|e,0\rangle$ starts to empty. In addition the exponentially suppressed sinusoidal oscillations of the photon profile are seen to appear clearly in the behavior of the laser profile, for large values of η.

An interesting question is of course if there is any limitation to the photon emission efficiency associated with the different photon profiles. In [29] an examination of this topic is conducted, and it is shown that maximum attainable efficiency will vary from profile to profile. A more thorough treatment of this subject would indeed be interesting, but will not be prioritized in this thesis.

In this brief chapter we have demonstrated how a predefined temporal photon profile can be used to specify required laser behavior. With the help of the effective Schrödinger equation and the Lindblad equation, we produced an expression for the laser profile $\Omega(t)$, in terms of the given photon shape. Finally, the explicit laser profiles corresponding to three selected photon shapes were calculated. With this we lay our theoretical investigation of the three-level Λ-system to rest, and head for the very last chapter of this thesis, concerning the experimental challenges of quantum optics.

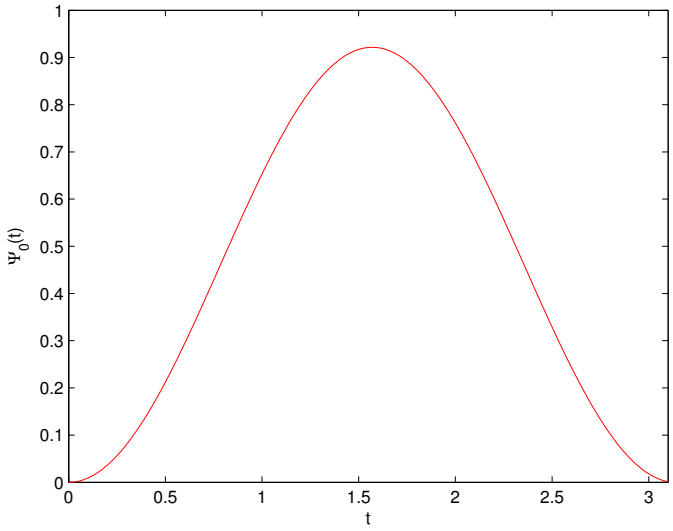

(a) The photon profile $\psi_{\rm ph}(t) = \sqrt{\frac{8}{3T}} \sin^2\left(\frac{\pi t}{T}\right)$.

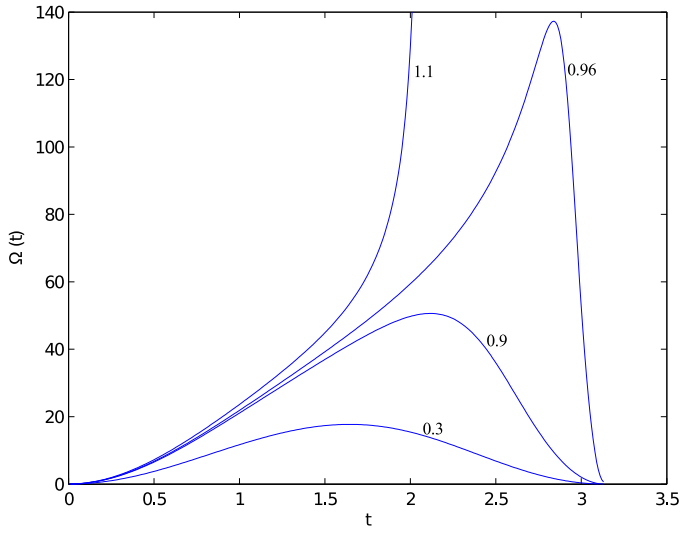

(b) The laser profiles for different photon emission efficiencies.

Figure 5.1: Figure (a) displays the predetermined photon profile, with photon emission probability $\eta = 1$. Figure (b) shows the corresponding laser profiles $\Omega(t)$ for varying photon emission efficiencies $\eta = 1.1, 0.96, 0.9, 0.3$, as indicated in the figure. $\Omega(t)$ is measured in MHz. Time is measured in μs.

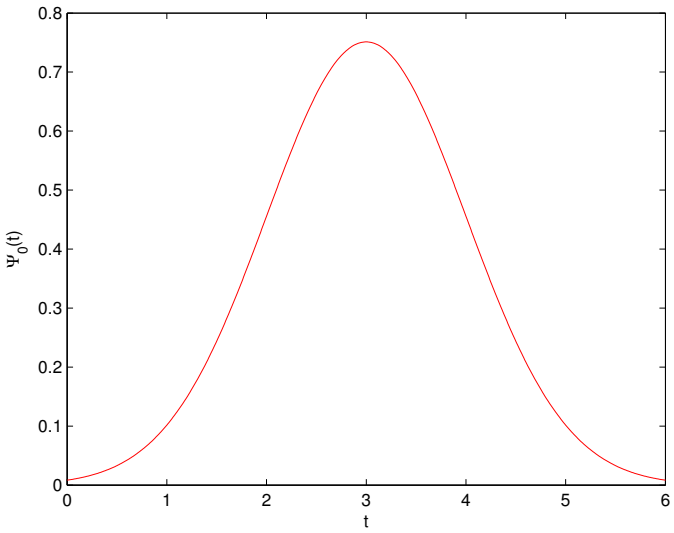

(a) The photon profile $\psi_{\mathrm{ph}}(t) = \pi^{-\frac{1}{4}} e^{-\frac{(t-3)^2}{2}}$.

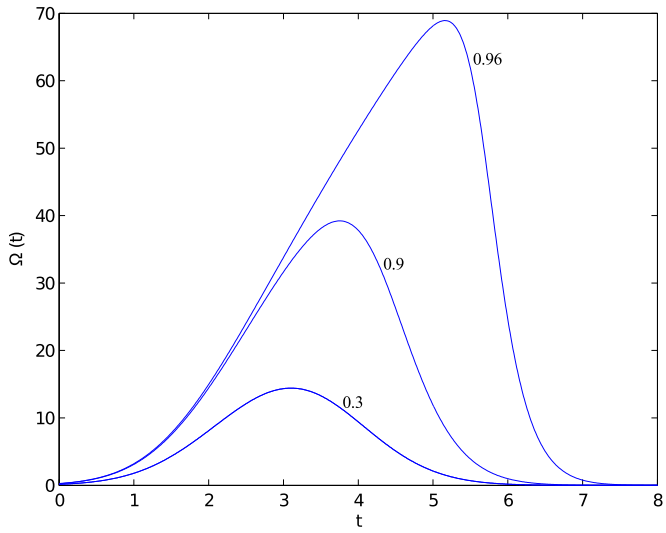

(b) The laser profiles for different photon emission efficiencies.

Figure 5.2: Figure (a) displays the predetermined photon profile, with photon emission probability $\eta = 1$. Figure (b) shows the corresponding laser profiles $\Omega(t)$ for varying photon emission efficiencies $\eta = 0.96, 0.9, 0.3$, as indicated in the figure. $\Omega(t)$ is measured in MHz. Time is measured in μs.

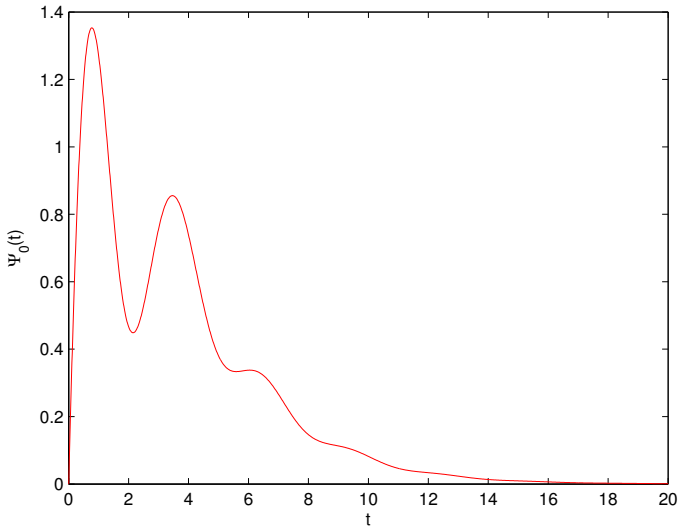

(a) The photon profile $\psi_{\rm ph}(t) = \frac{1}{N}(\sin(2.1t) + t)e^{-0.5t}$.

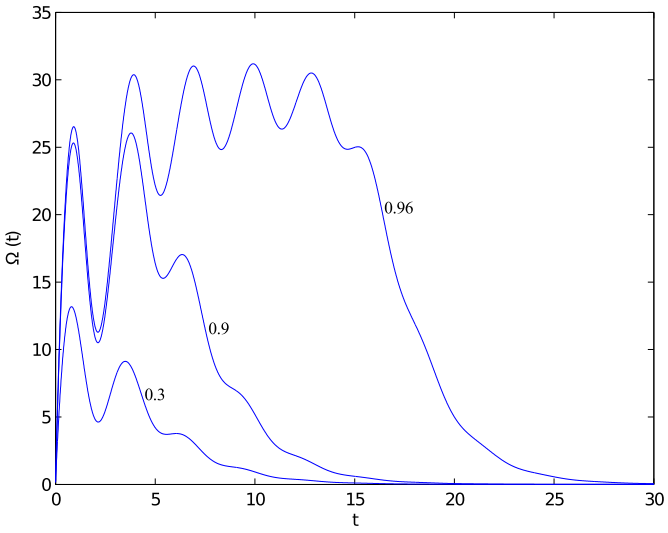

(b) The laser profiles for different photon emission efficiencies.

Figure 5.3: Figure (a) displays the predetermined photon profile, with photon emission probability $\eta = 1$. Figure (b) shows the corresponding laser profiles $\Omega(t)$ for varying photon emission efficiencies $\eta = 0.96, 0.9, 0.3$, as indicated in the figure. $\Omega(t)$ is measured in MHz. Time is measured in μs.

Chapter 6

Experimental Challenges and Concluding Remarks

Throughout this thesis we have presented a theoretical description of the set-up of a cavity-based single photon source, consisting of a three-level atom coupled to an optical cavity and a laser. In recent years the realization of such systems have been accomplished, and proven to be useful devices for quantum processing purposes.

Our work up until this point has been of pure theoretical character. In this chapter we will devote some attention to the experimental side of cavity QED, and the impressive techniques that have been developed. Techniques that allow detailed physical manipulation at single atom and single photon level. Finally, we will conclude our efforts with some closing comments on our work, and the future outlook of cavity quantum electrodynamics.

6.1 Realistic Atom-Cavity Systems

As theoreticians we are in many ways privileged as compared to our experimental fellows. The models we have worked with throughout this thesis have been simplified in several ways, and we have elegantly leaped across obstacles that would offer great difficulties in realistic situations. To give a more complete picture of the challenges that face experimental performers of the quantum art, we will devote this section to a brief study of the realization of an actual Λ-system based single photon source, as reported by Hijlkema et al. in [6]. The aim of the following description will be to give a general overview of the work needed to implement a real life single photon source.

6.1.1 The Set-up

To get some perspective on the physical dimensions of a typical optical cavity we will here give a short description of the set-up used in the experiments performed by Hijlkema and co-workers. Figure 6.1 gives a simplistic visualization of the set-up.

The optical cavity has length 0.5 mm and mode waist of 29 μm. In light of the extent of detailed control one is now able to impose on such systems, this is extraordinarily small. Yet, compared to the atom that is placed inside the cavity, and subjected to most

of the manipulation during the experiment, the cavity is relatively large. The cavity finesse is given as

$$\mathcal{F} = \frac{\Delta\lambda}{FWHM_\lambda} = 3 \times 10^4, \tag{6.1}$$

where $\Delta\lambda$ is the gap in wavelength between the different modes of the cavity, and $FWHM_\lambda$ is the full-with half-maximum of the wavelength distribution of the cavity mode. We remember from Chapter 1, that increasing $\Delta\lambda$ also increased the atom-cavity coupling. Thus, it is in our interest to make this as large as possible. $FWHM_\lambda$ measures the sharpness of the cavity mode energy. As we are interested in extracting photons of a well-defined frequency from the cavity, we naturally want this to be as small as possible. The conclusion is that large cavity finesse is desirable. With $\mathcal{F}$ in the order of 10^4, this cavity qualifies as a high-finesse cavity. Ultra-high finesse cavities with finesse values in the order of 10^6 are also achievable. To get a well defined direction of photon emission, one of the cavity mirrors is set to have 50 times higher transmittance than the other.

Starring in the role of the atom is the rubidium isotope ^{85}Rb. The three participating atomic levels are the hyperfine states $F = 3$ and $F = 2$ of the ground state $5^2\mathcal{S}_{1/2}$ and the $F' = 3$ excited state $5^2\mathcal{P}_{3/2}$. In the language of our previous Λ-model study, we have the following correspondence $F = 3 \rightarrow |e\rangle$, $F' = 3 \rightarrow |x\rangle$ and $F = 2 \rightarrow |g\rangle$. The familiar atom-cavity parameters, namely the atom-cavity coupling, the cavity mode decay rate and the atomic decay rate are measured to be $\{g_0, \kappa, \gamma_x\} = 2\pi \times \{5, 5, 3\}$ MHz. This puts this particular atom-cavity system in the intermediate coupling regime.

Starting with the atom in the $F = 3$ state, a trigger laser works together with the cavity field, to perform the STIRAP-process, transferring the atom to the $F = 2$ state. The procedure generates a cavity photon, which is emitted from the mirror with the highest degree of transparency. When the photon is successfully emitted, the atom is pumped back into starting position by the recycling laser, resonant with the atomic $F = 2 \leftrightarrow F' = 3$ transition. Once the atom reaches the initial $F = 3$ once again, the process can be reinitialized.

The recycling laser can, in addition to having a recycling function, be shown to also have a cooling effect on the atom, contributing to prolonging the time of its captivity. The average time of captivity for the atom in this set-up is in the order of 10 s. Although quite short, this is relatively good compared to other set-ups. The time scale at which the atom-cavity system operates is so small that the cavity will manage to emit a fair number of photons before the atom escapes. One of the great challenges when handling neutral atoms is to manage to keep them captive long enough for experiments to be carried out.

6.1.2 Capturing Single Atoms

One of the challenges we have yet to mention is how to actually place an atom inside our optical cavity. We cannot merely pick up a single atom and place it at our liking. We will here give a simplified account of how one captures a single atom. As will be evident, the expression "placing our atom inside the cavity", does not quite do justice

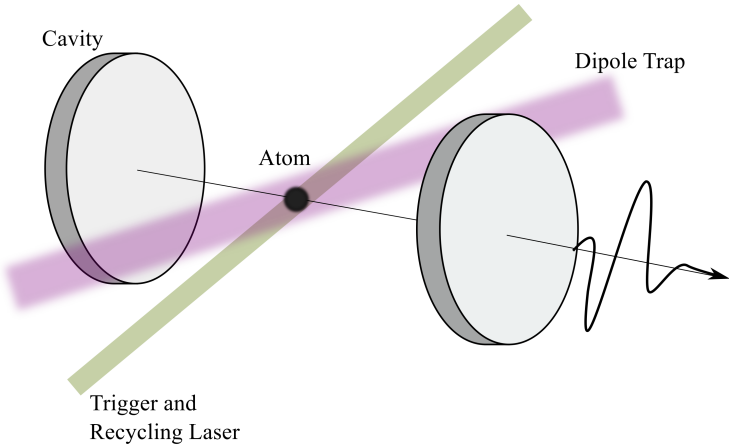

Figure 6.1: A simplified visualization of an atom-cavity set-up. The atom is held captive by a standing wave dipole trap, while the trigger laser and the cavity field work together to drive the STIRAP-process. Between succeeding photon emissions the system is reinitialized by a recycling laser.

to the actual process.

First a sample of ^{85}Rb atoms are collected from a vapor, with the help of a magneto-optical trap. This is a device that uses both laser cooling and a magnetic trap to cool and capture atoms. A simple magneto-optical trap can be constructed from applying so called Doppler cooling in combination with a spatially varying magnetic field. The term laser cooling refers to a variety of techniques, where lasers slow down atoms. In Doppler cooling, lasers with frequency just beneath one of the energy transitions of the atoms are applied from different directions. Due to the Doppler effect, laser light propagating in the opposite direction of an atom, will have the best energy match with its atomic transition, as seen from the atom. As a consequence the atoms to be more likely to absorb photons from counter propagating laser light, causing them to lose momentum, and eventually cool down.

The spatially varying magnetic field contributes to the process by functioning as a trap. It is designed to shift the energy levels of the atoms. The atomic energy transition makes a better match with the lasers when the atoms are further away from the trap center. So if an atom is headed out of the trap, it will soon swallow a photon traveling in the opposite direction, causing it to lose speed. In this way the atoms are persuaded to gather at the center of the trap.

After being captured and cooled, the atoms are placed in a running-wave dipole trap, and transported into the cavity. A dipole trap uses lasers to create an electromagnetic potential for the atomic ground state. These are usually categorized in two different types; standing wave and running wave traps. A standing wave dipole trap is constructed from two counter propagating, strongly focused lasers, of equal frequency. These will form a standing wave, creating a static potential. Such a trap is used to keep atoms at a fixed position. The running wave trap can be formed by simply turning off one of the lasers. This will cause a net flow of energy in one direction, which can be

used to transport atoms from one place to another.

When the atoms arrive at the cavity, the running-wave dipole trap is transformed into a standing wave dipole trap. Further manipulations are required to see to it that only a single atom is trapped inside the cavity. These techniques, called three-dimensional cavity cooling, exploit an additional laser and the presence of the cavity. A detailed description of the latter process can be found in [24]. When the whole process of capturing, cooling, transporting and cooling once again is over, control measurements need to be conducted to assure that there is actually a single atom inside the cavity. Given that the procedure ended in success, the actual atom-cavity experiment can finally begin.

6.1.3 Quantum Degrees of Coherence

In our theoretical investigation of cavity based photon sources, we have taken for granted that the photons being produced are in fact single photons. Remembering that in the derivation of the Jaynes-Cummings Hamiltonian, which is crucial to all the models we have looked at, we neglected all terms in the interaction Hamiltonian concerning processes of more than one photon at the time. To be certain that a photon source actually is producing non-classical single photons, the photon statistics needs to be measured. The nature of different types of light is usually experimentally determined by measuring the degree of second order coherence.

It can be shown [16] that for a single mode of the electromagnetic field the degree of second order coherence can be expressed

$$g^{(2)}(\tau) = \frac{\left\langle \hat{a}^\dagger(0)\hat{a}^\dagger(\tau)\hat{a}(\tau)\hat{a}(0) \right\rangle}{\left\langle \hat{a}^\dagger\hat{a} \right\rangle^2}, \tag{6.2}$$

where $\hat{a}(t)$ is the time dependent annihilation operator of the single mode in question. Here it is assumed that the field is stationary, in the sense that correlations will only depend on the difference in time of two measurements $\tau = t_2 - t_1$. For light in a quantum mechanical Fock state $|n\rangle$, this gives

$$g^{(2)}(0) = \frac{\langle n|\, \hat{a}^\dagger\hat{a}^\dagger\hat{a}\hat{a}\, |n\rangle}{\langle n|\, \hat{a}^\dagger\hat{a}\, |n\rangle} = \frac{n(n-1)}{n^2} = 1 - \frac{1}{n} < 1. \tag{6.3}$$

We see that for a single photon we have $g^{(2)}(0) = 0$. It can similarly be shown that for coherent light we have $g^{(2)}(0) = 1$, and for light in a chaotic thermal state we have $g^{(2)}(0) \geq 1$. This shows that measuring $g^{(2)}(0)$ will in fact determine what kind of light we can expect to receive from a photon source. For a thorough introduction to the concepts of quantum coherence, see for instance [22].

But exactly how can $g^{(2)}(0)$ be measured? In [6], a so-called Hanbury-Brown and Twiss detection scheme is applied in this regard. This consists of a beam-splitter and two photon detectors. See Figure 6.2.

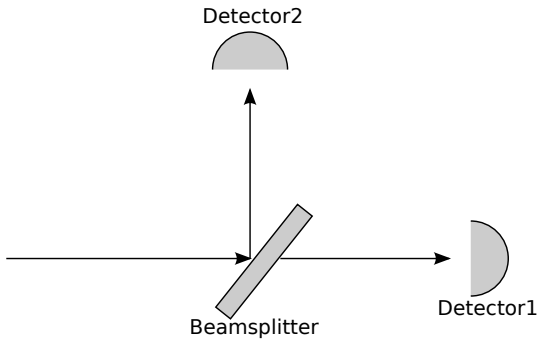

Figure 6.2: A schematic presentation of a Hanbury-Brown and Twiss detection scheme. It consists of a 50/50 beamsplitter and two photon detectors.

The operator responsible for the interaction between the field and the photon detection device will contain the annihilation operator of the field $\hat{a}$. So the probability of detecting a photon at time t will obey

$$P(t) \propto \left\langle |\hat{a}(t)|^2 \right\rangle . \tag{6.4}$$

Looking at $g^{(2)}(\tau)$ we have

$$g^{(2)}(\tau) = \frac{\left\langle |\hat{a}(\tau)\hat{a}(0)|^2 \right\rangle}{\left\langle |\hat{a}(0)|^2 \right\rangle \left\langle |\hat{a}(\tau)|^2 \right\rangle} = \frac{P_{12}(\tau)}{P_1(0)P_2(\tau)}. \tag{6.5}$$

Here $P_{12}(\tau)$ is the joint probability of detecting a photon at time $t = 0$ and $t = \tau$, while $P_1(0)$ and $P_2(\tau)$ is the probabilities of detecting a photon at time $t = 0$ and $t = \tau$.

For $\tau = 0$, P_{12} corresponds to the simultaneous detection of a photon at both detectors, while P_1 and P_2 are the respective probabilities of detecting a photon either at Detector 1 or Detector 2. By measuring these probabilities over a series of cavity photon emission, one determines the nature of the photons from the cavity based photon source. $g^{(2)}(0) = 0$ indicates the ideal single-photon Fock state. This simply reflects that if the emitted field contains only one photon, it will never be possible to have a simultaneous detection of photons at both detectors. $0 < g^{(2)}(0) < 1$ indicates a Fock state of several photons, while $g^{(2)}(0) \geq 1$ reports of classical light.

Of the 526 distinct experiment runs that are reported by Hijlkema and co-workers, 454 of them passed the coherence test, producing true single photon data.

6.2 Concluding Remarks

With this brief review of the experimental aspects of cavity quantum electrodynamics, we have hopefully brought some attention to the great achievements behind realizing the models we have been working with throughout this thesis. Extreme precision and craftsmanship is required at all stages of the experiments, and success is by no means a given. It should come as no surprise that one of the major challenges facing quantum schemes based on atom-cavity set-ups is the technical complexity necessary for operating them.

Seeing all the work that is put into realizing such simple systems, raises the question of whether or not we will ever be able to meet the final goal of realizing a fully functional quantum processor or communication network. To answer this question we quote the famous words of the American novelist Don Williams Jr

> The road of life twists and turns and no two directions are ever the same.
> Yet our lessons come from the journey, not the destination.

The advances made within physics in the name of quantum information technology are many, and has significantly deepened our understanding of natures behavior on microscopic scales. Regardless of whether or not the final goal of building a quantum computer is ever reached, the journey towards it has not been in vain.

This thesis gives a guided tour through the realms of cavity quantum electrodynamics, and its applications within single photon production. Starting with the basic interaction between a single cavity mode and a two-level atom, and adding to it piece by piece, we have gradually built more complex and useful systems. In the two-level Jaynes-Cummings model, a great deal was accomplished in terms of photon emission efficiency by adjusting the coupling strength and decay rates. In the upgraded three-level Λ-model one of the main parts was played by the laser. By adjusting its coupling to the atom, we could control both the photon emission efficiency and the temporal photon profile. Adding to our understanding of the behavior of decaying quantum systems was the numerical Monte Carlo wavefunction method [17].

In spite of the simplicity of the theoretical models studied throughout this thesis, our efforts have been very rewarding. After all our hard work we are not only left with clever schemes to obtain maximal photon emission efficiency or specific photon shapes, but a deeper understanding of the world of quantum optics.

There has recently been successful realizations of quantum state transfer, entanglement between distant nodes and the storage and retrieval of a single photon, with the use of an atom-cavity Λ-system [28]. These set-ups are expected to play a central role in further implementations of quantum network schemes. Optical cavities, though difficult to maneuver, have turned out to be extremely useful devices, which has lead to a wealth of atom physics development during the last decades. As of this writing, the latest Nobel Prize in Physics was awarded for advances in cavity quantum electrodynamics.

Appendices

Appendix A

The Rotating Wave Approximation

We consider the case of an atom-cavity system, where two of the atomic levels $|g\rangle$ and $|x\rangle$ are strongly interacting with only one of the cavity modes, as described by the Hamiltonian

$$\begin{aligned}\hat{H} &= \hat{H}_0 + \hat{H}_{AF},\\ \hat{H}_{AF} &= -\hbar g_0\Big(\hat{a} + \hat{a}^\dagger\Big)\Big(\,|x\rangle\langle g| + |g\rangle\langle x|\,\Big).\end{aligned} \tag{A.1}$$

Here $\hat{H}_0$ describes the bare atom and field, while $\hat{H}_{AF}$ describes their interaction.

The energy of the cavity mode $\hbar\omega_k$ is assumed to be close to the energy transitions $\hbar(\omega_x - \omega_g)$ of the atom. This assumption allows us to simplify the Hamiltonian of the atom-cavity interaction. To see how, we must go to the interaction picture, by transformation with the unitary operator

$$\hat{U}_0(t) = e^{-\frac{i}{\hbar}\hat{H}_0 t}. \tag{A.2}$$

In this picture the time evolution of an operator $\hat{A}$ is given by

$$\hat{A}_I = \hat{U}_0(t)^\dagger(t)\hat{A}_S\hat{U}_0(t) = e^{\frac{i}{\hbar}\hat{H}_0 t}\hat{A}e^{-\frac{i}{\hbar}\hat{H}_0 t} = \hat{A} + [\hat{H}_0, \hat{A}] + \frac{1}{2}[\hat{H}_0, [\hat{H}_0, \hat{A}]] + \ldots, \tag{A.3}$$

and the state kets are transformed as

$$|\psi(t)\rangle_I = \hat{U}_0^\dagger(t)\,|\psi(t)\rangle\,. \tag{A.4}$$

The time evolution of the state kets is determined by the modified Scrödinger equation

$$i\hbar\frac{d}{dt}\,|\psi(t)\rangle_I = \hat{H}_I\,|\psi(t)\rangle_I\,, \tag{A.5}$$

with the interaction Hamiltonian

$$\hat{H}_I = \hat{U}_0^\dagger(t)\hat{H}_{AF}\hat{U}_0(t). \tag{A.6}$$

The corresponding time evolution operator is

$$\hat{U}_I(t,t_0) = \sum_{n=0}^{\infty} \left(\frac{-i}{\hbar}\right)^n \int_{t_0}^{t} dt_1 \int_{t_0}^{t_1} dt_2 \ldots \int_{t_0}^{t_{n-1}} dt_n \hat{H}_I(t_1)\hat{H}_I(t_2)\ldots\hat{H}_I(t_n). \tag{A.7}$$

We are now interested in the time evolution of the creation and annihilation operators $\hat{a}^\dagger$ and $\hat{a}$, as well as the atomic lowering and raising operators $|g\rangle\langle x|$ and $|x\rangle\langle g|$. To lighten the calculations of this subsection we introduce the operator notation

$$|\alpha\rangle\langle\beta| = \hat{\sigma}_{\alpha\beta}. \tag{A.8}$$

To find the time development of an operator we must evaluate the expression of (A.3). We observe that since the raising and lowering operators for both field and atom are Hermitian conjugates of each other, it will suffice to find the time evolution of one of them. Determining the commutators $[\hat{H}_0, \hat{a}^\dagger]$ and $[\hat{H}_0, \hat{\sigma}_{xg}]$ seems like a reasonable place to start. Before setting out on the necessary calculations we take the time to note some useful operator relations

$$[\hat{a}, \hat{a}^\dagger] = 1, \quad [\hat{\sigma}_{\alpha\alpha}, \hat{\sigma}_{\alpha\beta}] = \hat{\sigma}_{\alpha\beta}, \quad [\hat{\sigma}_{\alpha\alpha}, \hat{\sigma}_{\beta\alpha}] = -\hat{\sigma}_{\beta\alpha} \tag{A.9}$$

With these relations at hand we can easily calculate the commutators in question

$$[\hat{H}_0, \hat{a}^\dagger] = \hbar\omega_k[\hat{a}\hat{a}^\dagger, \hat{a}^\dagger] = \hbar\omega_k(\hat{a}[\hat{a}^\dagger, \hat{a}^\dagger] + [\hat{a}, \hat{a}^\dagger]\hat{a}^\dagger) = \hbar\omega_k\hat{a}^\dagger, \tag{A.10}$$

$$[\hat{H}_0, \hat{\sigma}_{gx}] = \hbar[\omega_x\hat{\sigma}_{gg} + \omega_x\hat{\sigma}_{xx}, \hat{\sigma}_{gx}] = -\hbar(\omega_x - \omega_g)\hat{\sigma}_{gx} = -\hbar\omega_{xg}\hat{\sigma}_{gx}. \tag{A.11}$$

The commutators in (A.11) and (A.10) are both of the form

$$[\hat{H}_0, \hat{A}] = \hbar\kappa\hat{A}, \quad \text{for } \kappa = \text{const.} \tag{A.12}$$

Inserting this into (A.3) we find a time evolution given by

$$\hat{A}_I = \hat{A} + i\kappa\hat{A}t + (i\kappa)^2\hat{A}t^2 + \cdots + (i\kappa t)^n\hat{A} + \cdots = \hat{A}e^{i\kappa t}. \tag{A.13}$$

From this result we immediately know the the time evolution of our four operators

$$\hat{a}_I^\dagger = \hat{a}^\dagger e^{i\omega_k t}, \qquad \hat{\sigma}_{gx}^I = \hat{\sigma}_{gx}e^{-i(\omega_x-\omega_g)t},$$
$$\hat{a}_I = \hat{a}e^{-i\omega_k t}, \qquad \hat{\sigma}_{xg}^I = \hat{\sigma}_{xg}e^{i(\omega_x-\omega_g)t}.$$

In terms of the newly introduced $\hat{\sigma}$-operators the interaction Hamiltonian can be written

$$\begin{aligned}\hat{H}_I =& \hat{U}_0^\dagger\hat{H}_{AF}\hat{U}_0 \\ =& -\hbar g_0\Big(\hat{a}\hat{\sigma}_{xg}e^{i(\omega_{xg}-\omega_k)t} + \hat{a}\hat{\sigma}_{gx}e^{-i(\omega_{xg}+\omega_k)t} \\ &+ \hat{a}^\dagger\hat{\sigma}_{xg}e^{i(\omega_{xg}+\omega_k)t} + \hat{a}^\dagger\hat{\sigma}_{gx}e^{-i(\omega_{xg}-\omega_k)t}\Big).\end{aligned} \tag{A.14}$$

To first order the time evolution operator in (A.7) can be approximated to

$$\hat{U}_I(t,t_0) \approx 1 - \frac{i}{\hbar}\int_{t_0}^{t} \hat{H}_I(t_1)dt_1. \tag{A.15}$$

Assume the system is in state $|\psi(0)\rangle$ at $t_0 = 0$, then at a later time t it will be in

$$\begin{aligned}
|\psi(t)\rangle &= \hat{U}_I(t)\,|\psi(0)\rangle \\
&= |\psi(0)\rangle - \frac{i}{\hbar}\int_0^t \hat{H}_I(t_1)dt_1\,|\psi(0)\rangle \\
&= |\psi(0)\rangle + ig_0\int_0^t \hat{a}\hat{\sigma}_{xg}e^{i(\omega_{xg}-\omega_k)t_1} + \hat{a}\hat{\sigma}_{gx}e^{-i(\omega_{xg}+\omega_k)t_1} \\
&+ \hat{a}^\dagger\hat{\sigma}_{xg}e^{i(\omega_{xg}+\omega_k)t_1} + \hat{a}^\dagger\hat{\sigma}_{gx}e^{-i(\omega_{xg}-\omega_k)t_1}dt_1\,|\psi(0)\rangle \\
&= |\psi(0)\rangle + g_0\Big(\frac{1}{\omega_{xg}-\omega_k}\hat{a}\hat{\sigma}_{xg}e^{i(\omega_{xg}-\omega_k)t} - \frac{1}{\omega_{xg}+\omega_k}\hat{a}\hat{\sigma}_{gx}e^{-i(\omega_{xg}+\omega_k)t} \\
&+ \frac{1}{\omega_{xg}+\omega_k}\hat{a}^\dagger\hat{\sigma}_{xg}e^{i(\omega_{xg}+\omega_k)t} - \frac{1}{\omega_{xg}-\omega_k}\hat{a}^\dagger\hat{\sigma}_{gx}e^{-i(\omega_{xg}-\omega_k)t}\Big).
\end{aligned} \tag{A.16}$$

Now since $\omega_k \approx \omega_{xg}$, the terms with $\omega_{xg} - \omega_k$ in the denominator will be much larger than the ones with $\omega_{xg} + \omega_k$. This justifies the so-called *rotating wave approximation*, which involves dropping the terms of the Hamiltonian with $\omega_{xg} + \omega_k$ in the exponent. Inspecting the Hamiltonian, we see that it contains four different types of terms

$\hat{a}\hat{\sigma}_{gx}$ Annihilates a photon and lowers the atom from the excited state to the ground state.

$\hat{a}^\dagger\hat{\sigma}_{xg}$ Creates a photon and excites the atom from the ground state to the excited state.

$\hat{a}\hat{\sigma}_{xg}$ Annihilates a photon and excites the atom from the excited state to the ground state.

$\hat{a}^\dagger\hat{\sigma}_{gx}$ Creates a photon and lowers the atom from the excited state to the ground state.

In the rotating wave approximation the terms containing $\hat{a}\hat{\sigma}_{gx}$ and $\hat{a}^\dagger\hat{\sigma}_{xg}$ are dropped. So the terms that are neglected in this approximation are those that do not conserve the total energy of the the atom and the cavity mode. That is, the terms that either lower or raise both the energy of the atom and the field. It seems reasonable that these terms should give a negligible contribution in comparison to the ones that do respect conservation of energy.

In the rotating wave approximation the atom-cavity interaction Hamiltonian in the Schrödinger picture is reduced to

$$\hat{H}_{AF} = -\hbar g_0\Big(\hat{a}\,|x\rangle\langle g| + \hat{a}^\dagger\,|g\rangle\langle x|\Big). \tag{A.17}$$

Appendix B

Fourth Order Runge-Kutta Simulation of The Λ-system

Here we give an account for the implementation of the fourth order Runge-Kutta simulation of the decaying Λ-system. A general description is found in Chapter 3. After a brief explanation of the practical procedure follows the program implementation in C++.

Generally a state of the three-level system can be expressed as a superposition of the form

$$|\psi(t)\rangle = c_g(t)\,|g,1\rangle + c_e(t)\,|e,0\rangle + c_x(t)\,|x,0\rangle\,. \tag{B.1}$$

The system evolution is simulated numerically through the coefficients $c_g(t), c_e(t)$ and $c_x(t)$. Before we begin the simulations we start by choosing a time interval $[0, t_{\max}]$, which is divided into N segments each corresponding to a time step δt. This time interval is represented numerically by an array of length N. We then make corresponding arrays to keep track of the coefficients $c_g(t), c_e(t)$ and $c_x(t)$ as functions of time. The system state is then initialized from screen, and the simulations can start.

```
1  using namespace std;
2
3  # include <iostream>    //writing to and from screen
4  # include <fstream>     //writing to file
5  # include <iomanip>     //manipulation of output to file
6  # include <cmath>       //mathematical functions
7  # include <complex>     //handling complex numbers
8
9
10 //Defining types
11 typedef complex<double> cmplx;
12
13 //Defining global variables
14 cmplx imag_i(0,1);
15 double PI = 4.0*atan(1.0);
16
17
18 //Declaring Methods
```

```
19 void initialize(cmplx *, cmplx *, cmplx *, cmplx *, double *, double, int,
       double);
20 double omega_function(double);
21 void rk4(cmplx *, double, double, double, double, double);
22 void calc_k(cmplx *, cmplx *, double, double, double, double, double);
23 cmplx function_g(cmplx, cmplx, double, double);
24 cmplx function_e(cmplx, double);
25 cmplx function_x(cmplx, cmplx, cmplx, double, double, double);
26 void output(double *, cmplx *, cmplx *, cmplx *, int);
27
28
29 int main(){
30
31   //Declaring variables
32   int N;
33   double t_max, t_min, h, g_0, kappa, gamma_x;
34
35   t_max = 20.0; //Upper time limit
36   t_min = -20.0;
37   N = 200000; //Number of subintervals - 1
38   h = (t_max-t_min)/N;
39   //Coupling constant and decay rates
40   g_0 = 9*PI;
41   kappa = 0.0;
42   gamma_x = 500*PI;
43
44   //Reserving memory for arrays
45   cmplx *c, *c_g, *c_e, *c_x;
46   double *t;
47
48   t = new double[N+1]; //Time array
49
50   c = new cmplx[3]; //Arrays containing the coefficients of the system
       state
51   c_g = new cmplx[N+1];
52   c_e = new cmplx[N+1];
53   c_x = new cmplx[N+1];
54
55   //Initializing coefficients
56   initialize(c_g, c_e, c_x, c, t, h, N, t_min);
57
58   for(int i=1; i<=N; i++){
59     rk4(c, kappa, g_0, gamma_x, h, t[i]);
60     c_g[i] = c[0];
61     c_e[i] = c[1];
62     c_x[i] = c[2];
63   }
64
65   output(t, c_g, c_e, c_x, N);
66
67   //Free memory
68   delete [] t;
69   delete [] c;
70   delete [] c_g;
71   delete [] c_e;
72   delete [] c_x;
```

```
}



//*****************************************************************
//                              METHODS
//*****************************************************************

void initialize(cmplx *c_g, cmplx *c_e, cmplx *c_x, cmplx *c,
    double *t, double h, int N, double t_min){

  //Reading initial coefficient values from screen
  cout << "Initial value of c_g:" << "\n";
  cin >> c_g[0];
  cout << "Inital value of c_e:" << "\n";
  cin >> c_e[0];
  cout << "Initial value of c_x:" << "\n";
  cin >> c_x[0];

  c[0] = c_g[0];
  c[1] = c_e[0];
  c[2] = c_x[0];

  //Initializing time array
  for(int i=0; i<=N; i++){
    t[i] = t_min + i*h;
  }

  return;
}//End initialize()


void rk4(cmplx *c, double kappa, double g_0, double gamma_x, double h,
   double t){

  double omega, t_temp;

  cmplx *c_temp, *k1, *k2,*k3, *k4;
  c_temp = new cmplx[3];
  k1 = new cmplx[3];
  k2 = new cmplx[3];
  k3 = new cmplx[3];
  k4 = new cmplx[3];

  omega = omega_function(t);

  //Calculating k1
  calc_k(k1,c,kappa, g_0, omega, gamma_x, h);

  for(int i=0; i<=2; i++){
    c_temp[i] = c[i] + 0.5*h*k1[i];
  }
  t_temp = t + 0.5*h;
  omega = omega_function(t_temp);
```

```
129
130   //Calculating k2
131   calc_k(k2, c_temp, kappa, g_0, omega, gamma_x, h);
132
133   for(int i=0; i<=2; i++){
134     c_temp[i] = c[i] + 0.5*h*k2[i];
135   }
136
137   //Calculating k3
138   calc_k(k3, c_temp, kappa, g_0, omega, gamma_x, h);
139
140   for(int i=0; i<=2; i++){
141     c_temp[i] = c[i] + h*k3[i];
142   }
143   t_temp = t + h;
144   omega = omega_function(t_temp);
145
146   //Calculating k4
147   calc_k(k4, c_temp, kappa, g_0, omega, gamma_x, h);
148
149   //Estimating values of coefficients
150   for(int i=0; i<=2; i++){
151     c[i] = c[i] + (1/6.0)*(k1[i] + 2.0*k2[i] + 2.0*k3[i] + k4[i]);
152   }
153
154   //Free memory
155   delete [] c_temp;
156   delete [] k1;
157   delete [] k2;
158   delete [] k3;
159   delete [] k4;
160     return;
161 }//End rk4()
162
163
164 void calc_k(cmplx *k, cmplx *c, double kappa, double g_0, double omega,
165       double gamma_x, double h){
166   k[0] = h*function_g(c[0], c[2], kappa, g_0);
167   k[1] = h*function_e(c[2], omega);
168   k[2] = h*function_x(c[0], c[1], c[2], g_0, omega, gamma_x);
169     return;
170 }//End calc_k()
171
172
173 //Function controlling the laser profile
174 double omega_function(double t){
175   double omega = 14*2*PI*9*exp(-(t/3*PI)*(t/3*PI));
176   return omega;
177 }//End omega()
178
179
180 cmplx function_g(cmplx c_g, cmplx c_x, double kappa, double g_0){
181   cmplx f = -kappa*c_g + imag_i*g_0*c_x;
182   return f;
183 }//End function_g()
184
```

```
185
186 cmplx function_e(cmplx c_x, double omega){
187   cmplx f = imag_i*omega/2.0*c_x;
188   return f;
189 }//End function_e()
190
191
192 cmplx function_x(cmplx c_g, cmplx c_e, cmplx c_x, double g_0, double omega
      ,
193       double gamma_x){
194   cmplx f = imag_i*g_0*c_g + imag_i*omega/2.0*c_e - gamma_x*c_x;
195   return f;
196 }//End function_x()
197
198
199 //Writing output to file
200 void output(double *t, cmplx *c_g, cmplx *c_e, cmplx *c_x, int N){
201   ofstream xfile("rungeSTIRAP.txt");
202   xfile << setiosflags(ios::showpoint | ios::uppercase);
203
204   for(int i=0; i<=N; i++){
205     xfile << setw(15) << setprecision(8) << t[i];
206     xfile << setw(15) << setprecision(8) << pow(abs(c_g[i]),2);
207     xfile << setw(15) << setprecision(8) << pow(abs(c_e[i]),2);
208     xfile << setw(15) << setprecision(8) << pow(abs(c_x[i]),2) << "\n";
209   }
210   return;
211 }//End output()
```

./C++/RK4.cpp

Appendix C

Monte Carlo Simulation of The Λ-system

Here we give an account for the implementation of the Monte Carlo wavefunction method for the decaying Λ-system. A general description is found in Chapter 4. After a brief explanation of the practical procedure and a schematic representation of the program structure, follows the program implementation in C++.

Generally a state of the three-level system can be expressed as a superposition of the form

$$|\psi(t)\rangle = c_g(t)\,|g,1\rangle + c_e(t)\,|e,0\rangle + c_x(t)\,|x,0\rangle\,. \tag{C.1}$$

The system evolution is simulated numerically through the coefficients $c_g(t), c_e(t)$ and $c_x(t)$. Before we begin the Monte Carlo simulations we start by choosing a time interval $[0, t_{\max}]$, which is divided into N segments each corresponding to a time step δt. This time interval is represented numerically by an array of length N. We then make corresponding arrays to keep track of the coefficients $c_g(t), c_e(t)$ and $c_x(t)$ as functions of time. The system state is then initialized from screen, and the Monte Carlo simulations can start. A schematic representation of the program structure is given in Figure C.1.

To calculate the continuous part of the time evolution, a standard fourth-order Runge-Kutta method, as described in Section 3.2.4, has been used. To generate uniformly distributed random numbers between 0 and 1, the ran3 generator [26] is used.

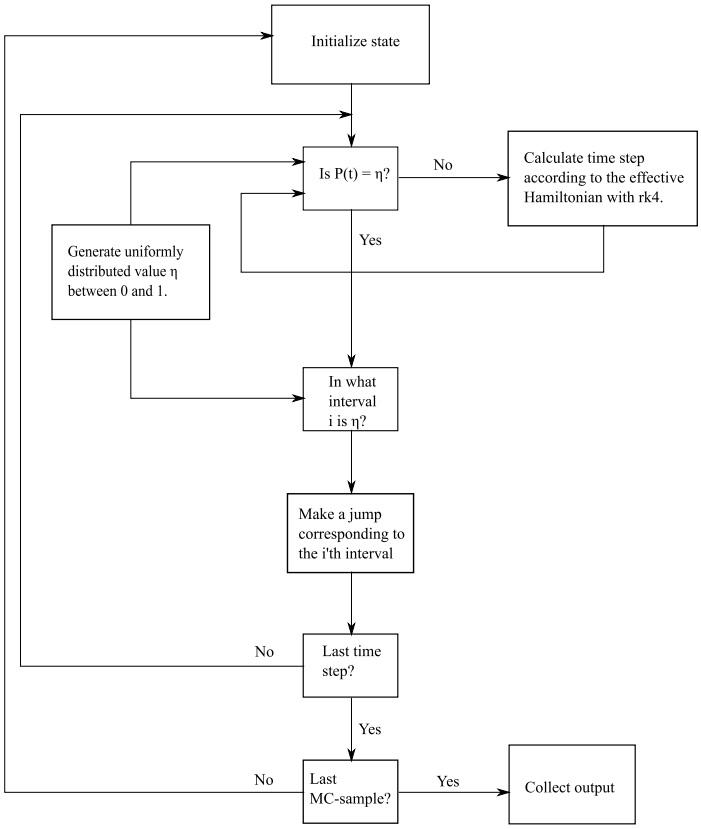

Figure C.1: Schematic description of the program using the Monte Carlo wave function method to simulate the atom-cavity system.

```
using namespace std;

# include <iostream>       //writing to and from screen
# include <fstream>        //writing to file
# include <iomanip>        //manipulation of output to file
# include <cmath>          //mathematical functions
# include <complex>        //handling complex numbers
# include "lib.h"          //random number generators
# include <time.h>         //timing

//Defining types
typedef complex<double> cmplx;

//Defining global variables
cmplx imag_i(0,1);
double PI = 4.0*atan(1.0);


//Declaring Methods
void initialize(cmplx *, cmplx *, cmplx *, cmplx *, cmplx *, double *,
    double,
    int, double);
void monteCarloSampling(cmplx *, double *, double *, double *, cmplx *,
    cmplx *,
      cmplx *, cmplx *, double *, double, double, double,
      double, double, double, int, int);
double waitingTimeDist(cmplx *);
double omega_function(double);
void rk4(cmplx *, double, double, double, double, double);
void calc_k(cmplx *, cmplx *, double, double, double, double, double);
cmplx function_g(cmplx, cmplx, double, double);
cmplx function_e(cmplx, double);
cmplx function_x(cmplx, cmplx, cmplx, double, double, double);
void quantumJump(cmplx *, double, double, double, double);
void output(double *, double *, double *, double *, int);


int main(){

  //Declaring variables
  int N, numberOfSamples;
  double t_max, t_min, h, g_0, kappa, gamma_xg, gamma_xe, gamma_x;

  t_max = 20.0; //Upper time limit
  t_min = -20.0;
  N = 60000; //Number of subintervals - 1
  numberOfSamples = 10000; //Number of Monte_Carlo samples
  h = (t_max-t_min)/N;
  //Coupling constant and decay rates
  g_0 = 9*PI;
  kappa = 0.25*PI;
  gamma_xg = 15*PI;
  gamma_xe = 60*PI;
  gamma_x = gamma_xg + gamma_xe;

  //Reserving memory for arrays
```

```
55    cmplx *c_init, *c, *c_g, *c_e, *c_x;
56    double *t, *c_gSquared, *c_eSquared, *c_xSquared;
57
58    t = new double[N+1]; //Time array
59    c = new cmplx[3];     //Arrays containing the coefficients of the system
          state
60    c_init = new cmplx[3];
61    c_g = new cmplx[N+1];
62    c_e = new cmplx[N+1];
63    c_x = new cmplx[N+1];
64    c_gSquared = new double[N+1];
65    c_eSquared = new double[N+1];
66    c_xSquared = new double[N+1];
67
68    //Initializing coefficients
69    initialize(c_g, c_e, c_x, c, c_init, t, h, N, t_min);
70
71    //Monte-Carlo simulation
72    monteCarloSampling(c_init, c_gSquared, c_eSquared, c_xSquared, c, c_g,
          c_e,
73            c_x, t, kappa, g_0, gamma_x, gamma_xg, gamma_xe, h, N,
74            numberOfSamples);
75
76    //Writing output to file
77    output(t, c_gSquared, c_eSquared, c_xSquared, N);
78
79    //Free memory
80    delete [] t;
81    delete [] c;
82    delete [] c_init;
83    delete [] c_g;
84    delete [] c_e;
85    delete [] c_x;
86    delete [] c_gSquared;
87    delete [] c_eSquared;
88    delete [] c_xSquared;
89
90 }//End main()
91
92
93
94
95 //*************************************************************
96 //                              METHODS
97 //*************************************************************
98
99
100 void initialize(cmplx *c_g, cmplx *c_e, cmplx *c_x, cmplx *c, cmplx *
        c_init,
101     double *t, double h, int N, double t_min){
102
103    //Reading initial coefficient values from screen
104    cout << "Initial value of c_g:" << "\n";
105    cin >> c_init[0];
106    cout << "Inital value of c_e:" << "\n";
107    cin >> c_init[1];
```

```
108   cout << "Initial value of c_x:" << "\n";
109   cin >> c_init[2];
110
111   //Initializing time array
112   for(int i=0; i<=N; i++){
113     t[i] = t_min + i*h;
114   }
115
116   return;
117 }//End initialize()
118
119
120 void monteCarloSampling(cmplx *c_init, double *c_gSquared, double *
      c_eSquared,
121       double *c_xSquared, cmplx *c, cmplx *c_g, cmplx *c_e,
122       cmplx *c_x, double *t, double kappa, double g_0,
123       double gamma_x, double gamma_xg, double gamma_xe,
124       double h, int N, int numberOfSamples){
125   double P, eta, rho, squared_g, squared_e, squared_x, norm;
126   long idum = -time(NULL);
127
128     for(int i=0; i<numberOfSamples; i++){
129
130       //The coefficients must be initialized before each MC-sample.
131       for(int j=0; j<3; j++){
132   c[j] = c_init[j];
133       }
134       c_g[0] = c_init[0];
135       c_e[0] = c_init[1];
136       c_x[0] = c_init[2];
137
138
139
140       //Calculating the time evolution
141       eta = ran3(&idum);
142       for(int k=1; k<=N; k++){
143
144   P = waitingTimeDist(c);
145
146   if(P<eta){
147     rk4(c, kappa, g_0, gamma_x, h, t[k]);
148   }
149   else{
150     rho = ran3(&idum);
151     quantumJump(c, gamma_xg, gamma_xe, kappa, rho);
152     eta = ran3(&idum);
153   }
154   c_g[k] = c[0];
155   c_e[k] = c[1];
156   c_x[k] = c[2];
157       }
158
159
160       //Computing average populations
161       for(int l=0; l<=N; l++){
162
```

```
163   squared_g = abs(c_g[l])*abs(c_g[l]);
164   squared_e = abs(c_e[l])*abs(c_e[l]);
165   squared_x = abs(c_x[l])*abs(c_x[l]);
166   norm = squared_g + squared_e + squared_x;
167
168   if(norm != 0){
169     if(i==0){
170       c_gSquared[l] = squared_g/norm;
171       c_eSquared[l] = squared_e/norm;
172       c_xSquared[l] = squared_x/norm;
173     }
174     else{
175       c_gSquared[l] += squared_g/norm;
176       c_eSquared[l] += squared_e/norm;
177       c_xSquared[l] += squared_x/norm;
178     }
179   }
180   if(norm == 0){
181
182     if(i==0){
183       c_gSquared[l] = squared_g;
184       c_eSquared[l] = squared_e;
185       c_xSquared[l] = squared_x;
186     }
187     else{
188       c_gSquared[l] += squared_g;
189       c_eSquared[l] += squared_e;
190       c_xSquared[l] += squared_x;
191     }
192   }
193
194       }
195     }//End for()
196
197   for(int m=0; m<=N; m++){
198     c_gSquared[m] /= numberOfSamples;
199     c_eSquared[m] /= numberOfSamples;
200     c_xSquared[m] /= numberOfSamples;
201   }
202
203
204 }//End monteCarloSampling()
205
206
207
208 double waitingTimeDist(cmplx *c){
209   double P = 1 - (pow(abs(c[0]),2) + pow(abs(c[1]),2) + pow(abs(c[2]),2));
210   return P;
211 }//End waitingTimeDist()
212
213
214 void rk4(cmplx *c, double kappa, double g_0, double gamma_x, double h,
215    double t){
216
217   double omega, t_temp;
218
```

```
219   cmplx *c_temp, *k1, *k2,*k3, *k4;
220   c_temp = new cmplx[3];
221   k1 = new cmplx[3];
222   k2 = new cmplx[3];
223   k3 = new cmplx[3];
224   k4 = new cmplx[3];
225
226   omega = omega_function(t);
227
228   //Calculating k1
229   calc_k(k1,c,kappa, g_0, omega, gamma_x, h);
230
231   for(int i=0; i<=2; i++){
232     c_temp[i] = c[i] + 0.5*h*k1[i];
233   }
234   t_temp = t + 0.5*h;
235   omega = omega_function(t_temp);
236
237   //Calculating k2
238   calc_k(k2, c_temp, kappa, g_0, omega, gamma_x, h);
239
240   for(int i=0; i<=2; i++){
241     c_temp[i] = c[i] + 0.5*h*k2[i];
242   }
243
244   //Calculating k3
245   calc_k(k3, c_temp, kappa, g_0, omega, gamma_x, h);
246
247   for(int i=0; i<=2; i++){
248     c_temp[i] = c[i] + h*k3[i];
249   }
250   t_temp = t + h;
251   omega = omega_function(t_temp);
252
253   //Calculating k4
254   calc_k(k4, c_temp, kappa, g_0, omega, gamma_x, h);
255
256   //Estimating values of coefficients
257   for(int i=0; i<=2; i++){
258     c[i] = c[i] + (1/6.0)*(k1[i] + 2.0*k2[i] + 2.0*k3[i] + k4[i]);
259   }
260
261   //Free memory
262   delete [] c_temp;
263   delete [] k1;
264   delete [] k2;
265   delete [] k3;
266   delete [] k4;
267     return;
268 }//End rk4()
269
270
271 void calc_k(cmplx *k, cmplx *c, double kappa, double g_0, double omega,
272       double gamma_x, double h){
273   k[0] = h*function_g(c[0], c[2], kappa, g_0);
274   k[1] = h*function_e(c[2], omega);
```

```
275   k[2] = h*function_x(c[0], c[1], c[2], g_0, omega, gamma_x);
276     return;
277 }//End calc_k()
278
279
280 //Function controlling the laser profile
281 double omega_function(double t){
282   double omega = 14*2*PI*9*exp(-(t/3*PI)*(t/3*PI));
283   return omega;
284 }//End omega()
285
286
287 cmplx function_g(cmplx c_g, cmplx c_x, double kappa, double g_0){
288   cmplx f = -kappa*c_g + imag_i*g_0*c_x;
289   return f;
290 }//End function_g()
291
292
293 cmplx function_e(cmplx c_x, double omega){
294   cmplx f = imag_i*omega/2.0*c_x;
295   return f;
296 }//End function_e()
297
298
299 cmplx function_x(cmplx c_g, cmplx c_e, cmplx c_x, double g_0, double omega
      ,
300      double gamma_x){
301   cmplx f = imag_i*g_0*c_g + imag_i*omega/2.0*c_e - gamma_x*c_x;
302   return f;
303 }//End function_x()
304
305
306 void quantumJump(cmplx *c, double gamma_xg, double gamma_xe, double kappa,
307      double rho){
308
309   double p_xg, p_xe, p_ph, p_tot, pCond_xg, pCond_xe, pCond_ph;
310
311   p_xg = 2*gamma_xg*pow(abs(c[2]),2);
312   p_xe = 2*gamma_xe*pow(abs(c[2]),2);
313   p_ph = 2*kappa*pow(abs(c[0]),2);
314   p_tot = p_xg + p_xe + p_ph;
315
316   pCond_xg = p_xg/p_tot;
317   pCond_xe = p_xe/p_tot;
318   pCond_ph = p_ph/p_tot;
319
320   if(rho <  pCond_xg+pCond_ph){
321     for(int i=0; i<=2; i++){
322       c[i]=0;
323     }
324   }
325   else{
326     if(rho >= pCond_xg+pCond_ph){
327       c[0]=0;
328       c[1]=1;
329       c[2]=0;
```

```
330       }
331     }
332
333     return;
334 }//End quantumJump()
335
336
337 void output(double *t, double *c_gFinal, double *c_eFinal, double *
      c_xFinal, int N){
338     ofstream xfile("mcSTIRAP.txt");
339     xfile << setiosflags(ios::showpoint | ios::uppercase);
340
341     for(int i=0; i<=N; i++){
342       xfile << setw(15) << setprecision(8) << t[i];
343       xfile << setw(15) << setprecision(8) << c_gFinal[i];
344       xfile << setw(15) << setprecision(8) << c_eFinal[i];
345       xfile << setw(15) << setprecision(8) << c_xFinal[i];
346       xfile << setw(15) << setprecision(8) << c_xFinal[i] +
347         c_gFinal[i] + c_eFinal[i] << "\n";
348     }
349     return;
350 }//End output()
```

./C++/MC.cpp

Bibliography

[1] The 2012 Nobel Prize in Physics - Press Release. Nobelprize.org. 29 Nov 2012 *http* : *//www.nobelprize.org/nobelprizes/physics/laureates/*2012/*press.html*, 2012.

[2] Heinz-Peter Breuer and Francesco Petruccione. *The theory of open quantum systems*. Oxford University Press, 2006.

[3] R. Dum, P. Zoller, and H. Ritsch. Monte Carlo simulation of the atomic master equation for spontaneous emission. *Physical Review A*, 45, 1991.

[4] Charles Fabry and Alfred Pérot. Comparison of quantum and semiclassical radiation theories with application to the beam maser. *Annales de chimie et physique*, 12, 1897.

[5] C. Henry Edwards and David E. Penney. *Elementary Differential Equations*. Pearson Education, 2009.

[6] Markus Hijlkema, Holger P. Specht Bernhard Weber, Simon C. Webster, Axel Kuhn, and Gerhard Rempe. A single-photon server with just one atom. *Nature Physics*, 3, 2007.

[7] Morten Hjorth-Jensen. *Lecture Notes on Computational Physics*. University of Oslo, 2010.

[8] D. Hunger, T. Steinmetz, Y. Colombe, C. Deutcsh, T. W. Hänsch, and J. Reichel. Fiber Fabry-Perot cavity with high finesse. 2010, 1005.0067v1.

[9] David J. Griffiths. *Introduction to Quantum Mechanics*. Pearson Education, 2005.

[10] J.I. Cirac, P. Zoller, H.J. Kimble, and H. Mabuchi. Quantum Transfer and Entanglement Distribution among Distant Nodes in a Quantum Network. *Physical Review Letters*, 78, 1996.

[11] C. K. Law and H. J. Kimble. Deterministic generation of a bit-stream of single-photon pulses. *Journal of Modern Optics*, 44, 2009.

[12] A. Kuhn, M. Hennrich, T. Bondo, and G. Rempe. Controlled generation of single photons from a strongly coupled atom-cavity system. *Applied Physics B*, 69, 1996.

[13] Axel Kuhn, Markus Hennrich, and Gerard Rempe. Deterministic Single-Photon Source for Distributed Quantum Networking. *Physical Review Letters*, 89, 2002.

[14] Axel Kuhn and Daniel Ljunggren. Cavity-based single-photon sources. *Contemporary Physics*, 51, 2009.

[15] Jay L. Devore and Kenneth N. Berk. *Modern Mathematical Statistics with Applications*. Thomson Brooks/Cole, 2007.

[16] Peter Lambropoulos and David Petrosyan. *Fundamentals of Quantum Optics and Quantum Information*. Springer, 2007.

[17] Klaus Mølmer, Yvan Castin, and Jean Dalibard. Monte Carlo wave-function method in quantum optics. *Journal of the Optical Society of America B*, 10, 1992.

[18] Edward M. Purcell. Proceedings of the American Physical Society. *Physical Review*, 69, 1946.

[19] Jon Magne Leinaas. Lecture Notes on Non-relativistic Quantum Mechanics, 2010.

[20] Dieter Meschede. *Optics, Light and Lasers*. Wiley, 2007.

[21] Nicholas Metropolis and S. Ulam. The Monte Carlo Method. *Journal of the American Statistical Association*, 44, 1949.

[22] Hanne-Torill Mevik. Coherence in Classical Electromagnetism and Quantum Optics. Master's thesis, University of Oslo, 2009.

[23] G. Nogues, A. Rauschenbeutel, S. Osnaghi, M. Brune, J. M. Raimond, and S. Haroche. Seeing a single photon without destroying it. *Letters to Nature*, 1999.

[24] Stefan Nußmann, Karim Murr, Markus Hijlkema, Bernhard Weber, Axel Kuhn, and Gerhard Rempe. Vacuum-stimulated cooling of single atoms in three dimensions. *Nature Physics*, 1, 2005.

[25] Marlan O. Scully and M. Suhail Zubairy. *Quantum Optics*. The press syndicate of the University of Cambridge, 1997.

[26] W.H Press, B.P Flannery, S.A Teukolsky, and W.T Vetterling. *Numerical Recipes in C++, The art of scientific Computing*. Cambridge University Press, 1999.

[27] G. Rempe, R. J. Thompson, and H. J. Kimble. Measurement of ultraslow losses in an optical interferometer. *Optics Letters*, 17, 1992.

[28] Stephan Ritter, Christian Nölleke, Carolin Hahn, Andreas Reiserer, Andreas Neuzner, Manuel Uphoff, Martin Mücke, Eden Figueroa, Joerg Bochmann, and Gerhard Rempe. An elementary quantum network of single atoms in optical cavities. *Nature*, 484, 2012.

[29] Genko S. Vasilev, Daniel Ljunggren, and Axel Kuhn. Single photons made-to-measure. *New Jounal of Physics*, 12, 2010.

[30] E. T. Jaynes and F. W. Cummings. Sur les fringes des lames minces argenteés et leur application à la mesure de petites é passeurs d'air. *Proceedings of the IEEE*, 51, 1963.

[31] Amnon Yariv. *Optical Electronics*. Saunders College Publishing, 1991.